RELIABILITY ANALYSIS OF A ROCK SLOPE IN SUMELA MONASTERY, TURKEY, BASED ON DISCRETE ELEMENT AND RESPONSE SURFACE METHODS

A THESIS SUBMITTED TO
THE GRADUATE SCHOOL OF NATURAL AND APPLIED SCIENCES
OF
MIDDLE EAST TECHNICAL UNIVERSITY

BY

NEDA DADASHZADEH

IN PARTIAL FULFILLMENT OF THE REQUIREMENTS
FOR
THE DEGREE OF MASTER OF SCIENCE
IN
MINING ENGINEERING

FEBRUARY 2015

Approval of the thesis:

RELIABILITY ANALYSIS OF A ROCK SLOPE IN SUMELA MONASTERY, TURKEY, BASED ON DISCRETE ELEMENT AND RESPONSE SURFACE METHODS

submitted by **NEDA DADASHZADEH** in partial fulfillment of the requirements for the degree of **Master of Science in Mining Engineering Department, Middle East Technical University** by,

Prof. Dr. Gülbin Dural Ünver   _____
Dean, Graduate School of **Natural and Applied Sciences**

Prof. Dr. Ali İhsan Arol   _____
Head of Department, **Mining Engineering**

Prof. Dr. H.Şebnem Düzgün   _____
Supervisor, **Mining Engineering Department, METU**

Examining Committee Members:

Prof. Dr. Candan Gökceoğlu   _____
Geological Engineering Department, Hacettepe University

Prof. Dr. H.Şebnem Düzgün   _____
Mining Engineering Department, METU

Prof. Dr. Levent Tutluoğlu   _____
Mining Engineering Department, METU

Prof. Dr. Haluk Akgün   _____
Geological Engineering Department, METU

Assist. Prof. Dr. Nurgül Gültekin   _____
Geological Engineering Department, Aksaray University

Date: **02/02/2015**

I hereby declare that all information in this document has been obtained and presented in accordance with academic rules and ethical conduct. I also declare that, as required by these rules and conduct, I have fully cited and referenced all material and results that are not original to this work.

Name, Last Name: Neda Dadashzadeh

Signature   :

ABSTRACT

RELIABILITY ANALYSIS OF A ROCK SLOPE IN SUMELA MONASTERY, TURKEY, BASED ON DISCRETE ELEMENT AND RESPONSE SURFACE METHODS

Dadashzadeh, Neda

M.S., Department of Mining Engineering

Supervisor: Prof. Dr. H.Şebnem Düzgün

February 2015, 121 pages

It is widely recognized that a single factor of safety (FOS) calculated by traditional deterministic analysis methods may not represent slope safety due to involved uncertainties. The First Order Reliability Method (FORM) is one of the extensively used probabilistic methods in slope stability studies to quantify the uncertainties in the parameters. FORM can be easily applied when the slope is analyzed based on limit equilibrium methods. However, the recent numerical techniques are almost substituted by the conventional limit equilibrium approaches due to their high performance of representing the real phenomena. Monte Carlo Simulation (MCS) technique is a widely used probabilistic tool to consider the uncertainties. However, although advanced modeling techniques in slope stability analysis are successfully used in deterministic studies, they have so far found little use in probabilistic analyses due to their high computation cost. Alternatively, FORM can calculate the probability of failure (P_f) in more efficient way rather than MCS method. However, in order to be able to perform

reliability studies, the corresponding limit state failure function is essential. It is not possible to generate an explicit failure function in cases simulated by numerical methods. The Response Surface Method (RSM) is usually used to approximate the implicit limit state failure function using an equivalent explicit mathematical function of the random variables. Since the approximated limit state function is explicit, the FORM can be applied to estimate the P_f. In this thesis, a reliability assessment methodology is developed by using three dimensional distinct element code, 3DEC, based on RSM. Once the limit state surface is generated, FORM is performed to calculate the P_f. The methodology is used to calculate the P_f of a selected potential rock wedge in Sumela Monastery, Turkey. The potential wedge is located at height of approximately 200 meters from the toe of the cliff with volume of about ten million m^3. Rockfall evidences on the wedge indicate the slope instabilities. The P_f of the wedge is calculated to be 16.3% by 84 simulations in 3DEC based on proposed methodology which is about 10% of the number of simulations required for a MCS. It is concluded that by converging to the limit state surface obtained from RSM, slope instabilities occur inside the model and cause increase in total displacements and vertical velocity. It is also revealed that after about 10 cm of total displacement, the slope represents a critical uncontrollable situation which requires development of risk mitigation strategies.

Keywords: Rock slope stability, Distinct Element Method, Response Surface Method, Reliability analysis, Probability of Failure.

ÖZ

SÜMELA MANASTIRINDA BİR KAYA ŞEVİNİN AYRIK ELEMAN VE TEPKİ YUZEYİ METODLARINA DAYALI GUVENİRLİK ANALİZİ

Dadashzadeh, Neda

Yuksek Lisans, Maden Mühendisliği Bölümü

Tez Yöneticisi : Prof. Dr. H. Şebnem Düzgün

Şubat 2015, 121 sayfa

Klasik deterministic analiz yöntemleri ile hesaplanan Emniyet Katsayısı (EK) kaya şev duraylığı analizlerindeki belirsizlikler nedeniyle şevin güvenliğini temsil etmeyebilir. Birinci Mertebe İkince Moment (BMİM) methodu şev duraylığı çalışmalarında parametrelerdeki belirsizliği ölçmek için yaygın olarak kullanılan olasılığa dayalı yöntemlerden biridir. BMİM limit denge yöntemleri kullanılarak kolayca uygulanabilir. Son yıllarda sayısal teknikler gerçek olguları modellemede yüksek performans gösterdiği için klasik limit denge methotlarının yerini almiştir. Yüksek hesaplama gerektiren Monte Carlo Simulasyonu (MCS) bir başka yaygın olarak kullanılan olasılığa dayalı methoddur. Sayısal metodlerle güvenirlik analizi yapılabilmesi için sayısal tekniklere dayalı bir yenilme fonksiyonunun tanımlanması gereklidir. Tepki Yüzeyi Methodu (TYM) limit denge fonksiyonunun,rassal değişkenlerle ifade edilen eşlenik bir fonksiyonla kestirimidir. Eşlenik fonksiyon analiz olarak rassal değişkenlerle ifade edilebildiğinden BMİM ile yenilme olasılığı (P_f) in tahmini yapılabilir. Bu tezde TSM'ne dayalı üç boyutlu Ayrık Elemanlar Codu (3AEC) kullanılarak güvenlik analizi metodolojisi geliştirilmiştir. Bin kere limit denge yüzeyi yaratılınca P_f hesaplamak için

BMİM uygulanmıştır. Metodoloji Türkiye'de Sümela Manastırında seçilen bir potansiyel kama türü kaya şevi için uygulanmıştır. Kayma potansiyeli olan kama şeklindeki şevin topuktan yüksekliği yaklaşık 200 m ve hacmi 10 milyon m^3 tür. MCS methodunun %10'una denk gelen 3AEC'te 84 adet benzetişim ile kamanın kayma olasılığı %16.3 olarak bulunmuştur. TYM ile limit dengenin elde edilip şev duraysızlığının gösterilebildiği sonucuna varılmıştır. Ayrıca şevin 10 cm'lik hareketi sonrası kontrol edilemeyerek yenileceği, bu nedenle de zarar azaltma stratejilerinin geliştirilmesi gerektiği ortaya çıkmıştır.

Anahtar Kelimeler: Kaya şev stabilitesi, Farklı elemanlar yöntemi, Tepki yuzeyi yöntemi, Güvenilirlik analizı, Başarısızlık olasılığı.

ACKNOWLEDGEMENTS

I must express my profound gratitude to my parents, whose mentorship was paramount in all stages of my life. They always encouraged me to not only grow as a human but also as an independent thinker and develop a positive individuality and self-sufficiency.

I would also send special thanks to my sister, Hoda, for her tremendous understanding and kindness.

Finally, I send my deepest appreciation to my husband, Ali, for always encouraging me to pursue my desires and goals. His endless support and patience is my most precious property. Thank you.

TABLE OF CONTENTS

LIST OF TABLES

TABLES

LIST OF FIGURES

FIGURES

LIST OF ABBREVIATIONS

3DEC	3 Dimensional Discrete Element Code
BEM	Boundary Element Method
DEM	Distinct Element Method
DoE	Design of Experiments
FDM	Finite Difference Method
FEM	Finite Element Method
FORM	First Order Reliability Method
FOS	Factor of Safety
MCS	Monte Carlo Simulation
MPP	Most Probable Point
RBM	Rigid Body Motion
RQD	Rock Quality Designation
RSM	Response Surface Method
P_f	Probability of Failure
SORM	Second Order Reliability Method

CHAPTER 1

INTRODUCTION

A "rock slope failure" is the movement of a mass of rock downward in response to gravity, when it cannot anymore hold its original position after a disturbing phenomena or strength loss. The movement can vary from very slow, barely perceptible for many years, to rapid speed in a few minutes causing sudden hazards. According to the mechanism of the event, the rock slope failure may follow different scenarios like slides, falls and flows (Hungr et al. 2013). Most of the rock slope failures are mainly triggered by the changes in stress field of the slope or decrease in shear strength due to external disturbance like pore pressure increase, erosion, weathering or seismic activity (Turner and Schuster 1996). Due to their large affected areas and high energy, slope failures are rated as the second destructive natural hazards after earthquakes, but are considered as the most frequent geohazard (USGS 2000). According to the database prepared by the Centre for Research on the Epidemiology of Disasters, landslides killed approximately 61,000 people around the world over the period 1900 – 2009 (Gutiérrez et al. 2010). In 1963, a catastrophic landslide known as Vaiont Landslide, occurred on the southern slope of the Vajont reservoir dam in Italy, and caused death of 2,500 people (Voight and Faust 1992). This is the most deadly landslide ever recorded in Europe. Hence, it is essential to have a better understanding of the slope failure mechanism in order to predict, design or implement protection measures for a safe environment. There are a considerable number of studies performed on different aspects of slope stability (Wu and Kraft 1970; Tang et al. 1976; Wong 1985; Matsui and San 1992; Duzgun et al.

1

1995; Park and West 2001; Stead et al. 2001; Jiang et al. 2003; Duzgun and Bhasin 2008; Lee et al. 2012). However, it is still one of the most concerning geological hazards due to its nondeterministic nature. It is widely accepted that great variability and data deficiency exist in natural phenomena (Phoon 2008). Accordingly, reliability and probabilistic approaches which allow the systematic and quantitative treatment of these uncertainties have become a topic of increasing interest in rock slope engineering area in the past couple of decades (Wong 1985; Duzgun et al. 2003; Jimenez-Rodriguez et al. 2006; Duzgun and Bhasin 2008; Stanković et al. 2013; Tan et al. 2013; Dadashzadeh et al. n.p.) . The performance of a rock slope is represented in the form of probability of failure (P_f) rather than a single factor of safety (FOS) in reliability and probabilistic methods. On the other hand, with the development of modern computation techniques, the rock slope stability analysis methods have also faced imrovements through decades. Recent numerical techniques are widely implemented in slope stability studies because of their capabilitis and advantages rather than conventional limit equilibrium methods (Zou and Williams 1995; Matsui and San 1992; Duncan 1996; Swan and Seo 1999; Griffiths and Lane 1999; Dolezalova et al. 2001; Wang et al. 2013; Kainthola et al. 2014).

It is recognized that a single FOS calculated by traditional deterministic analysis methods can not represent slope safety due to many uncertainties involved in the analysis owing to inadequate information for site characterization and inherent variability and measurement errors in geological and corresponding parameters (Phoon 2008). Consequently, reliability-based approaches that allow the systematic and quantitative treatment of these uncertainties have become a topic of increasing interest in rock slope engineering. On the other hand, since the slope stability analysis based on numerical methods do not require any assumptions on failure surfaces and modes like limit equilbrium methods, they are extensively applied to rock slope stability assessments. However, the numerical methods take a deterministic value of the input variables and can not directly consider the randomness of the parameters. Monte Carlo simulation (MCS) technique is one of the well known methods which overcomes this

drawback. However, the main disadvantage of this technique is the extensive computational time which increases substantially in the numerical analyses (Wong 1985). On the contrary, reliability methods can wisely search for the P_f with less time and effort. Defining a limit state failure function of the system is mandatory in reliablity analysis. The failure function of a slope can easily be obtained by limit equilibrium methods. However, it is not possible to generate an explicit failure function from numerical methods. Response Surface Method (RSM) can approximate the implicit limit state failure function using an equivalent explicit mathematical function of the random variables.

In this study, a methodology is proposed to generate the failure function of a slope simulated by Three Dimensional Distinct Element Code (3DEC) according to Response Surface Method. Once the explicit limit state function is generated, the First Order Reliability Method (FORM) is applied to estimate the P_f.

This thesis involves five chapters. An introduction of the problem to be considered is given in Chapter I. Chapter II provides a literature review of rock slope stability techniques as well as reliability and response surface methods. The proposed methodology is described in Chapter III. In Chapter IV, the methodology is implemented on a selected case study in Turkey in order to show the application of the proposed approach. The overall results are discussed in Chapter V.

CHAPTER 2

OVERVIEW ON ROCK SLOPE STABILITY ANALYSIS METHODS

2.1 Limit Equilibrium Methods in Rock Slope Stability Analysis

The limit equilibrium methods for slope stability are one of the most common methods of analysis among engineers because of their ease of application. The main developments are performed in 1950s and 1960s (Bishop 1955; Lowe and Karafiath 1960; Morgenstern and Price 1965; Spencer 1967). Considerable number of studies has been performed on the application and performance of these methods through the decades (Hoek 1973; Hoek and Bray 1981; Nash 1987; Duncan 1996; Jiang et al. 2003; Huang and Li 2012; Chen et al. 2013; Wang and Ji 2013). The limit equilibrium methods are mainly based on the geometry assumptions and force interactions. Generally, at shallow depth where stress levels are low, the behavior of the rock mass is governed by discontinuities and bedding planes rather than intact rock. Accordingly, based on the geological structure of the rock mass, the failure modes of a rock slope may commonly appear in form of plane failure, wedge failure or toppling failure. Rock slope stability studies based on limit equilibrium methods are mainly performed for plane and wedge failure. According to limit equilibrium techniques, the mass of rock is assumed to fail along potential sliding surfaces. Once the failure surface of a simple shape is assumed, the material above the surface is considered to be a free body and the corresponding FOS is calculated based on force and/or moment equilibrium equations.

The plane failure mode in rock slopes involves shear failure along a single planer surface. According to Hoek and Bray (1981), two conditions must be satisfied in order to form a plane failure,

1) $\Psi_f > \Psi_p > \varphi$
2) The strike of the sliding plane should be within ±20° of the slope face.

Where,

Ψ_f = Inclination of the slope face
Ψ_p = Inclination of the failure plane
φ = Friction angle

Figure 2.1 illustrates the basic mechanism of a plane failure stated by Hoek and Bray (1981).
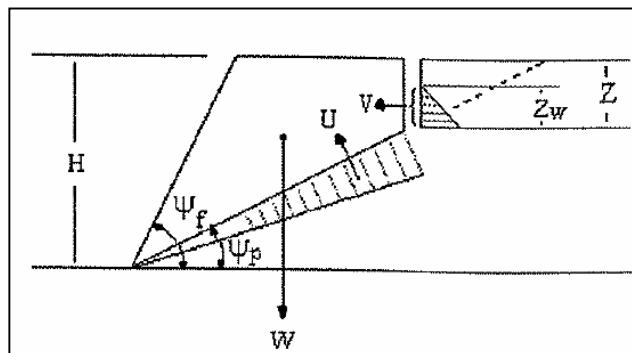
Figure 2.1 – Forces acting on a block for the plane failure when there is a tension crack in the upper slope surface (Hoek and Bray, 1981)

According to Hoek and Bray (1981), the FOS of a plane failure (Figure 2.1) based on limit equilibrium method can be written as,

6

$$FOS = \frac{CA+(W.Cos\Psi_p-U-V.Sin\Psi_p)Tan\varphi}{W.Sin\Psi_p+V.Cos\Psi_p} \qquad (2.1)$$

$$W = 1/2\gamma H^2 \cdot \left[(1-(Z/H)^2) \cdot Cot\Psi_p - Cot\Psi_f\right] \qquad (2.2)$$

$$U = 0.5\gamma_w . Z_w(H-Z).Cosec\Psi_p \qquad (2.3)$$

$$V = 0.5\gamma_w . Z_w^2 \qquad (2.4)$$

$$A = (H-Z) \cdot Cosec\Psi_p \qquad (2.5)$$

Where,

FOS = Factor of Safety

C = Cohesion of the intact rock

A = Area of the failure surface

W = Weight of the sliding block

V = Force due to water pressure in the tension crack

U = Uplift force due to pressure on the sliding surface

Z = Height of the tension crack from the upper surface of the slope

Z_w = Height of water in tension crack

H = Height of the slope

γ = Unit weight of rock

γ_w = Unit weight of water

A wedge failure happens when the discontinuities strike across the slope crest and the sliding takes place along the line of intersection of two planes (Figure 2.2).
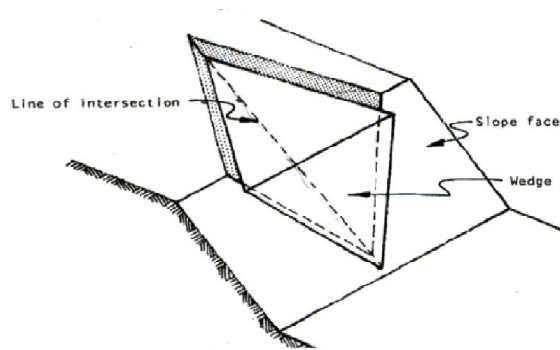
Figure 2.2 – Wedge failure geometry (Hoek and Bray, 1981).

According to Hoek and Bray (1981) the general condition for a wedge failure to take place is,

$$\Psi_{f_i} > \Psi_i > \varphi$$

Where,
Ψ_{f_i} = Inclination of the slope face
Ψ_i = Dip of the line of intersection
φ = Friction angle

For a wedge shown in Figure 2.3, in case the friction angle is the same for both planes, Hoek and Bray (1981) formulated the FOS as,
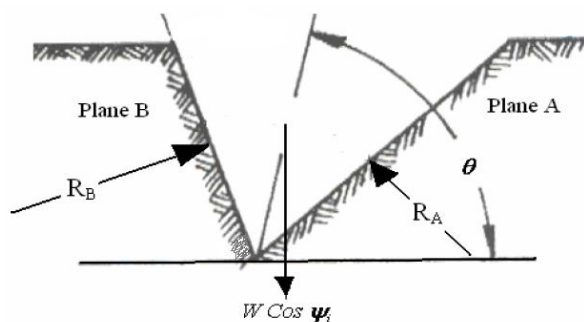
Figure 2.3 – Forces acting on a wedge slope (Hoek and Bray, 1981)

8

$$FOS = \frac{(R_A + R_B).Tan\varphi}{W.Sin\Psi_i} \qquad (2.6)$$

$$R_A + R_B = \frac{W.Cos\Psi_i.Sin\theta}{Sin\frac{1}{2}\xi} \qquad (2.7)$$

Where,

W = Weight of the wedge block

R_A = Normal reaction provided by plane A

R_B = Normal reaction provided by plane B

ξ = Angle of the intersection line

As it is clear, the relative stability of a slope in deterministic limit equilibrium methods are represented in the form of FOS. The parameters of the resisting and driving forces take a single value, generally mean value, and generate a single FOS accordingly.

The limit equilibrium methods have been popular in rock engineering assessments for many decades. However, they have been generated through assumptions like elastic behavior, homogeneous, isotropic material, time independent behavior and quasi-static loading. It is obvious that rock mass is a massively Discontinuous, Inhomogeneous, Anisotropic and Non-Elastic (DIANE) material (Harrison and Hudson 2000). Hence, the assumptions followed by limit equilibrium methods may limit a better representation of rock mass behavior in complex problems. Recent developments in computational approaches and increase in application of sophisticated mathematical methods provide a better understanding of materials and more reliable analytical techniques, accordingly.

2.2 Numerical Methods in Rock Slope Stability Analysis

Despite improvements in engineering designs and predictions, geotechnical problems still reveals important concerns due to inadequate knowledge of the material and complex failure mechanisms. Accordingly, the assumptions and simplifications of conventional limit equilibrium slope stability methods which cannot consider the development of strain, may not be sufficient to represent the behavior of complex slope problems (Stead et al. 2001). Benefiting the recent advancements in computational approaches, it is possible to model the slope stability problems in a more realistic manner. The numerical simulation methods are currently adopted in many geotechnical programs (Jiang 1990; Matsui and San 1992; Griffiths and Lane 1999). These methods divide the slope into a finite number of zones or elements and calculate the forces and strains of each element using appropriate constitutive laws. There is no necessity for pre-defined failure surface and mode or statical assumptions. Moreover, multiple failure surfaces can be taken into account (Jing 2003). According to Eberhardt (2003), the most common numerical methods of analysis applied for rock slope stability can be divided into three approaches: continuum, discontinuum and hybrid modeling. Considering the different fracture circumstances in rock mechanics problems, Figure 2.4 illustrates the alternative choices appropriate to simulate the system.
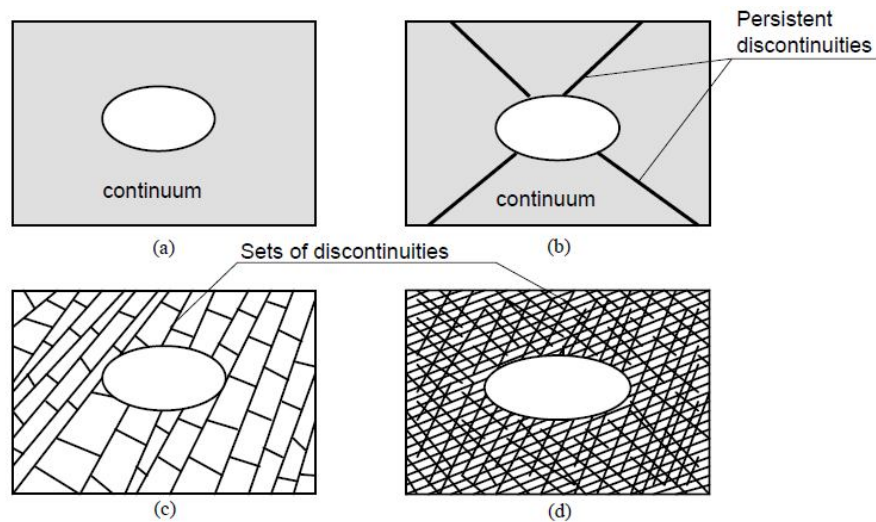
Figure 2.4 – Appropriate numerical methods for different rock mass systems: (a) continuum method; (b) either continuum with fracture elements or discrete method; (c) discrete method; and (d) continuum method with equivalent properties (Jing 2003).

According to this classification (Figure 2.4), the choice of continuum or discontinuum methods mainly depends on the geometry of the fracture system. Generally, continuum approaches are used for mediums with no fractures or with intense fractures (Figure 2.4a and d). In cases where a few discontinuities exist and not very big displacements are expected through discontinuities, continuum methods may also be applicable (Figure 2.4b). However, in situations where failure along the discontinuities rather than intact rock are expected to govern the problem, or the number of fractures are high to be simulated by continuum methods, discontinuum techniques are more suitable (Figure 2.4c).

In rock slope stability analyzes, the level of confining stress is very low in comparison to underground problems. Hence, the slope is mainly confronted with large movements of individual blocks rather than material deformation. Accordingly, discontinuum methods are more appropriate to be utilized in slope stability analyses (Anon 2013).

Since this study uses the discontinuum approach to model the slope behavior, a brief overview of continuum and hybrid models is presented while the discontinuum approach is discussed in detail.

2.3 Continuum and Hybrid Modeling

Continuum modeling assumes a continuous material throughout the body which is best suited for the analysis of slopes that are comprised of intact rock, soil-like or heavily fractured rock masses (Stead et al. 2001). The discontinuities are treated as special cases by introducing interfaces between continuum bodies. However, continuum modeling can typically simulate a few numbers of discontinuities with no fracture opening or complete block detachment which is not appropriate for blocky mediums. The common continuum methods used in recent commercial software are the Finite Difference Method (FDM), Finite Element Method (FEM) and Boundary Element Method (BEM). In these techniques, the problem domain is discretized into a set of sub-domains or elements. The solution procedure may then be based on numerical approximations of the governing equations, i.e. the differential equations of equilibrium, the strain-displacement relations and the stress-strain equations (Eberhardt 2003).

FLAC2D, FLAC3D (Itasca), Phase2 (Rocscience), ABAQUS and VISAGE (VIPS 2001) are common continuum modeling commercial tools for rock slope cases. There is considerable number of studies performed by continuum methods which proves the strong application of numerical modeling in slope stability analysis. As an example, Griffiths and Lane (1999) compared the results of several examples of finite element slope stability analysis against limit equilibrium methods. Wu (2008) studied a slope stability case in central Asia under severe seismic event using finite difference program FLAC3D and Finite Element program QUAKE/W. Yang (2011) evaluated the slope

12

stability of North Opencast coal mine of YiMei, and validated the results based on rigid body limit equilibrium method. Wang et al. (2012), have also utilized the finite difference method to determine the landslide static stability of Zhu Jiadeng slope in Chongqing, china. Kainthola et al. (2013) analyzed a road cut slope from Deccan traps of Mahabaleshwar, India, using FLAC SLOPE 5.0. Guo et al. (2013), studied the deformation and stability of soft rock slope using FLAC3D. Sdvizhkova et al. (2014) studied the stability of slopes in the regions of Crimea, Ukraine by using finite element method software Plaxis and Phase2.

Each numerical method may include definite limitations and disadvantages. Moreover, complex models of analysis require high performance numerical codes and computational expenses. In such cases, it is often unnecessary to apply one method to the whole problem in order to provide adequate representation. Hybrid methods involve the coupling of continuum and discontinuum techniques to maximize their key advantages. The initial representation of the idea started with the studies of Lorig and Brady (1984) in which the far-field rock is modeled as a transversely isotropic continuum using the Boundary Element Method (BEM) and the near-field rock as a set of discrete element blocks defined by rock fractures (Figure 2.5).
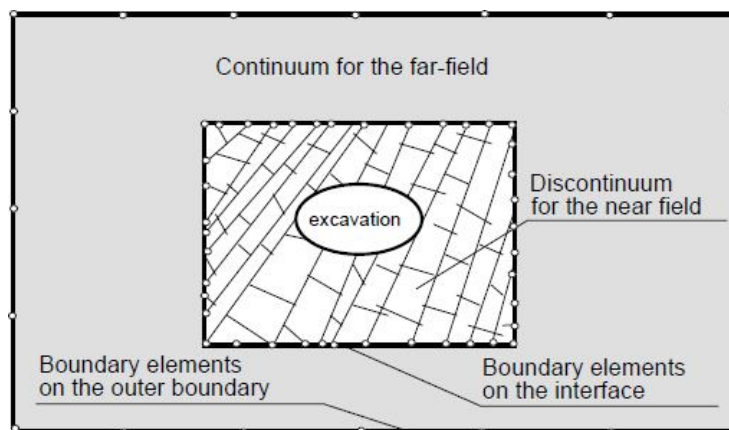
Figure 2.5 - Hybrid DEM-BEM model for a rock mass containing an excavation (Jing 2003)

13

The disturbed rock mass near the excavation can be efficiently handled by the DEM or FEM, while the surrounded material is simulated by a BEM linear material behavior without fractures. The reason for the assumption of the far-field is that the variation of the physical parameters, such as stress, displacement or flow, decrease rapidly with distance from the excavation. By the combined way of modeling, a higher efficiency of numerical techniques can be achieved. Recent advances include coupled particle flow and finite-difference analyses using FLAC-3D and PFC-3D (Itasca 2012). ELFEN (ELFEN 2001) is one of the other hybrid codes with adaptive remeshing routines, which has been successfully applied to the simulation of surface mine blasting, mineral grinding, retaining wall failure and underground rock caving (Munjiza et al. 1995). The hybrid techniques also show significant potential in the investigation of piping slope failures, and the influence of high groundwater pressures on the failure of weak rock slopes (Stead et al. 2001). The FEM-FDM codes use a finite element mesh to represent the blocks of a slope bounded by fractures and combine a discrete element model to simulate the behavior of the discontinuities. If the stresses inside the rock slope exceed the failure criteria of the finite element model, a crack is initiated. The propagation of the new cracks through the finite element mesh can be possible by remeshing.

2.4 Discontinuum Modeling

The upper crust of the Earth is comprised of fractured rock mass which is a discrete system. Simulating the exact material behavior is not practically possible. Hence, by different material and geomechanical assumptions, numerical methods have been developed for continuous and discrete systems. According to the assumptions of a continuum method, no points of a system domain can be open or broken into pieces (Jing 2003). When geotechnical problems are dealing with moderately fractured rock masses, where the behavior of the system is mainly controlled by the discontinuities, the

continuum methods can not satisfy the requirements. Continuum methods are limited to model the blocky media in one or more of the following ways;

1) They are inefficient when many intersecting faces are used,
2) They cannot automatically generate new contacts during the analysis,
3) The formulation cannot simulate large scale displacements of blocks (Anon 2013).

In 1971 Cundall generated a new methodology by introducing the Discrete Element Method (DEM) in a landmark paper about the progressive movements of rock masses considered as 2D rigid block assemblages and overcome the problem associated with the large displacements of discontinuum medium. The approach was then developed in 1970's (Cundall 1971; Cundall 1974; Chappel 1972; Chappel 1974; Byrne 1974). Fundamentally, the DEM treats the fractured medium as an assemblage of rigid or deformable blocks connected by discontinuities in the problem domain, and solve the dynamic equations of motion and treatment of contacts between the blocks which allows the deformation and movement of blocks relative to each other. Large displacements caused by rigid body motion of individual blocks, including rotation, sliding and opening of rock discontinuities or complete detachments is straightforward in the DEM, which are not possible in the FDM, FEM or BEM. The important difference between the continuum and discrete methods is the treatment of displacements. In the continuum methods, the displacement compatibility must be enforced between the neighboring internal elements. However, the displacement compatibility is not required between blocks in the DEM, and is replaced by the contact conditions between blocks with specially developed constitutive models for point contacts or fractures (Jing 2003). The rigid body mode and deformable mode of blocks in DEM are individually treated. The rigid body motion logic produces large scale block displacements but cannot generate strains in the elements. Hence, it is not generally included in continuum methods. Accordingly, a continuous model reflects mainly the "material deformation" of the system while the discrete model reflects mainly the "member movement" of the system (Anon 2013) . The key concept of DEM which is also one of the draw backs of

15

continuum methods is that the contact pattern between the blocks/particles/bodies needs to be continuously updated during the deformation and motion process.

Cundall (1971) is originally the main developer of the Discrete Element Method. Cundall and Marti (1979) extended the study on discontinuum medium by using the DEM and Rigid Body Motion (RBM) code to approximate the deformation of blocks of 2-D geometries. The code called CRACK was able to consider fracturing, cracking and splitting of intact blocks under loading, based on a tensile failure criterion. However, the code was not able to make compatibility between the complex block geometries. This difficulty was overcome later by using full internal discretization of blocks by finite volume meshes of triangle elements, leading to early versions of the code UDEC (Cundall 1980; Cundall and Hart 1985). Later studies were developed on three dimensional analyses by Cundall (1988) and Hart et al. (1988) leading to the introduction of the code 3DEC, 3 dimensional Discrete Element Code. 3DEC, as the result of a period of over 40 years progression, is a powerful code on performing 3D calculations of discontinuum medium on computers. It is well suited to the jointed rock slopes because in one hand it is capable to simulate large displacements due to slip or detachment along discontinuities and on the other hand, it can model the deformation and material yielding of the intact rock blocks bounded by fractures (Rathod et al. 2012). This becomes highly relevant for slopes composed in weak rock, flexural-topples and other complex modes of rock slope failure (Eberhardt 2003). There are several published schemes that appear to resemble discrete element methods like the ones consider the stability of bodies using limit equilibrium methods (Hoek 1973; Warburton 1981; Goodman and G.-H. 1985; Lin and Fairhurst 1988). However, they lack modeling the deformation of blocks or detection of new contacts.

3DEC V 5.0 (Itasca 2013) is a three-dimensional numerical program based on the discrete element method for discontinuum simulation. It simulates the response of the jointed rock mass subjected to either static or dynamic loading. The discontinuities are treated as boundary conditions between blocks rather than individual elements. Each

block behaves as either rigid or deformable material. Deformable blocks are subdivided into a mesh of finite difference elements, and each element responds according to a prescribed linear or nonlinear stress-strain law. The relative motion of the discontinuities is also governed by linear or nonlinear force-displacement relations for movement in both the normal and shear directions. The equation of dynamic equilibrium for each block is formulated and repeatedly solved until the boundary conditions and laws of contact and motion are satisfied. The new block position and contact displacement increments (or velocities) are provided by integrating the law of motion. Later, the sub-contact force-displacement law is applied to obtain the new sub-contact forces to be used in the next time step. 3DEC is based on Lagrangian calculation scheme which is appropriate to model the large movements and deformations. It also detects the new contacts between the particles generated from block motions (3DEC 2013).

The major advantage of 3DEC over the other published discrete element methods is the ability to represent the block material behavior bounded by the discontinuities in rigid or deformable form (3DEC 2013). The early distinct element codes were ignoring the deformability of the blocks by assuming rigid material for any problem condition. However, the importance of including block deformability in stability analyses is undeniable particularly when the problem is dealing with buried structures and confined rock mass with high values of stress distributions (Zeng et al. 2006).

It is sufficient to assume material rigidity when the stresses and deformations in the blocks are low and major deformation in the system occurs by the movement on the discontinuities. This condition happens in unconfined set of rock blocks at a low stress level, such as shallow slopes in jointed rock where the movements consist mainly of sliding and rotation of blocks, and of opening and interlocking of interfaces (Anon 2013). For rigid block analysis, an explicit time-marching scheme is used to solve the dynamic equations of motion, based on a dynamic or static relaxation scheme, or an FDM approach in the time domain (Jing 2003). However, it is not reasonable to ignore the compressibility of the intact rock in underground problems.

When the deformation of the block material cannot be neglected, in order to introduce deformability to the bodies, the block is discretized into internal elements for increasing the number of degrees-of-freedom. The solution strategies follow two methods. One is explicit solution with finite volume discretization of the block interiors, without the need for solving large-scale matrix equations. The other is an implicit solution with finite element discretization of the block interiors, which leads to a matrix equation representing the deformability of the block systems (Jing 2003).

3DEC provides four material models in order to define the intact rock properties;

1)   Elastic, isotropic,
2)   Elastic, anisotropic,
3)   Mohr-Coulomb plasticity,
4)   Bilinear strain-hardening/softening, ubiquitous joint.

The elastic, isotropic model is appropriate for homogeneous, isotropic, continuous materials which show linear stress-strain behavior. The elastic, anisotropic model is valid for elastic materials that exhibit elastic anisotropy. The Mohr-Coulomb plasticity model is suited for materials that yield when subjected to shear loading. The bilinear strain-softening, ubiquitous joint model, is a modified form of the Mohr-Coulomb model. The Mohr-Coulomb model is more computationally efficient than the bilinear model in terms of calculation time and memory space. However, plastic strain cannot be studied in the Mohr-Coulomb model. Consequently, the bilinear model is generated in 3DEC for the applications in which the post-failure response is important such as yielding pillars, caving or backfilling studies (3DEC manual 2013).

There are two available models in 3DEC to represent the joint behavior;

1)   Coulomb slip criteria,
2)   Continuously yielding model.

The Coulomb slip model is valid for closely packed blocks with area contact. It provides a linear representation of joint stiffness and yield limit, which is based on elastic stiffness, frictional, cohesive and tensile strength properties, and dilation characteristics of the joint. The continuously yielding joint model simulates displacement-weakening of the joint by loss of cohesive and tensile strength at the onset of shear or tensile failure. According to Anon (2013) the model is appropriate for the rock discontinuities displaying progressive damage and hysteretic behavior and is applicable in dynamic analysis, cyclic loading and load reversal with predominant hysteretic loop (3DEC manual 2013).

One of the most important concepts in geohazard evaluations, particularly in slope stability studies, is the evaluation of the FOS in the concerning problem. FOS is a value that is used to examine the stability state of slopes. Generally, a slope fails when its material shear strength on the sliding surface is insufficient to resist the applied in-situ shear stresses. According to Anon (2013), a "FOS" index can be defined for any relevant problem by taking the ratio of the calculated parameter value under given conditions to the critical value of the same parameter, at which the onset of an unacceptable outcome manifests itself. Once the definition is clarified, the effort must be performed on identifying the actual and critical parameters. In recent numerical techniques, this goal is achieved based on parameter reduction techniques (Shen 2012). According to this method, the actual parameter value is achieved by direct resolution of field and constitutive equations governing the problem, while the critical parameter is calculated by solving inverse boundary value problem. In numerical simulations this can be achieved using a trial-and-error technique for a range of parameter values until the critical value is found (Diederichs et al. 2007).

The calculation of the FOS in 3DEC is performed based on strength reduction method. The strength reduction method is an increasingly popular numerical technique to evaluate FOS in geomechanics (Dawson and Roth 1999; Griffiths and Lane 1999).

According to this method, the FOS is calculated by progressively reducing the shear strength of the material to bring the slope to a state of limiting equilibrium. The method is commonly applied with the Mohr-Coulomb failure criterion. In this case, the FOS is defined according to the following equations,

$$FOS = \frac{\tau}{\tau_{trial}} \tag{2.8}$$

Where τ is the actual strength being obtained from the material properties and corresponding constitutive models, and τ_{trial} is the critical strength of the problem. τ_{trial} is obtained from,

$$\tau_{trial} = C_{trial} + \sigma_n tan\varphi_{trial} \tag{2.9}$$

$$C_{trial} = \frac{1}{SRF} C \tag{2.10}$$

$$\emptyset_{trial} = \arctan\left(\frac{1}{SRF} tan\emptyset\right) \tag{2.11}$$

Where SRF is strength reduction factor that is obtained by a series of simulations using trial values of the SRF to reduce the cohesion, C, and friction angle, φ, until slope failure occurs.

There are several slope stability studies performed by 3DEC in the literature. Sainsbury et al. (2007) has developed the 3DEC codes for the south wall of Newcrest Mining Ltd's Cadia Hill Open Pit. Brideau et al. (2008) used 3DEC to perform a preliminary slope stability analysis of the 2007 Mount Steele rock and ice avalanche. Firpo et al. (2011) made a rock slope stability analysis based on digital terrestrial photogrammetric techniques and 3DEC. Rathod et al. (2012) used 3DEC for predicting the behavior of the jointed rock slope of the abutments of the bridge at Chenab, India. Noroozi et al. (2012) proposed a new 3D key-block method for slope stability in which the key blocks are

searched and if no such blocks are found to be unstable, it is concluded that the whole of the rock mass is stable. The stability analysis of the block has been performed by 3DEC in this study. Wang et al. (2013) used 3DEC to simulate the excavation of a rock slope in Puli-Xuanwei Expressway in Yunnan Province. Gheibie et al. (2013) performed a Probabilistic-Numerical Modeling of a Rock Slope in Amasya-Turkey by using 3DEC. Weida et al. (2014) proposed a new method (kinetic vector method, KVM) for analyzing the dynamic stability of wedge in rock slope by using 3DEC for dynamic simulations.

The modeling of geoengineering processes is different from the design of fabricated materials. The inherent variability and lack of site-specific data followed by rock and soil structures constrains a tough situation to the corresponding studies and designs. Accordingly, even any sophisticated and well developed computational tools and codes must be used by cautious to approach to the reality. The computer codes should never be considered as a "black box" which accept any input data and produce acceptable predictions of the site behavior. It is widely accepted that in order to gain a better understanding of the problem, any analysis technique (limit equilibrium or numerical techniques) must be followed by systematic and quantitative treatment of the uncertainties of the input variables.

2.5 The First Order Reliability Method (FORM) and its application in rock slope stability analysis

The engineering design processes are generally constrained by limited resources. Consequently, the information available for analysis is incomplete and decisions are made under uncertainty. Uncertainties in natural systems may be associated with inherent randomness of the material, which is called aleatory uncertainty, or with simulations and estimations of reality performed under inadequate site information

called uncertainty (Phoon 2008) . It is widely accepted that high amount of variability and data deficiency exist in natural phenomena. Hence, in order to achieve a realistic evaluation of the system's safety under consideration, any analysis and engineering design must include the uncertainties of the basic variables affecting the system performance.

Probability tools allow engineers to formulate a mathematical model in which uncertainty can be quantified. Reliability methods are rational ways of contributing quantified uncertainties in modeling and designs. According to Harr (1989), Reliability is theoretically defined as probability of a system performing its required function adequately for a specified period of time under stated conditions. In other words, problems of engineering reliability may be formulated as the determination of the supply capacity of an engineering system to meet certain demand requirements (Ang and Tang 1984). The reliability technique has become a topic of interest in recent years due to its powerful ability of treating the uncertainties in a systematic way. Monte Carlo Simulation Method (MCS) is another well known probabilistic technique in engineering studies. However, In spite of its wide application, the method requires large number of realizations to provide an acceptable P_f of a system. This drawback particularly causes a considerable increase in computational expenses of engineering concepts. On the contrary, reliability techniques can wisely search for the P_f with less effort.

The reliability techniques investigate the performance of a system by defining a limit state where the system fails if it performs under the limit state and survives if it exists above it. Due to the sophistication of the treatment of the problem as well as the approximation of a given limit state function, reliability approach is generally divided into two levels: Conventional Reliability and Level II.

The conventional reliability is based on the full probabilistic descriptions of the load and resistance factors and gives the exact value of P_f. However, the difficulty in computing this probability and the problems of the evaluation of the exact distributions of random

variables on the other hand have led to the development of approximation methods categorized as level II techniques (Zhao and Ono 1999).

In the level II techniques, the reliability of a system is evaluated by approximating a defined limit state function beyond which a system can no longer fulfill the desired condition. The failure function is approximated either linearly or nonlinearly in higher orders. The First Order Reliability Method (FORM) is considered to be the most common technique in evaluating the P_f because of its efficiency (Bjerager 1991). However, its accuracy deteriorates when the nonlinearity of limit-state function increases. The Second Order Reliability Method (SORM) overcomes this drawback with a cost of low efficiency in terms of the number of function calls and computation expenses (Zhang and Du 2010).

Rock slope stability analysis, as well as other geological fields, deals with high degrees of uncertainty. Accordingly, employing reliability and probabilistic tools has increasingly become a topic of interest in the last couple of decades (Duzgun et al. 1995; Duzgun et al. 2003; Duzgun and Bhasin 2008; Jimenez-Rodriguez et al. 2006; Stanković et al. 2013). Slope stability is one of the most widely reported applications of reliability among other geosciences (Lee et al. 2012). The behavior of the slope is evaluated in terms of failure probability rather than a single FOS originated from traditional deterministic methods. The conventional FOS, which only uses characteristic values of the uncertain parameters, cannot consider different possible scenarios associated with the same FOS since it cannot contribute the variability of the parameters (Nadim et al 2005). There is considerable number of studies on reliability based slope stability analyses. Most of these studies are based on FORM (Low 1997; Jimenez-Rodriguez et al. 2006; Duzgun et al. 1995; J.C. et al. 2000; Li et al. 2009). According to Zhang et al. (2010) there is a slight difference between the P_f derived from FORM and SORM. However, this discrepancy is highlighted when the problem is dealing with very low values of failure probability (like in the field of structural engineering). Dadashzadeh et al. (n.p.) has studied the application of SORM in slope stability

problems. According to their observations, FORM can provide adequate accuracy of failure probability in slope stability studies except when the problem is dealing with very low rates of failure probability (e.g. P_f in the order of 10^{-3} or above). Consequently, FORM is going to be adopted in this thesis due to its higher efficiency.

In the practice of level II reliability analysis, the reliability of a system is expressed in terms of reliability index (β) or probability of survival (alternatively failure). At this level of reliability, a limit state function beyond which a system or part of it can no longer fulfill the satisfied condition, must be defined. The limit state function $g(X_i)$ must be defined in such a way that the operating scenario is the availability of a resistance greater than the load:

$$g(X_i) = R(X_i) - S(X_i) > 0 \tag{2.12}$$

and the non-operating or failure scenario is:

$$g(X_i) = R(X_i) - S(X_i) < 0 \tag{2.13}$$

Where X_i is the vector of basic variables, $R(X_i)$ represents the resistance function and $S(X_i)$ represents the load function of the system.

Cornell (1969) defined the reliability index, β_c, as the ratio of the expected value of $g(X_i)$, $\mu_{g(X_i)}$, over its standard deviation, $\sigma_{g(X_i)}$, which can be obtained according to the Taylor series approximation at the mean vector:

$$\beta_c = \frac{\mu_{g(X_i)}}{\sigma_{g(X_i)}} \tag{2.14}$$

The P_f in this case is defined as:

$$P_f = 1 - \emptyset(\beta_c) \tag{2.15}$$

Where $\emptyset(.)$ is the cumulative Gaussian distribution. However, the β_c lacks the failure function invariance, which may result in different reliability indexes for mechanically equivalent limit state functions of the same failure criterion.

To compensate for the non-invariance of Cornell reliability index (β_c), Hasofer and Lind (1974) performed a transformation of variables to a new space of statistically independent Gaussian variables, with zero mean and unit standard deviations. The transformation from physical space (X_i) to standardized space or normalized space (U_i) is immediate in the case of independent Gaussian variables:

$$U_i = \frac{X_i - \mu_{X_i}}{\sigma_{X_i}} \tag{2.16}$$

When random variables are not Gaussian or independent, a transformation must be applied to convert the variables into uncorrelated standard normal parameters. There are several transformation methods (Rosenblauth 1952; Nataf 1962; Fiessler and Rackwitz 1979) among which the Fiessler-Rackwitz has widely been used in reliability studies. Once the variables are transformed to the standard Gaussian U space, the reliability index of Hasofer-Lind, β_{HL}, is defined as the distance between the origin O and the point U^*, closest to the origin in the limit-state surface. U^* is the most probable failure point (MPP) named also as the design point (Figure 2.6) .
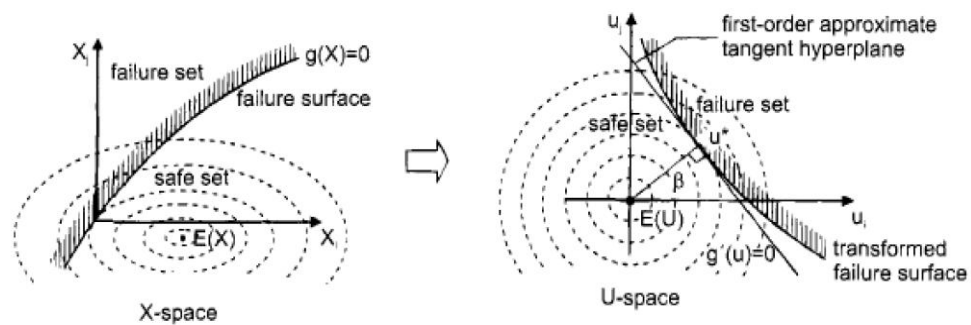
Figure 2.6 – Graphical representation of the FORM approximation.

25

The direction cosine (α) of the corresponding design point (U^*) will iteratively be obtained by:

$$\alpha_i = \frac{-\frac{\partial g}{du_i}(\beta.\bar{\alpha})}{\left[\sum_{j=1}^{n}\frac{\partial g}{du_i}(\beta.\bar{\alpha})^2\right]^{1/2}} \quad , \ i = 1,2,\dots,n \tag{2.17}$$

Where β is searched by:

$$g(\beta.\alpha_1, \beta.\alpha_2, \dots, \beta.\alpha_n) = 0 \tag{2.18}$$

In this method, the failure function is approximated by a linear function (hypersurface) tangent to the limit state surface in the design point. The Cornell Reliability Index is the same as the Hasofer-Lind Reliability Index when the failure function is a hypersurface or the Taylor expansion is implemented around the design point in the nonlinear failure functions.

The reliability analysis of slope based on limit equilibrium techniques have been widely discussed in literature. Tang et al. (1976) presented one of the earliest comprehensive studies of reliability based slope stability analysis. Duzgun et al. (1995) applied the FORM to analyze the planar failure of a rock slope. Low (1997) prepared a reliability study of rock wedge failures. Duncan (2000) discussed the factors of safety and reliability in geotechnical engineering. Duzgun et al. (2003) introduced a methodology for reliability based design of rock slopes. Rodriguez et al. (2006) proposed a system reliability approach to rock slope stability. Duzgun and Bhasin (2008) applied reliability techniques to investigate the stability of a rock slope in Norway. Li et al. (2009) presented a system reliability approach for rock wedges.

The mandatory step to initiate the reliability studies is the definition of the limit state failure function. As it was mentioned, the initial studies of reliability based slope stability analysis were based on limit equilibrium methods. The limit equilibrium methods investigate the equilibrium of the driving forces of the slope mass with the resistance forces. Accordingly, this definition can be applied to generate the failure function of a slope due to limit equilibrium assumptions:

$$g(X_i) = R(X_i) - S(X_i) \tag{2.19}$$

Where $R(X_i)$ denotes the resistance forces of the slope mass and $S(X_i)$ denotes all the driving forces on the slope. According to the different failure criteria for the rock mass of the slope as well as different failure mechanisms, the performance function may vary from case to case. The limit state function for a plane failure following the Mohr-Coulomb criteria will be defined as (Figure 2.7),
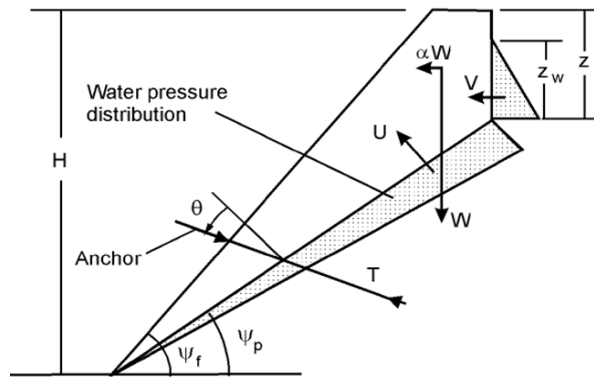
Figure 2.7 – Forces of a rock block subjected to the plane failure.

$$g(X_i) = \left[cA + \left(W(cos\Psi_p - \alpha sin\Psi_p) - U - Vsin\Psi_p + Tcos\theta\right)tan\varphi\right] - \left[W(sin\Psi_p + \alpha cos\Psi_p) + Vcos\Psi_p - Tsin\theta\right] \tag{2.20}$$

Where,

C = Cohesion of the discontinuity

A = Area of the failure surface

W = Weight of the sliding block

V = Force due to water pressure in the tension crack

U = Uplift force due to pressure on the sliding surface

T= Resisting force of the anchor

Ψ_f= Slope face angle

Ψ_p= Discontinuity plane angle

φ = Friction angle

H = Slope height

Z = Height of the tension crack from the upper surface of the slope

Z_w = Height of water in tension crack

The limit state function is easy to define explicitly in limit equilibrium techniques. However, if a reliability analysis is desired to be performed based on numerical simulation of the slope stability, it is not possible to explicitly define a limit state surface based on the effecting variables.

The failure function of a slope presented in Equation 2.18 can also be written as:

$$g(X_i) = FOS(X_i) - 1 \qquad\qquad (2.21)$$

Where $FOS(X_i)$ denotes the factor of safety of the slope with all random parameters affecting the performance of the slope (X_i). The reliability analysis would be possible to implement on numerically simulated slopes, once a function is defined for $FOS(X_i)$. Integrating the reliability analysis and numerical simulations can provide a better interpretation of the slope's performance.

There are several studies in which it is tried to consider the uncertainties in numerical simulations. However, most of these studies are based on probabilistic methods like MCS implemented on soil slopes. Griffiths and Lane (1999) proposed a Random Finite Element Method (RFEM) for soil slopes in a MCS framework to calculate the P_f. Suchomel and Masin (2008) studied a particular landslide in the fine-grained soil, Lodalen slide, Norway, using finite element method combined with random field theory and MCS. Hammah et al. (2009) explored the application of the finite element method to compute the P_f for soil slopes based on Point Estimate Method (PEM) and limited numbers of MCS's. Huang et al. (2010) applied RFEM to calculate the system reliability of soil slopes. Gheibi (2012) proposed a random methodology to find the P_f of a rock slope in Turkey, based on 3DEC. Shen and Abbas (2013) simulated a rock slope in China by UDEC and random set theory.

2.6 Response Surface Method (RSM)

Probabilistic tools are generally used in order to take the uncertainty into account. In principle, the Monte Carlo Simulation (MCS) method is considered as the most reliable probabilistic method for estimating the exact value of the failure probability of the complicated implicit systems (Tan et al. 2013). The main idea of the MCS method is to investigate the performance of the system using a random sampling technique in cases where the limit state cannot be easily expressed explicitly. In spite of the high accuracy of the MSC, it certainly requires large number of observations which results in considerable computational efforts. To reduce the total CPU time, FORM is a widely used alternative method (Wong 1985). Defining a limit state surface for the problem under consideration is mandatory in FORM. In cases where there is not a closed form

explicit equation of the failure surface, RSM is usually used for approximating the implicit limit state function (Youliang et al. 2008).

Response Surface Methodology (RSM) was first introduced by Box and Wilson (1951) as a technique in empirical study of relationships between response of parameters to a group of variables. Although it is originally referred to the process of identifying and fitting an appropriate response surface model from experimental data, it can be applied to numerical modeling studies, where each run can be regarded as an experiment (Zangeneh et al. 2002). According to Propst et al. (1992), the RSM can be considered in three major scenarios,

1) For the case of the well-discovered system performance, RSM can be used to obtain the best optimum value of the response.
2) For the case of limited number of experiments, RSM can be used to gain better understanding of the overall response system.
3) For the cases of requirement of complicated analysis with high effort and advanced computational resources, a simplified equivalent response surface may be obtained by a few numbers of runs to replace the complicated analysis.

The basic idea of the RSM is to approximate the implicit limit state function using an equivalent explicit mathematical function of the random variables involved in the limit state function. Because the approximated function is explicit, the FORM can be applied to estimate the P_f (Tan et al. 2013).

The RSM is based on a group of carefully designed mathematical and statistical experiments which is used to develop an adequate functional relationship between a response of interest (output variable) influenced by several independent variables (input variables). An experiment is a series of tests, called runs, in which changes are made in the input variables in order to identify the reasons for changes in the output response. In general, the structure of the relationship between the inputs and output (response) is

unknown but can be truly approximated by the RSM in which the convergence to the real relation improves by a number of smooth functions (Khuri and Mukhopadhyay 2010).

The RSM is performed by two major steps, namely design and estimation (Wong 1985):

1) The estimation step is the calculations of fitting an approximate response to the real surface based on a number of wisely selected sample points on the space.

2) The design step deals with how to select the best sample points at which experiments will be run so that the fitting of the surface to the true one is satisfied.

According to the estimation step, it is assumed that the true response, $g(X_i)$, of a system depends on i number of input variables, $X_1, X_2, \dots, X_i$, as:

$$g(X_i) = f(X_1, X_2, \dots, X_i) + \varepsilon \quad (2.21)$$

Where the function f is the true unknown and complicated response function, and ε is treated as a statistical error. There are several response surface functions proposed to approximate a limit state surface (Wong 1985; Bucher and Bourgund 1990; Rajashekhar and Ellingwood 1993; Kim and Na 1997; Zheng and Das 2000). The most common approach is the low-degree quadratic polynomial (C. Bucher and Bourgund 1990) due to their advantages of being simple and known properties. The main idea of the polynomial-based RSM is to adjust correctly the polynomials to the limit state function using sample points, particularly in the neighborhood of the design point (Tan et al. 2013).

If $g(X_i)$ represents the real limit state surface of a system, the approximated surface due to response surface function based on quadratic polynomial is:

$$\hat{g}(X_i) = a + \sum_{i=1}^{n} b_i X_i + \sum_{i=1}^{n} c_i X_i^2 \quad (2.22)$$

where $\mathfrak{g}(X_i)$ is the response surface function (i.e., the approximate limit state function); X_i is the ith random variable ($i = 1, 2, ..., n$); n is the number of basic variables; a, b_i, c_i are the polynomial coefficients which must be calculated. According to equation 2.18, it is obvious that $2n + 1$ number of sample points is required to be able to obtain the constants.

According to Box and Draper (1987), the most important part of the RSM is the design of experiments (DoE). The objective of DoE is the selection of the points where the response should be evaluated. The choice of the sampling points can have a large influence on the cost of convergence to the response surface. Among various sampling methods (Myers and Montgomery 1995; Montgomery 1997), a common approach is to evaluate $g(X)$ at $2n + 1$ (n is the number of random variables) combinations of central point, X_i, and along the line parallel to each coordinate axes at $X_i \pm f\sigma_{X_i}$. Parameter X_i is set to be the mean value (μ) of the ith random variable at the first iteration. f is usually set to be 1 for most of the approximations. However, there are several studies in which the importance of f is discussed (Youliang et al. 2008) . σ_{X_i} denotes the standard deviation of the ith random variable (Youliang et al. 2008). Figure 2.8 illustrates the sampling for a system with two random variables.
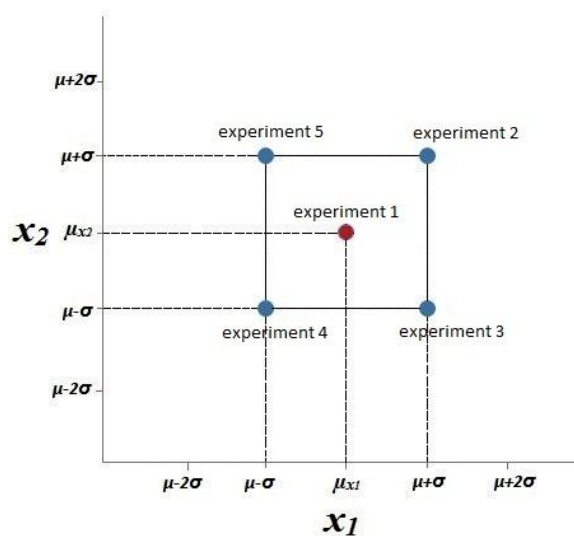
Figure 2.8– DoE around the mean in two random variable space (X_1, X_2).

It should be noted that the main limitation of the RSM is that it is a local analysis method, which means the developed response surface is invalid for regions other than the studied ranges of random variables.

The application of the RSM in engineering reliability analyses started at the end of 1980s and well developed in 1990s (Faravelli 1989; C. G. Bucher and Bourgund 1990; Rajashekhar and Ellingwood 1993; Ying Wei Liu and Moses 1994; S. H. Kim and Na 1997; Zheng and Das 2000; Adhikari 2004). However, most of these studies have been performed in structural engineering field. There are a few studies in reliability analysis of slope stability in which response surface method is applied. The first use of RSM in geotechnical application was performed by Wong (1985) in which a soil slope is modeled by finite element code and the reliability analysis is studied based on FORM. Wong (1985) repeated the slope model in MCS technique and received a reasonable match between the P_f obtained from MCS and RSM. Zangeneh et al. (2002) have employed the RSM to analyze the displacement of slopes in the earthquake studies. Moellmann et al. (2008) proposed a probabilistic finite element analysis approach for reliability study of embankment based on RSM and FORM. Li et al. (2011) proposed a stochastic response surface method for reliability analysis of rock slopes and showed that the accuracy of the proposed method is higher than that for the FORM and is much more efficient than Monte-Carlo simulation. Stanković et al. (2013) used FORM enforced with RSM to study the stability of an open pit coal mine in Monte Negro to obtain P_f with sufficient accuracy, but with various simplifications. Zhang et al. (2013) studied the system reliability of soil slopes with RSM. Tan et al. (2013) studied the application of RSM in slope stability analysis. It is to be noted that in spite of the fact that available discrete element codes like 3DEC requires high run time per model, no study has been performed on the application of the RSM is probabilistic analyses in discontinuum medium, up to now.

CHAPTER 3

DEVELOPMENT OF THE RELIABILITY ANALYSIS BASED ON NUMERICAL AND RESPONSE SURFACE METHODS FOR ROCK SLOPES

In this study, a methodology is developed for reliability analysis of rock slopes based on distinct element code, 3DEC. The limit state function for reliability analysis is defined by RSM and the FORM approach is adopted for calculating the P_f.

According to Equation 2.21, the limit state failure function of a slope to be analyzed by FORM is:

$$g(X_i) = FOS(X_i) - 1 \qquad (3.1)$$

The target is to generate a function to the $FOS(X_i)$ by simulating the slope in 3DEC. This objective is not directly possible by 3DEC. Hence, an explicit equation can be defined to $FOS(X_i)$ using RSM. The response surface of $FOS(X_i)$ represents the performance of the FOS of the slope according to different random variables of load and resistance (X_i) observed in 3DEC. Once an explicit function is generated for $FOS(X_i)$, the FORM can easily be performed for the slope. However, it is important to obtain satisfactory convergence to the real function of the FOS. Figure 3.1 illustrates the flow chart of the developed methodology. The proposed approach consists of 5 steps:
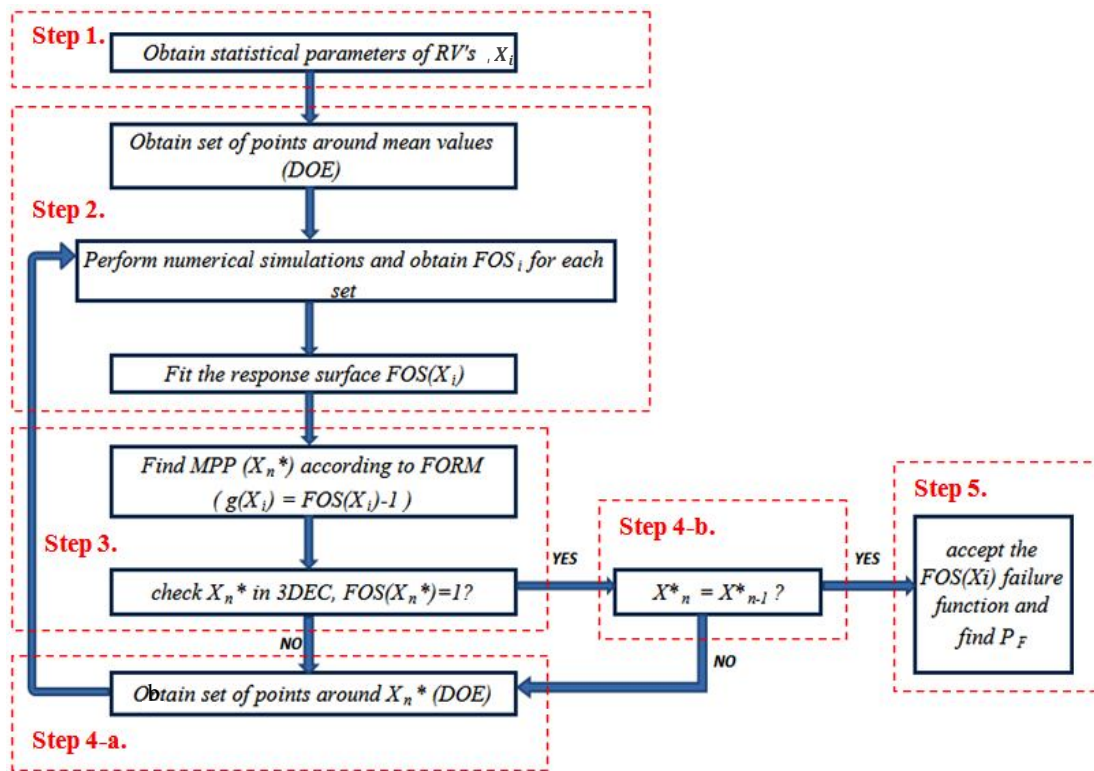
Figure 3.1 – The flowchart of the developed methodology.

Step 1: Any reliability analysis, in which the uncertainties in the parameters of the system are quantified, requires the statistical parameters of the random variables. According to the purpose of the study or sensitivity analysis of the system, the basic variables (X_i) that may affect the performance of a slope is determined. Once the deterministic and random parameters are decided, the statistical parameters of each random variable can be obtained according to the data of laboratory tests and field observations, as well as literature studies.

Step 2: In the next step the approximation of the FOS function is performed according to RSM. As it was mentioned before, the RSM tries to gradually converge to the real surface by iteratively fitting a number of equations for the selected sample points.

36

In the first iteration, the designing of the sample points is performed around the mean values of the random variables. For a quadratic response function, $2n + 1$ number of sample points is necessary to be able to calculate the coefficients of the Equation 2.23 (a_i, b_i, c_i). For instance, in a slope problem with two random variables, (X_1, X_2), five set of points are necessary (Table 3.1). Once the design of the points around mean is performed, each set is separately imported to the numerical simulation program (3DEC in this study) and the corresponding FOS is computed.

Table 3.1 – Design of the experiments around mean values of two random variables.

Set No.	1	2	3	4	5
X_1	μ_{X_1}	$\mu_{X_1} + \sigma_{X_1}$	$\mu_{X_1} + \sigma_{X_1}$	$\mu_{X_1} - \sigma_{X_1}$	$\mu_{X_1} - \sigma_{X_1}$
X_2	μ_{X_2}	$\mu_{X_2} + \sigma_{X_2}$	$\mu_{X_2} - \sigma_{X_2}$	$\mu_{X_2} + \sigma_{X_2}$	$\mu_{X_2} - \sigma_{X_2}$
FOS	FOS_1	FOS_2	FOS_3	FOS_4	FOS_5

Once the response of each set is obtained (FOS_i), the quadratic Equation (2.23) can easily be generated by calculating the coefficients. In this example (two variable case), the response function for the FOS in the region of mean points (first iteration) is:

$$FOS(X_1, X_2) = a_0 + b_1 X_1 + b_2 X_2 + c_1 X_1^2 + c_2 X_2^2 \tag{3.2}$$

Step 3: Since converging to a real surface by using the RSM is an iterative technique, it is important to figure out when the desired response is satisfied. In this study, in order to check whether the obtained $FOS(X_i)$ truly represents the performance of the corresponding slope, FORM is used.

Once the $FOS(X_i)$ is generated in step 2 in the region of the mean values, the limit state function of the slope is,

$$g(X_i) = FOS(X_i) - 1 \qquad\qquad\qquad (3.3)$$

According to FORM, the most probable point (X^*) of this limit state can be achieved. It is noted that due to the definition of FORM, the Most Probable Point (MPP) always locates on the limit state surface, $FOS(X^*) = 1.0$. Hence, in order to check the validity of the generated $FOS(X_i)$, the X^* is imported to 3DEC. If the obtained FOS in 3DEC is close to 1.0, the first condition of the methodology is fulfilled. Otherwise, the iteration is continued up to the level in which the obtained MPP (X^*) develop a value of $FOS(X^*) \approx 1.0$ in 3DEC.

Step 4-a: In order to continue the iteration levels, another set of sample points are required to be designed to define the new region in which $FOS(X_i)$ is fitted. The region in each new level is designed around the MPP of the previous level (X^*_{n-1}).

Step 4-b: Fulfilling the condition of $FOS \approx 1.0$ is not sufficient to confirm the validity of the approximated limit state function. The reason is that any point on the real limit state surface takes the value of $FOS = 1.0$. However, there is just one MPP on the real failure limit state function. On the other hand, the RSM is valid only for the local in which it is studied. Accordingly, the complete convergence only happens when the MPP determined in a subsequent level approach to the MPP in the preceding level. Therefore, the two conditions of the proposed methodology to be fulfilled are given as:

1) $FOS(X^*) \approx 1.0$
2) $X^*_n = X^*_{n-1}$

Figure 3.2 shows a schematic illustration of the methodology in a two variable problem. The origin of the axes represents the mean point of the random variables. The problem is converged in 6 levels to the target point, real MPP.
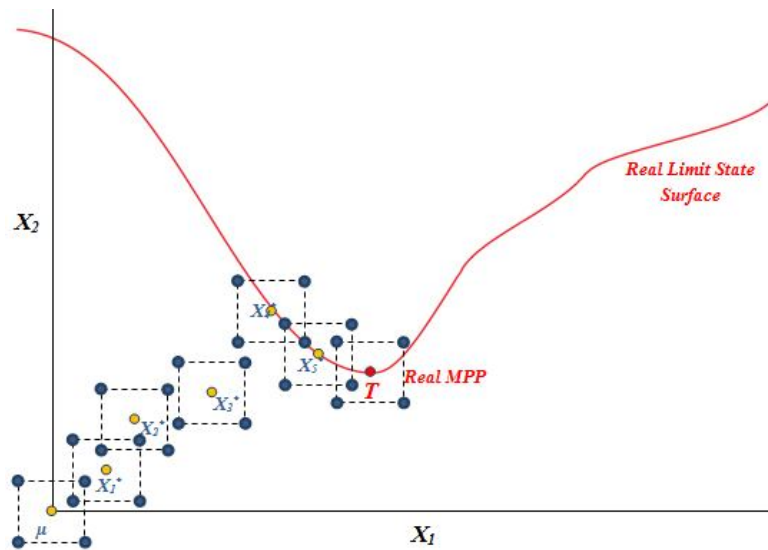
Figure 3.2 – Detection of real limit state surface due to RSM in a two random variable space.

Step 5: Once both of the conditions are fulfilled, the function of $FOS(X_i)$ in the last level can be accepted as a true approximation. Subsequently, the P_f of the slope under consideration is calculated according to FORM.

CHAPTER 4

IMPLEMENTATION OF THE PROPOSED APPROACH FOR A ROCK SLOPE IN SUMELA MONASTERY, TURKEY

4.1 Introduction

In order to examine the successful implementation of the methodology, it is applied to a selected hazardous rock slope in Sumela Monastery, Turkey. The Sumela Monastery is one of the major historical places of Turkey which hosts considerable number of tourists every year. Accordingly, the safety analysis of the slope is a fundamental issue in this region.

4.2 Study Area

The Sumela Monastery located in the Altindere National Park at Macka region of Trabzon city in Turkey, is a Greek Orthodox monastery dedicated to the Virgin Mary (Figure 4.1a). It was founded in AD 386 during the reign of the Emperor Theodosius I (375 - 395) by two priests from Athens, Barnabas and Sophronios (Miller 1968). The monastery had reached its final appearance by periodic enlargements and verifications during the sixth and thirteenth centuries (Wikipedia 2014). The structure of the monastery is constructed inside a steep rock cliff at a height of about 200 meters from

the toe of the cliff which is surrounded by the roads and settlements of the local citizens (Figure 4.1b and c). The Sumela Monastery is one of the major historical and touristic places of Turkey hosting around 180,000 local and foreign visitors every year (Gelisli et al. 2011).
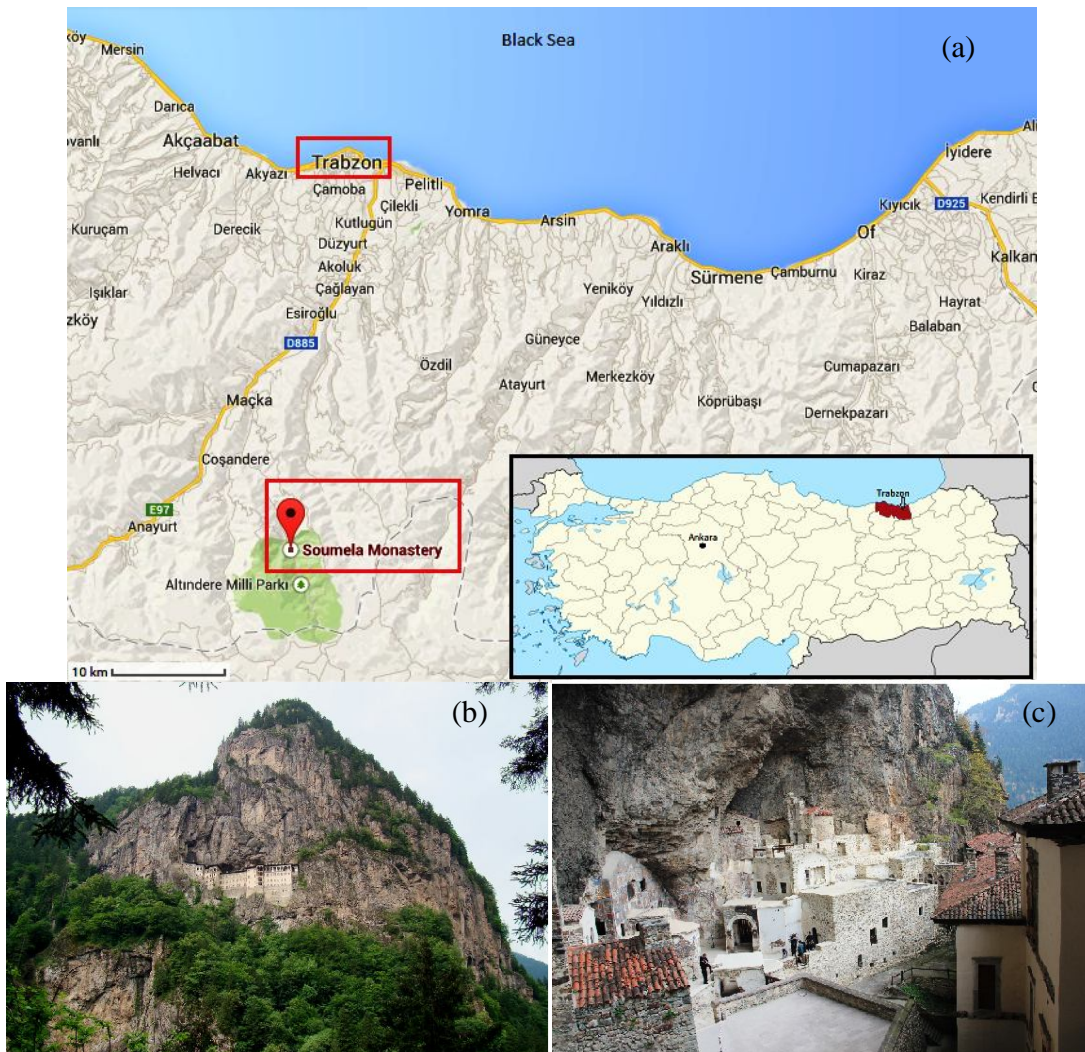
Figure 4.1 – (a) Location map of the Sumela Monastery, (b) Sumela Monastery located on a steep rock cliff, (c) structure of the Monastery caved inside the cliff.

The study area is located in the Northern Zone of the Eastern Pontide volcanic province on the Black Sea coast which is dominated by Late Cretaceous and Middle Eocene volcanics and volcaniclastic rocks (Gelisli et al. 2011). The formation of the Northern Zone consists of basaltic and andesitic lithic tuff, volcanogenic sandstone, shale, basaltic and andesitic lavas, and conglomerate deposited in a rift basin setting. The region evolved into a carbonate platform after the deposition of the Hamurkesen Formation as a result of a decrease in tectonic activity and filling of the rift basins, giving rise to the Berdiga Formation during the Late Jurassic-Early Cretaceous. Alluvial deposits formed of clay, silt, sand and gravel are widely displayed adjacent to the rivers in this region (Gelisli et al. 2011). Figure 4.2 illustrates the geological map of the study area.
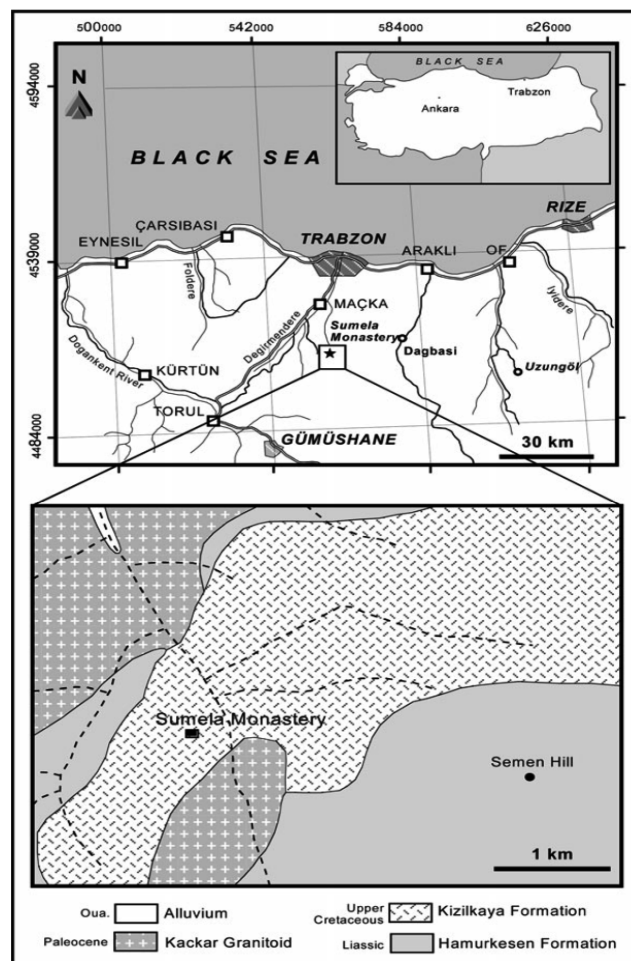
Figure 4.2 – Simplified geological map of the study area (Gelisli et al. 2011)

4.3 Field and Laboratory Studies

In order to investigate the stability problems in the region, the slope of the Sumela cliff is surveyed. Due to the geological structure of the cliff, the region is subjected to a high risk of slope instabilities. Considerable numbers of rockfall and slope failure evidences are observed around the cliff surface which proves the significance of stability analysis in the region. Figure 4.3a shows the damages of the plants and released rock blocks through a slope failure. Figure 4.3b illustrates a circular failure occurred on the highly weathered surface of the cliff. Figure 4.3c shows a large scale rock block detachments in the region. Figure 4.3d presents the damages of the pavements on the path to the monastery, due to rockfall hazards.

Figure 4.3 – Evidences of slope instabilities in the vicinity of Sumela Monastery.

In 2001, a hazardous rockfall event was reported causing damages to the monastery buildings and facilities. According to Gelisli et al. (2011), as it is show in Figure 4.4, the fallen blocks were detached from the crest of the cliff on top of the Monastery structure following a path toward the settlements.
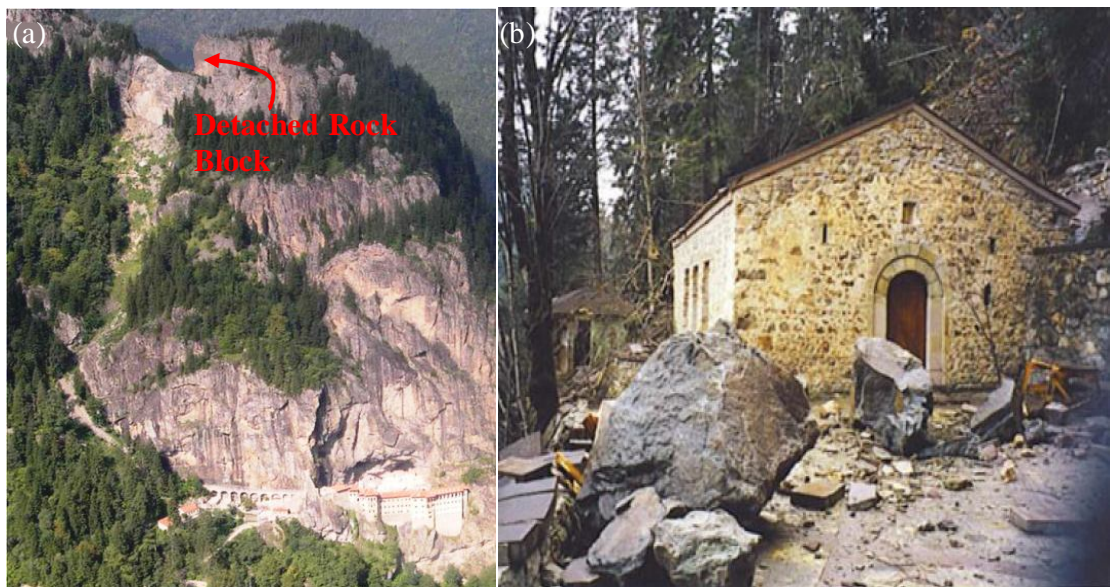
Figure 4.4 – (a) Location of detached rock block in 2001, (b) Rockfall event in 2001 (Gelisli et al. 2011)

According to the past evidences as well as field observations, a wedge failure is detected in the vicinity of the monastery which may threaten the structure as well as the downhill settlements. The potential wedge is marked in Figure 4.5. The rockfall event happened in 2001 had also been detached from the detected wedge. The wedge is highly fractured causing small block instabilities, potential to fall. More proofs of block detachments are obvious on the wedge even if they have not been reported. Therefore, in this study, it is tried to establish the probability of the wedge failure in the area based on the proposed methodology.

Figure 4.5 –Potential wedge failure and detached blocks from it.

In order to study the mechanical properties of the rock material, samples are collected to perform laboratory tests. Four uniaxial compressive tests and six Brazilan tests have been performed to define the Uniaxial Compressive Strength (UCS) and tensile strength of the rock respectively (Figure 4.6). The laboratory test results are listed in Table 4.1 and 4.2.
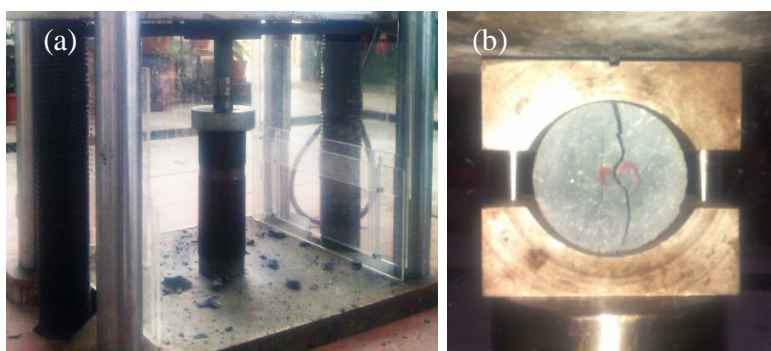
Figure 4.6 – (a) Uniaxial compressive test, (b) Brazilian test.

Table 4.1 - Results of uniaxial compressive test.

Sample No.	Diameter (mm)	Effective Area (mm^2)	Failure load (N)	UCS (MPa)
1	51.45	2077.975	511020	245.92
2	52.11	2131.63	472000	221.43
3	52.04	2125.907	482690	227.05
4	52.08	2129.176	461550	216.77

Table 4.2 – Results of Brazilian test.

Sample No.	Diameter (mm)	Height (mm)	Failure load (N)	Tensile strength (MPa)
1	51.97	30.48	35600	14.31
2	52.01	28.7	45450	19.39
3	51.86	29.31	36290	15.21
4	51.71	29.75	33400	13.83
5	52.17	30.58	38050	15.19
6	52.06	30.72	33110	13.19

The discontinuities of the study area are studied and the parameters are recorded. Generally, the discontinuities have rather wide aperture without infilling. This indicates that the study area is dealing with nearly large block sizes. Figure 4.7 shows typical rock blocks and discontinuities in the region.

Figure 4.7 – (a) Potential rock blocks, (b) Wide aperture of the discontinuities.

According to the surveyed geological parameters, the quality of the rock is classified based on Rock Mass Rating (RMR) system (After Bieniawski 1989). The results of the classification are given in Table 4.3, which indicates that the rock mass in the Monastery slope would be classified as fair rock. The table of the RMR is given in Appendix A.

Table 4.3 – Classification of rock mass based on RMR system.

	Parameter	Value	Rating		
1	UCS (MPa)	230	12	Friction Angle	25° - 35°
2	Rock Quality Designation, RQD (%)	40	8	Cohesion (KPa)	200 - 300
3	Spacing of discontinuities (m)	> 2	20		
4	Discontinuity length (m)	5 to 10	2	Class of the Rock	Fair Rock
	Separation (mm)	20 to 30	0		
	Roughness	smooth	1		
	Infilling	> 5 mm (soft)	0	Total RMR Rating	54
	Weathering	highly	1		
5	Ground water	damp	10		

Figure 4.8 illustrates the rock discontinuity distribution as well as the kinematic analysis of the region. According to this plot, two major discontinuity sets are detected and formation of wedge failure is clearly validated. Table 4.4 shows the statistical parameters of the discontinuity sets. The complete list of recorded discontinuity properties during field investigations are given in Table 4.5.
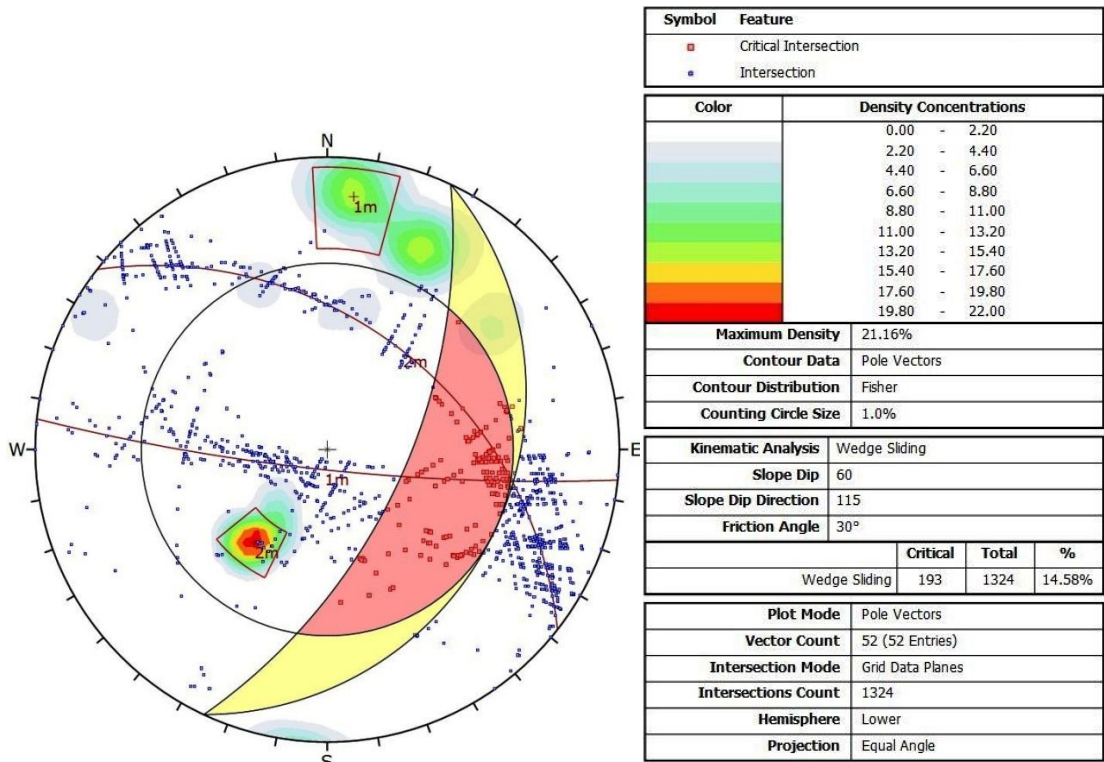
Figure 4.8 – Discontinuity distribution and kinematic analysis in the study region.

Table 4.4 – The discontinuity set properties in the study region.

Discontinuity set label	Mean Dip/Dip direction	Variability (99%)	Spacing (m)
1m	82.4 °/185.88 °	13.12 °	3.0
2m	43.8 °/38.5°	11.8°	5.0

Table 4.5 – Properties of the recorded discontinuities during field observations.

No.	Dip (deg.)	Dip Direction (deg.)	Rock Type	Schmidt Hammer	Aperture (mm)	No.	Dip (deg.)	Dip Direction (deg.)	Rock Type	Schmidt Hammer	Aperture (mm)
1	80	185	Basalt	51	3	26	75	235	Basalt	28	-
2	45	40	Basalt	58	2	27	80	185	Basalt	31	-
3	78	200	Basalt	53	5	28	40	290	Basalt	44	-
4	21	130	Basalt	48	5	29	80	120	Basalt	53	-
5	35	165	Basalt	38	5	30	85	180	Basalt	38	50
6	83	180	Basalt	56	10	31	85	187	Basalt	46	-
7	70	200	Basalt	49	15	32	75	190	Basalt	57	-
8	48	40	Basalt	48	15	33	65	155	Basalt	53	-
9	44	38	Basalt	52	10	34	90	300	Basalt	24	-
10	40	335	Basalt	36	20	35	65	235	Basalt	29	30
11	86	190	Basalt	50	5	36	83	191	Basalt	33	30
12	85	185	Basalt	42	5	37	47	225	Basalt	45	25
13	80	214	Basalt	54	1	38	70	205	Basalt	49	30
14	78	208	Basalt	47	1	39	47	45	Basalt	29	10
15	68	210	Basalt	39	-	40	48	175	Basalt	30	25
16	75	210	Basalt	46	10	41	60	160	Basalt	38	-
17	75	200	Basalt	26	15	42	70	230	Basalt	44	-
18	35	32	Basalt	37	10	43	45	49	Basalt	42	12
19	31	41	Basalt	30	10	44	42	37	Basalt	37	10
20	40	32	Basalt	44	-	45	55	195	Basalt	40	10
21	38	26	Basalt	50	-	46	50	190	Basalt	52	15
22	43	41	Basalt	38	50	47	26	52	Basalt	45	5
23	47	36	Basalt	24	60	48	45	39	Basalt	38	5
24	75	205	Basalt	32	50	49	34	33	Basalt	47	5
25	75	205	Basalt	36	50	50	26	40	Basalt	49	5

A simple schematic geometry of the wedge is sketched in Figure 4.9. The volume of the wedge is computed to be 10 million m^3 with a mass of 2.7 million tons.
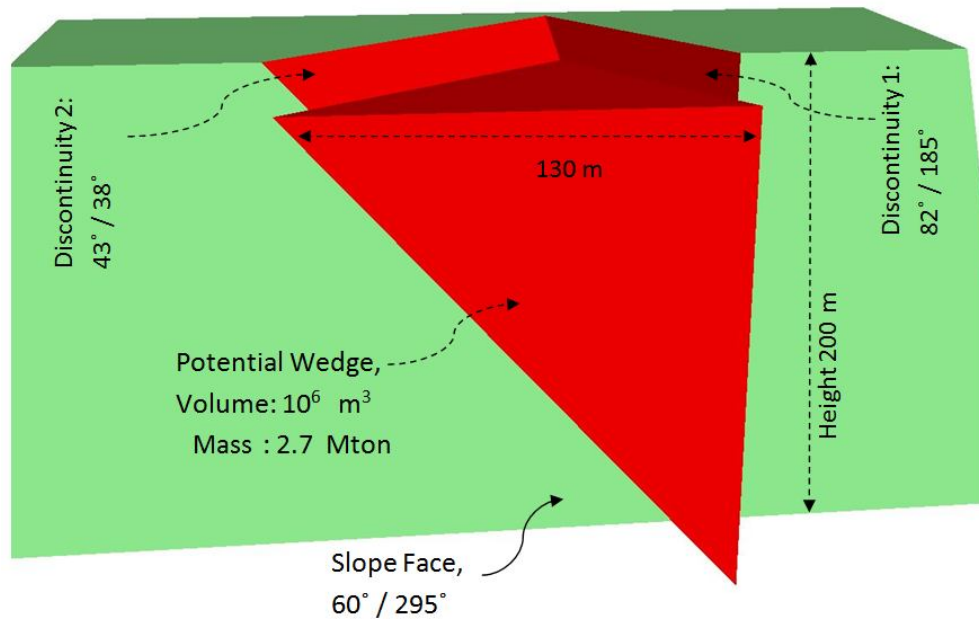
Figure 4.9 – schematic geometry of the wedge.

4.4 Implementation

Any simulation by 3DEC is performed in three fundamental steps,

1) Generating a model that represents the geometry of the problem,
2) Defining the material behavior and boundary conditions,
3) Results and interpretations.

The geometry of the slope is constructed considering the topographical conditions and field observations. Once the material behavior and boundary condition of the problem is assigned, and the model is brought to the initial equilibrium state, it is ready to be studied according to the proposed methodology. A sensitivity analysis is first performed to identify the random and deterministic parameters of the problem. Later, the P_f is calculated. This step is performed in two stages. First the response surface is generated according to the calculation of FOS and the corresponding P_f is obtained based on FORM. Then, in order to verify that the generated limit state function truly represents

the failure surface, the slope behavior is monitored and the results are discussed. The general procedure of the analysis is illustrated in Figure 4.10.
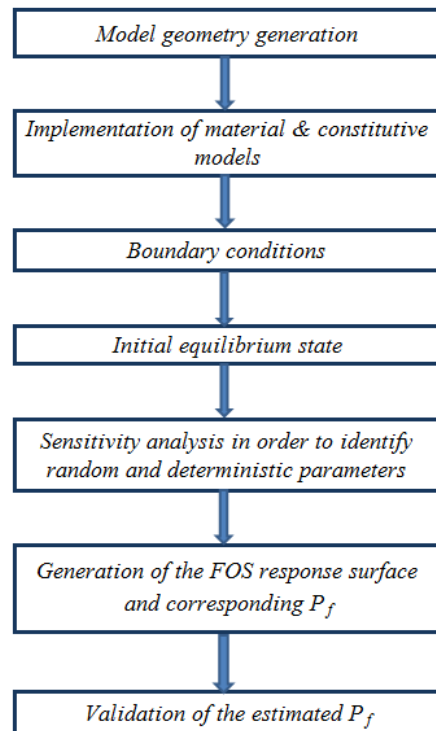
Figure 4.10 – Procedure of the calculation of P_f in the study area.

4.4.1 Geometry Generation

It is obvious that the accuracy of any simulation study depends on the equivalency of the generated model with real conditions of the problem under consideration. The geometry of the problem is one of the important factors of any simulation particularly in slope stability analysis. Recent improvements in model building tools of 3DEC provide a more realistic understanding of the problem. The geometry of a problem in 3DEC is created by cutting an original block in a way that the outcome represents boundaries of physical features in the problem. Previously, the original block was manually cut up to an approximate geometry to be obtained. However, it is now possible to generate any

desired geometry by modern techniques in 3DEC. Figure 4.11 illustrates the topography of the Sumela Monastery generated by conventional and modern building methods in 3DEC.
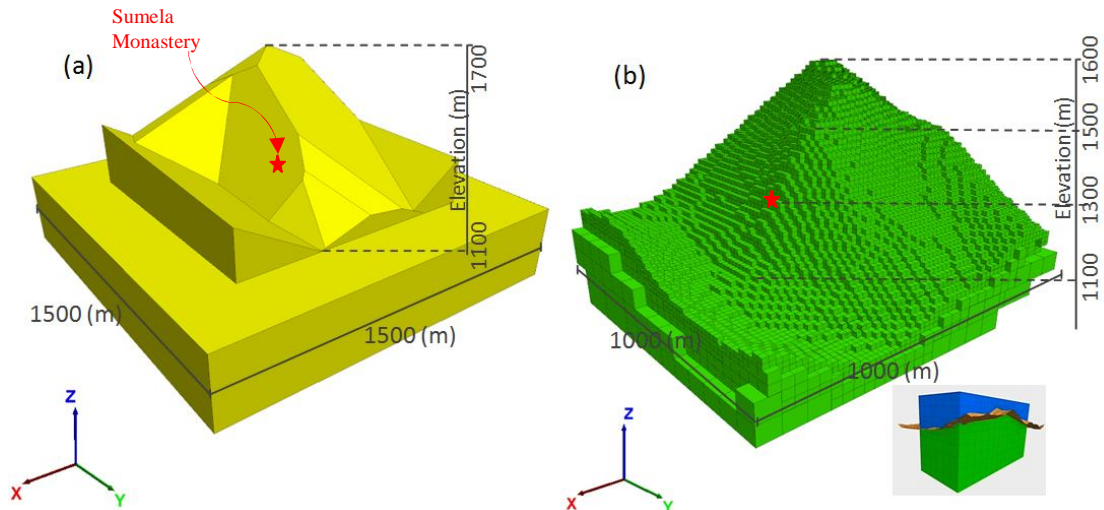
Figure 4.11 – Topography of Sumela monastery generated in 3DEC, (a) by manually cutting the original block, (b) by densifying the original block.

According to the new model building capabilities of 3DEC, any desired 3D geometry must first be created in a drawing program like AutoCAD, in the form of polygons. The geometry is then imported to 3DEC to cut the original block accordingly. The block is wisely divided into smaller pieces in a way that all the blocks that are touching the polygon surface have a higher resolution than the blocks away from the 3D surface. Once the block is divided, the upper pieces are deleted in order to achive a complete topography surface.

The geometry of the Sumela Monastery is created using SketchUp (2015) and Rhinoceros 5.0 tools. The topography is first obtained from SketchUp tool (Figure 4.12a). Later, it is imported to Rhinoceros 5.0 to create a 3D polygon surface (Figure 4.12b).
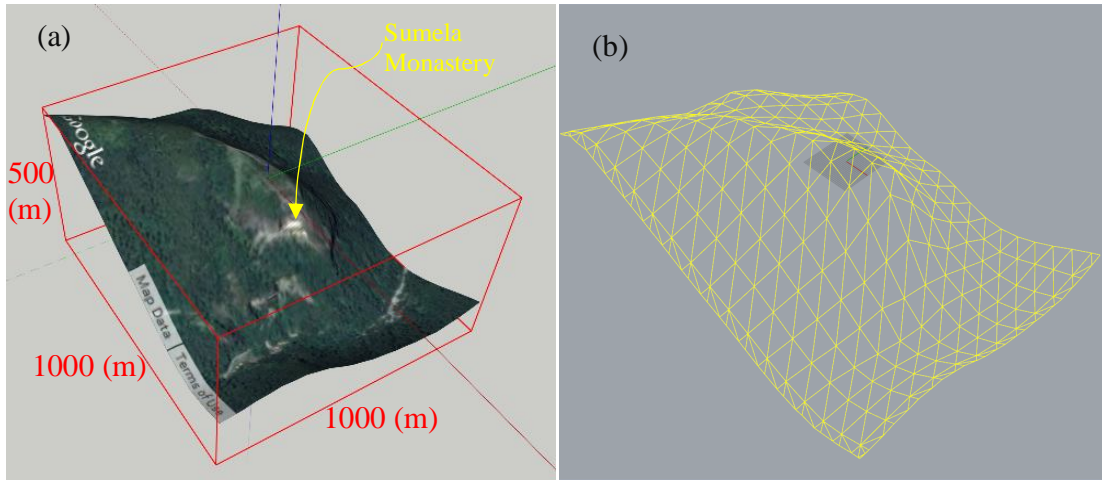
Figure 4.12 – (a) Topography of Sumela monastery created by SketchUp, (b) 3D polygon surface of the topography created by Rhinoceros 5.0.

The polygon geometry is then imported to 3DEC and the corresponding codes are established to merge and cut the original block with the imported geometry. Figure 4.13 shows how the final block model reasonably fits the topography surface.
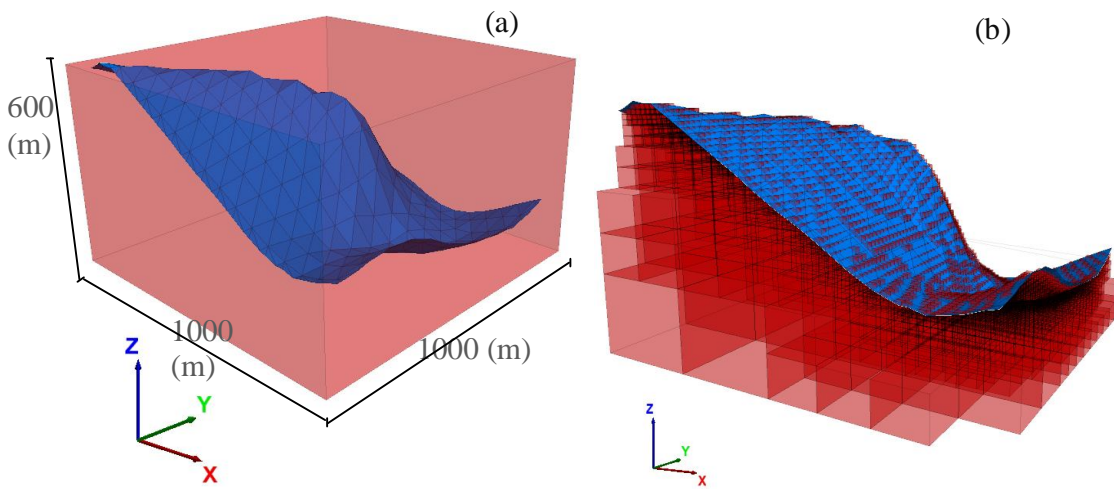
Figure 4.13 – (a) Topography of the Sumela Monastery merged by original block in 3DEC, (b) 3DEC block after cutting according to the topography.

In the next step, the surveyed discontinuity sets during the field studies are added to the model according to Table 4.4. Figure 4.14 indicates the final geometry of the concerning wedge in the Sumela Monastery.
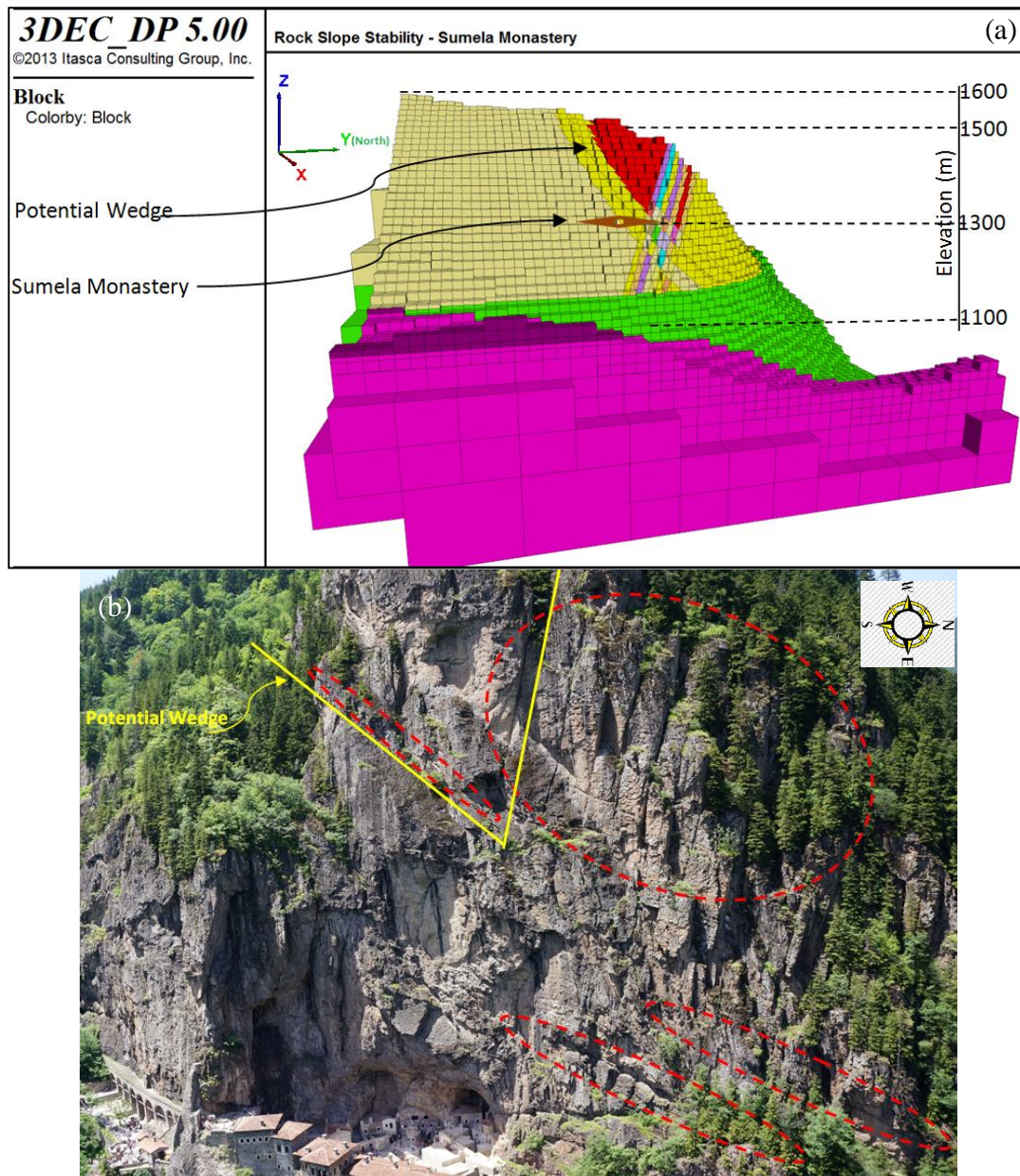
Figure 4.14 – (a) Final geometry of the study area developed in 3DEC, (b) Discontinuity sets and potential wedge in the study area.

4.4.2 Material Properties and Boundary Conditions

According to Anon (2013), when the problem is dealing with unconfined set of hard rock blocks at low stress level, such as shallow slopes in jointed rock where the movements consist mainly of sliding and rotation of blocks, it is reasonable to assume the infinite material rigidity in order to let the discontinuities dominate the problem. Accordingly, since the study area is comprised of unconfined hard basaltic rock blocks (Gelisli et al. 2011), the behavior of the intact material is assumed to be rigid rather than deformable. This let the model be mainly governed by the joints and discontinuities, which reflects the observed behavior in the field.

In order to dictate the type of response, the model displays under the applied in-situ conditions or upon any disturbance, the constitutive behavior and associated material and discontinuity properties must be introduced to the model. As it was discussed before, 3DEC provides four intact material models and two discontinuity models. According to Anon (2013), apart from special cases and purposes, the Mohr-Coulomb plasticity model is well suited for intact materials that yield when subjected to shear loading like rock and soil. Anon (2013) also states that among two predefined discontinuity constitutive models of 3DEC, the Coulomb slip model is most applicable for general engineering studies; while the continuously yielding joint model is applicable in dynamic analysis and cyclic loading. Consequently, the intact rock and discontinuity constitutive behavior of the wedge block under consideration is simulated with Mohr-Coulomb model and Coulomb slip model, respectively.

Since it was not possible to have reasonable number of experiments during this investigation, the final properties of the intact rock and discontinuities are prescribed by considering the values of the laboratory tests, RMR classifications, RocLab software and the literature review. The values of cohesion and friction angle obtained from different sources are listed in Table 4.6.

Table 4.6 – Cohesion and friction angle obtained from different approaches.

	Cohesion (MPa)	Friction angle
RMR	0.2 - 0.3	25-35
RocLab	2.9	47
Tilt test	-	38
literature	4.5	30

Based on the field observations, the discontinuities have wide aperture on the surface. However, considering the high value of the mass of 2.7 million tones, it is expected that the cohesion of the discontinuities will increase by depth as moving inside the slope and causes a high variability along the discontinuities of the wedge. Hence, the low values of cohesion obtained from RMR and Roclab may not be able to represent the reality. The RMR classification system provides the parameters of the rock mass. While in this study, the wedge is assumed to be intact created by intersection of two discontinuities. On the other hand, based on four triaxial tests, the results of the cohesion and friction angle of the intact rock are obtained close to the literature values. Consequently, the literature values of the intact rock and discontinuity properties are considered in this study (Kainthola et al. 2014; Schultz 1993). Table 4.7 indicates the properties considered as input parameters during the simulations. The results of triaxial tests are shown in Appendix B.

Table 4.7 – Intact rock and discontinuity properties considered during the simulations.

Material	Cohesion (MPa)	Friction angle	Tensile strength (MPa)	Young's Modulus (GPa)	Poisson's ratio	Normal Stiffness (GPa/m)	Shear Stiffness (GPa/m)
Intact rock	71	31	15	73	0.25	_	_
Disc. set	4.5	30	_	_	_	30	12

The boundary and initial condition in numerical simulations is the prescription of a constraint or controlled condition along a model boundary due to specified displacement, velocity or force to define the in-situ state of the problem. In this study, the gravitational acceleration is assigned in the negative z-direction and no outer loads are considered. The boundary condition is assigned in a way that the boundary blocks of the potential wedge are prevented from moving in order to better understand the behavior of the wedge.

4.4.3 Initial Equilibrium State

The 3DEC model must be at an initial force-equilibrium state before any simulation. The model is in equilibrium when the net nodal force vector at each centroid of rigid blocks, or gridpoint of deformable blocks, is zero (Anon 2013). The maximum nodal force vector is called the "unbalanced" or "out-of-balance" force. For a numerical analysis, the out-of-balance force never reaches exactly zero. However, it is sufficient to say that the model is in equilibrium when the maximum out of balance force is small compared to the total applied forces in the problem. During execution, inspection of maximum unbalanced force along with velocity and displacements can assess when the equilibrium has been reached.

In this study, before assigning the real material properties, a high value of cohesion and tensile strength is assigned to the model to prevent any slip or separation from occurring when the model in brought to an initial force-equilibrium state. In order to ensure that the model has reached to equilibrium, the history of maximum unbalanced force, vertical velocity (z-velocity) and total displacement is recorded and continuously monitored. The codes of 3DEC for the initial equilibrium state are listed in Appendix C. Figure 4.15 to 4.17 illustrate the plots of maximum unbalanced force, Z-velocity and total displacement respectively.
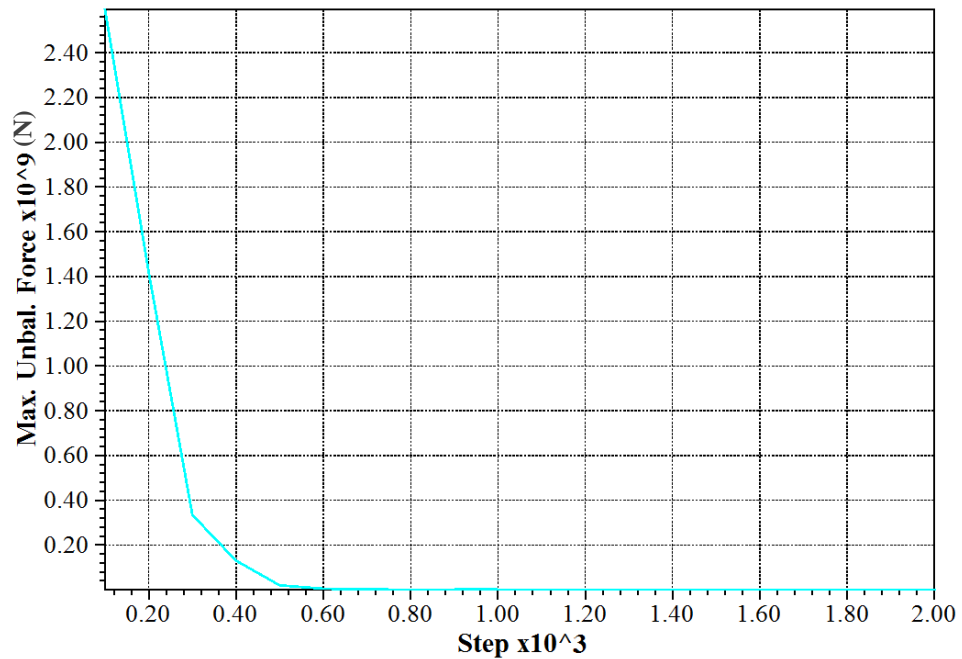
Figure 4.15 – History of maximum unbalanced force during equilibrium state.
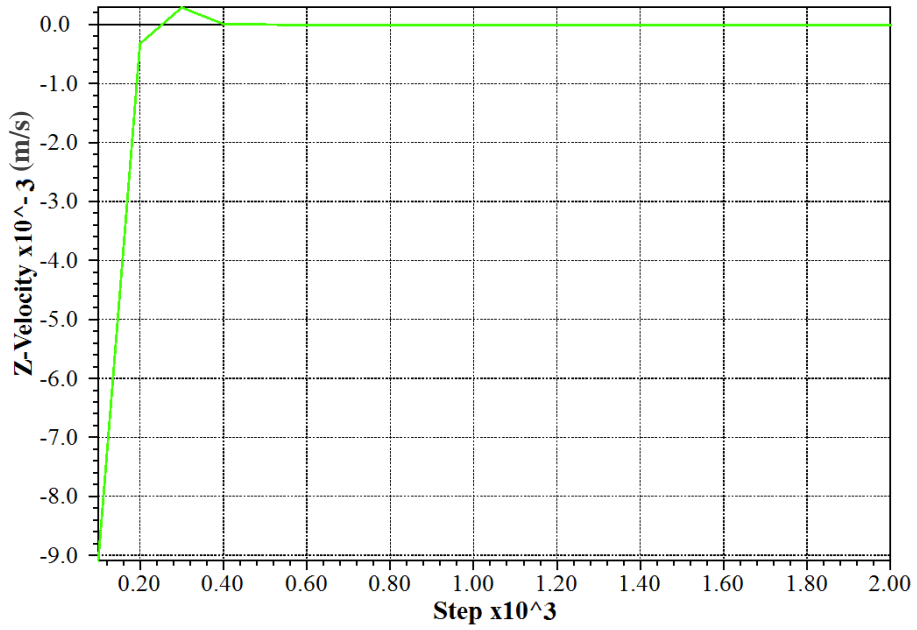
Figure 4.16 - History of vertical velocity during equilibrium state.
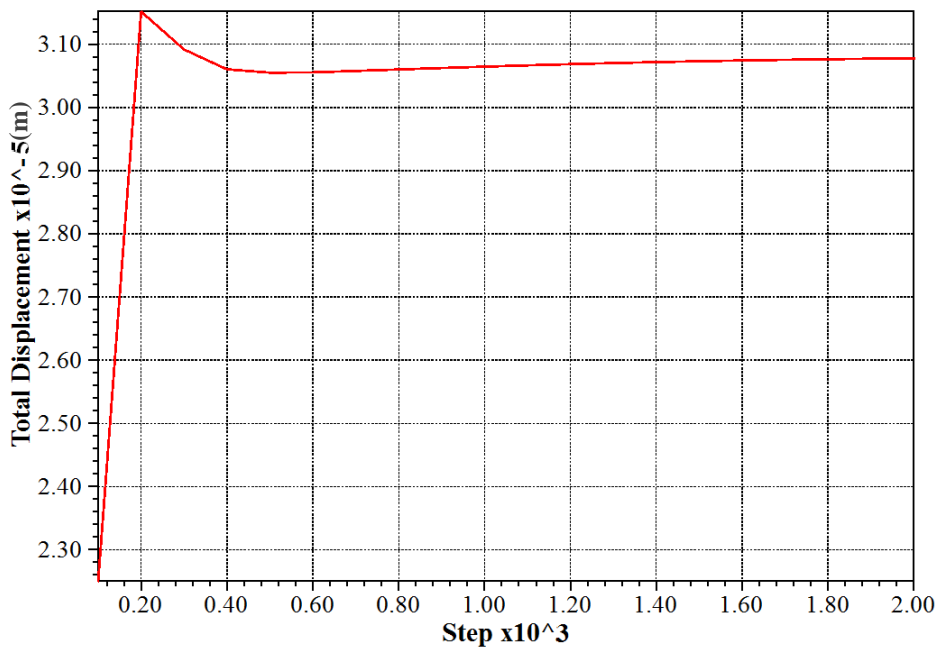
Figure 4.17 - History of maximum unbalanced force during equilibrium state.

According to Figure 4.15, it can be seen that the maximum unbalanced force has approached zero. Figure 4.16 illustrates the blocks in resting condition after 2000 steps. Moreover, history of total displacement in Figure 4.17 indicates that the block has slightly moved until reaching to equilibrium and kept a constant magnitude and stayed stable. This approves that no movements or slip occurrs within the model.

4.4.4 Sensitivity Analysis

According to Shen and Abbas (2013), it is important to note that both numerical and statistical studies demand a high calculation time and expenses. Hence, reducing the number of random variables, which may have negligible effect on model response, can considerably increase the efficiency. Prior to start the main simulations to estimate the P_f of the wedge, in order to define the deterministic and random input variables, a sensitivity analysis is performed to investigate how the uncertainty in each parameter may affect the FOS.

All the mechanical parameters of intact rock and joint sets are assumed to be random at initial step. In order to have a better understanding of uncertainty influence imposed by each variable, a constant coefficient of variation (C.O.V.) of 0.5 is implemented to all random variables. 25 models are run in 3DEC. In each set of models, the concerning random parameter is repeatedly verified while other parameters are kept constant in mean values and the corresponding FOS is recorded. Table 4.8 indicates the results of simulations. It is important to note that these simulations are only performed in order to decrease the number of random variables if they show a deterministic behavior and do not represent any understanding of the slope behavior.

Table 4.8 – Results of FOS with different values of material and joint properties.

C.O.V = 0.5		μ - 2σ	μ - σ	μ	μ + σ	μ + 2σ
Joint Cohesion (MPa)	Parameter	0	2.25	4.5	6.75	9
	FOS	0.16	1.48	2.93	4.38	5.21
Joint Friction Angle	Parameter	0°	15°	30°	45°	60°
	FOS	2.86	2.92	2.93	2.95	2.99
Joint Normal Stiffness (GPa/m)	Parameter	0	15	30	45	60
	FOS	0.78	2.26	2.93	3.33	3.49
Joint Shear Stiffness (GPa/m)	Parameter	0	6	12	18	24
	FOS	4.18	3.49	2.93	2.53	2.26
Block Cohesion (MPa)	Parameter	0	35.5	71	106.5	142
	FOS	2.93	2.93	2.93	2.94	0.94
Block Friction Angle	Parameter	0°	14°	28°	42°	56°
	FOS	2.93	2.93	2.93	2.93	2.93

Since the model is generated in rigid form, the discontinuities are mainly governing the problem rather than the intact rock blocks. It is revealed that the variability in discontinuity cohesion, normal stiffness (K_n) and shear stiffness (K_s) have the highest influence on FOS respectively (Figure 4.18). According to this investigation, it is reasonable to consider deterministic behavior for the rest of the parameters. Once the deterministic and random variables of the problem are defined, the model is ready to estimate the P_f according to the proposed methodology. The statistical parameters of the random variables are given in Table 4.9.
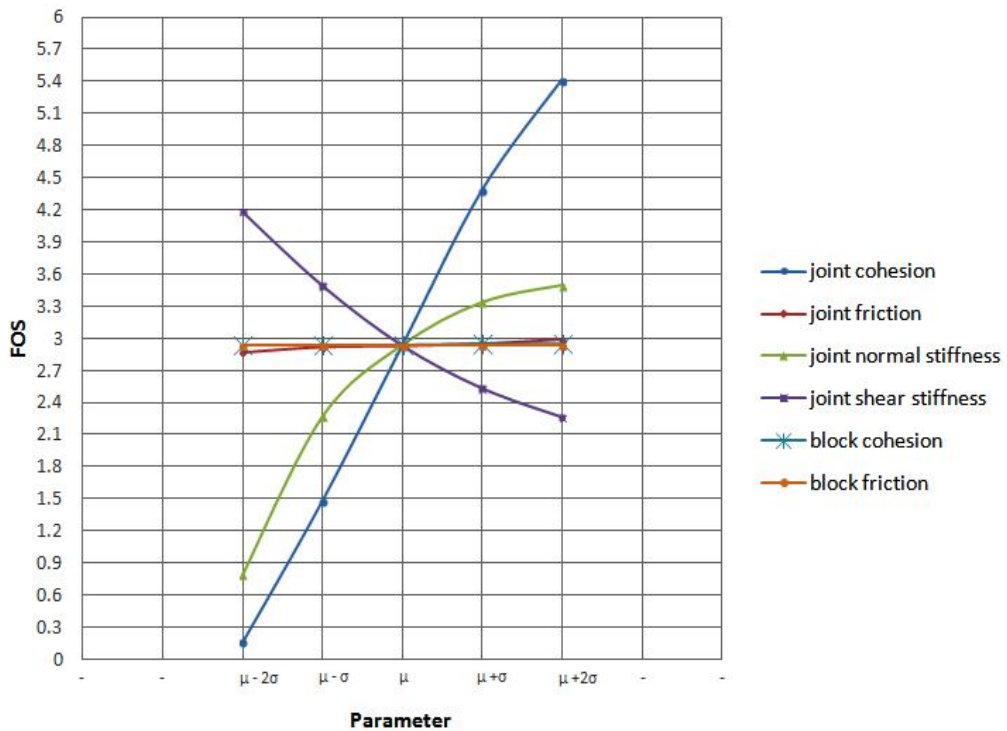
Figure 4.18 – Sensitivity analysis of FOS to the uncertainty in material properties.

Table 4.9 – Statistical parameters of the random variables.

Parameter	Discontinuity cohesion, JC (MPa)	Discontinuity normal stiffness, K_n (GPa/m)	Discontinuity shear stiffness, K_s (GPa/m)
Mean	4.5	30	12
Standard Deviation	1.8	9	2.4
Distribution	normal	normal	normal

4.4.5 Reliability Analysis

Once the model has been generated and brought to equilibrium, the proposed methodology can be implemented on the model in order to estimate the P_f. The main function of the methodology is to systematically define set of random material properties to 3DEC and obtain the corresponding FOS to generate the response surface accordingly. In order to converge to the true response surface of FOS, a number of iterations may be required.

The response surface of FOS must be adjusted around the mean values of the random variables at the initial iteration. For this purpose, the set of input points around the mean must be designed (DoE). Since this study consists of three random variables ($n = 3$), seven sets of points are necessary for each iteration ($2n + 1$). Once the set of input parameters are defined, each set is simulated in 3DEC and the corresponding FOS is obtained. Table 4.10 indicates the results of simulations around the mean values of random variables.

Table 4.10 – Design of points around mean and corresponding FOS.

Parameter	point 1	point 2	point 3	point 4	point 5	point 6	point 7
X_1 (JC), (MPa)	4.5	6.3	2.7	2.7	2.7	2.7	6.3
X_2 (K_n), (GPa/m)	30	39	21	39	39	21	21
X_3 (K_s), (GPa/m)	12	14.4	14.4	14.4	9.6	9.6	14.4
FOS	2.93	4.22	1.45	1.82	2.04	1.7	3.35

The design of points around the mean value is also plotted in Figure 4.19. It is clear that the points are systematically selected according to the DoE rules following a cubic pattern. However, six points around the mean is sufficient for this study to generate the response function of FOS.
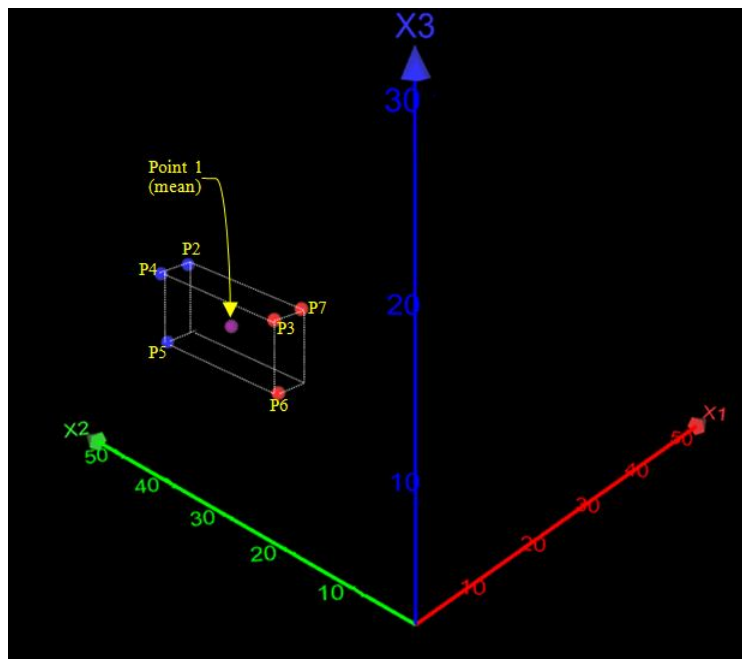
Figure 4.19 – 3D plot of sample points around the mean value in iteration 1.

65

According to equation 2.18, for three random variables, seven coefficients must be calculated to generate the response surface function of FOS. The coefficients can easily be obtained by solving seven equations with seven unknowns based on seven 3DEC simulations listed in table 4.9. Consequently, the response function of FOS for the first iteration is,

$$FOS(X_1, X_2, X_3) = (0.649) + (1.953*X_1) + (-0.445*X_2) + (0.509*X_3) +$$
$$(-0.143*X_1^2) + (0.008*X_2^2) + (-0.023*X_3^2) \qquad (4.1)$$

Therefore, the failure limit state surface for the first iteration can be written as,

$$g(X_1, X_2, X_3) = FOS(X_1, X_2, X_3) - 1 =$$
$$(0.649) + (1.953*X_1) + (-0.445*X_2) + (0.509*X_3) + (-0.143*X_1^2) +$$
$$(0.008*X_2^2) + (-0.023*X_3^2) - 1 \qquad (4.2)$$

Once the limit state failure function is generated, the FORM can be performed to find the most probable point (X_i^*). According to the methodology, the response function of FOS and corresponding failure limit state $g(X_i)$ is accepted when obtained design point illustrates a FOS close to 1.0 in 3DEC. Table 4.11 lists the results of design point in the first iteration and corresponding FOS in 3DEC. It is obvious that the iteration must be continued until the first condition of the methodology is satisfied in 3DEC ($FOS(X_i^*) \cong$ 1.0).

Table 4.11 – The most probable point and corresponding FOS in the first iteration.

X*			FOS (X*)
X_1^*	X_2^*	X_3^*	
3.85	28.3	12.6	2.72

Similarly, the iterations are continued by designing the input sets around the most probable point (design point) of the previous iteration (X_{n-1}^*). After pursuing 10 iterations, FOS converged to the desired condition ($\cong$ 1.0). However, as it has been

discussed before, any point on the failure function takes a value of $FOS \cong 1.0$. Since the RSM is locally valid, the true region must also be verified. This is obtained by satisfying the second condition of the methodology $(X_n^* = X_{n-1}^*)$. The second condition has been achieved by continuing two more iterations. All the results of the simulations are given in Appendix D.

The final failure function is obtained as,

$$
\begin{aligned}
g(X_i) = \\
(5.124) + (-0.073 * X_1) + (0.682 * X_2) + (-1.758 * X_3) + (0.147 * X_1^2) + \\
(-0.016 * X_2^2) + (0.066 * X_3^2) - 1 \qquad\qquad (4.3)
\end{aligned}
$$

Subsequently, by performing the FORM on equation 4.3, P_f of the wedge is computed as 0.163. The wedge is also modeled in Swedge 6.0 and probabilistic analysis is performed. The P_f is obtained to be 0.0984. It is observed that the Swedge software underestimates the P_f in comparison with 3DEC. Figure 4.20 shows the probability distribution of FOS obtained from Swedge modeling. The results of the simulations in Swegde are listed in Table 4.12. The challenging issue in reliability analysis of rock slopes is the lack of acceptable values of P_f (Duzgun and Bhasin 2008). A FOS of 1.3 to 1.5 is widely considered as an acceptable range in engineering practice. However, there is not a certain acceptable range for reliability studies in literature. Hence, in order to evaluate the safety of the studied slope, the P_f is compared with similar reliability studies of rock slopes in the literature. Generally, the studies are dealing with very low P_f of 10^{-3} orders. Accordingly, the P_f of 0.163 indicates a high hazard potential in this region.

Table 4.12 – Results of probabilistic simulation by Swedge.

No. of simulations	Mode of failure	FOS				P_f
		Mean	Standard deviation	Minimum	Maximum	
10000	Sliding on Joints 1&2	1.504	0.453	0.464	4.558	0.0984
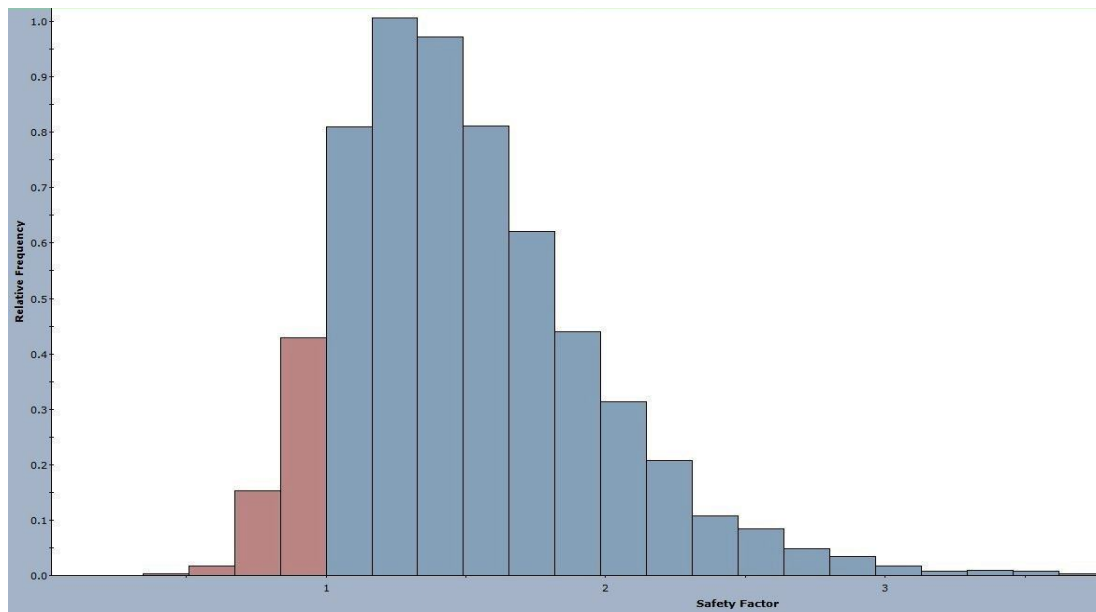
Figure 4.20 – Probability distribution of FOS obtained from Swedge.

4.4.6 Validation

In order to confirm the validation of the converged function of FOS, the response of the model is monitored in the center point of each iteration by plotting the z-velocity, displacements, and unbalanced force histories. It is revealed that the slope shows a steady state when the iterations are in the safe region, while by converging to the failure surface according to the RSM, the slope starts to fail in 3DEC as well.

Figure 4.21 illustrates the vertical velocity plots of iteration one and twelve. It is shown that, at the centerpoint of iteration one, where the FOS is calculated to be 2.93, the velocity of the slope follows almost constant rate of increasing due to the execution of the model; while by approaching to the failure surface, at the centerpoint of iteration twelve, a sudden increase in the z-velocity occurs after 14000 steps. Due to Anon (2013), any sudden increase in displacement or velocity of a model indicates a joint slip or block failure or plastic flow within the model.

68
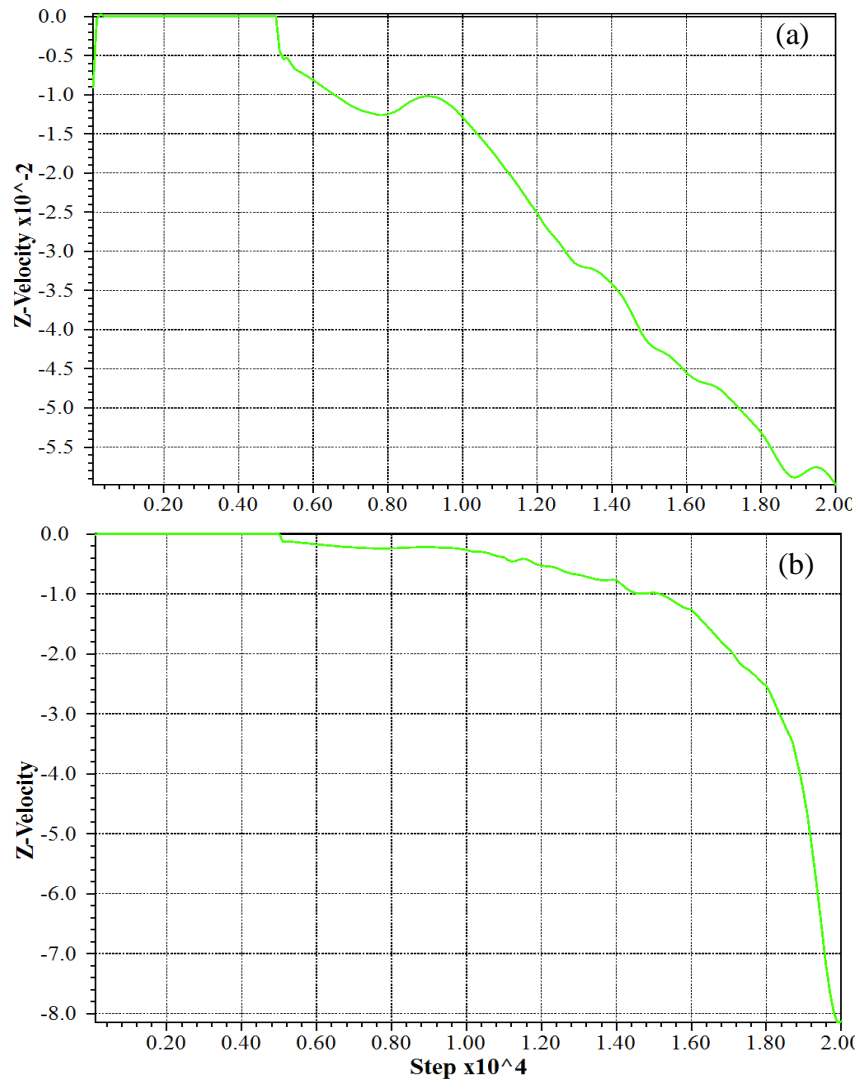
Figure 4.21 - History of vertical velocity in the centerpoint of (a) iteration one, (b) iteration twelve (m/s).

Moreover, according to the maximum unbalanced force plots illustrated in Figure 4.22, no instability conditions are observed in iteration one. The unbalanced force follows a constant value which indicates a constant movement within the model. However, iteration twelve shows a large force imbalance in the model after 16000 steps.
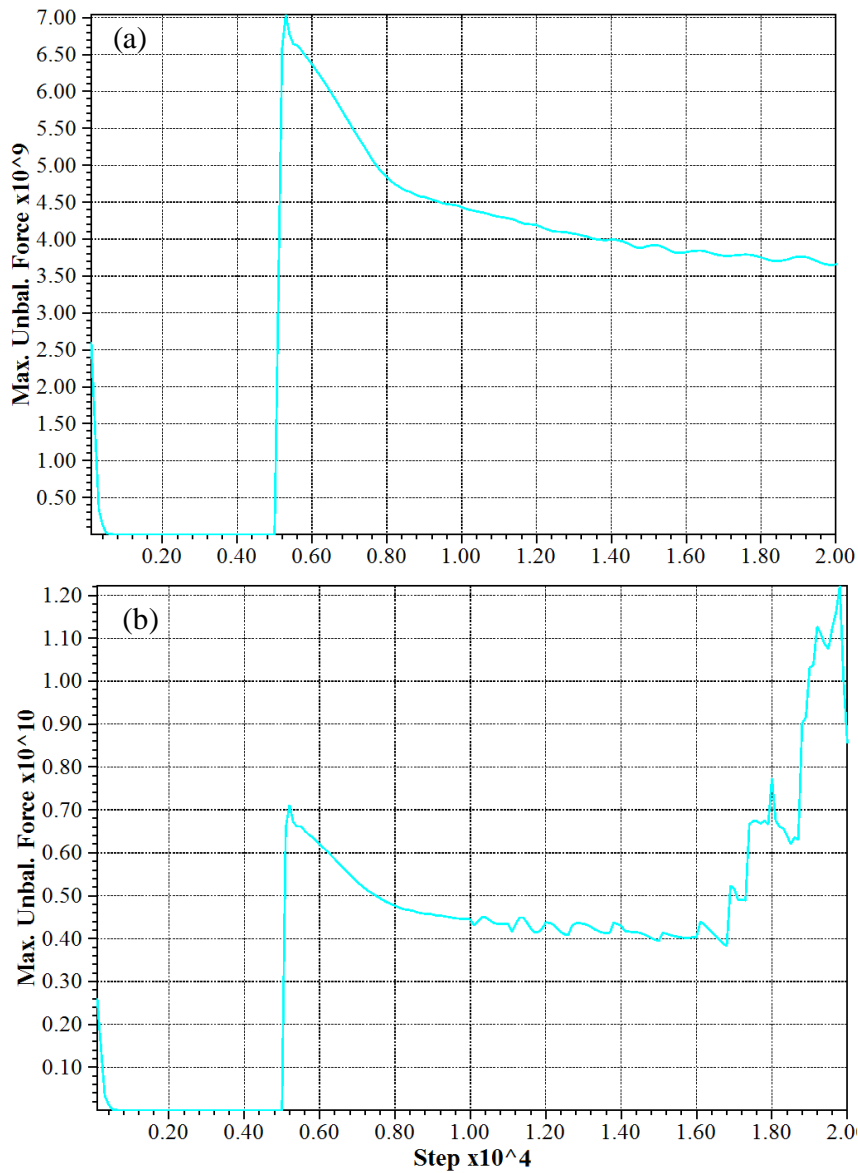
Figure 4.22 - History of maximum unbalanced force in the centerpoint of (a) iteration one, (b) iteration twelve (N).

Figure 4.23 illustrates the total displacement plots of iteration one and iteration twelve. It is obvious that the maximum total displacement is increased by approaching to the failure surface.

70
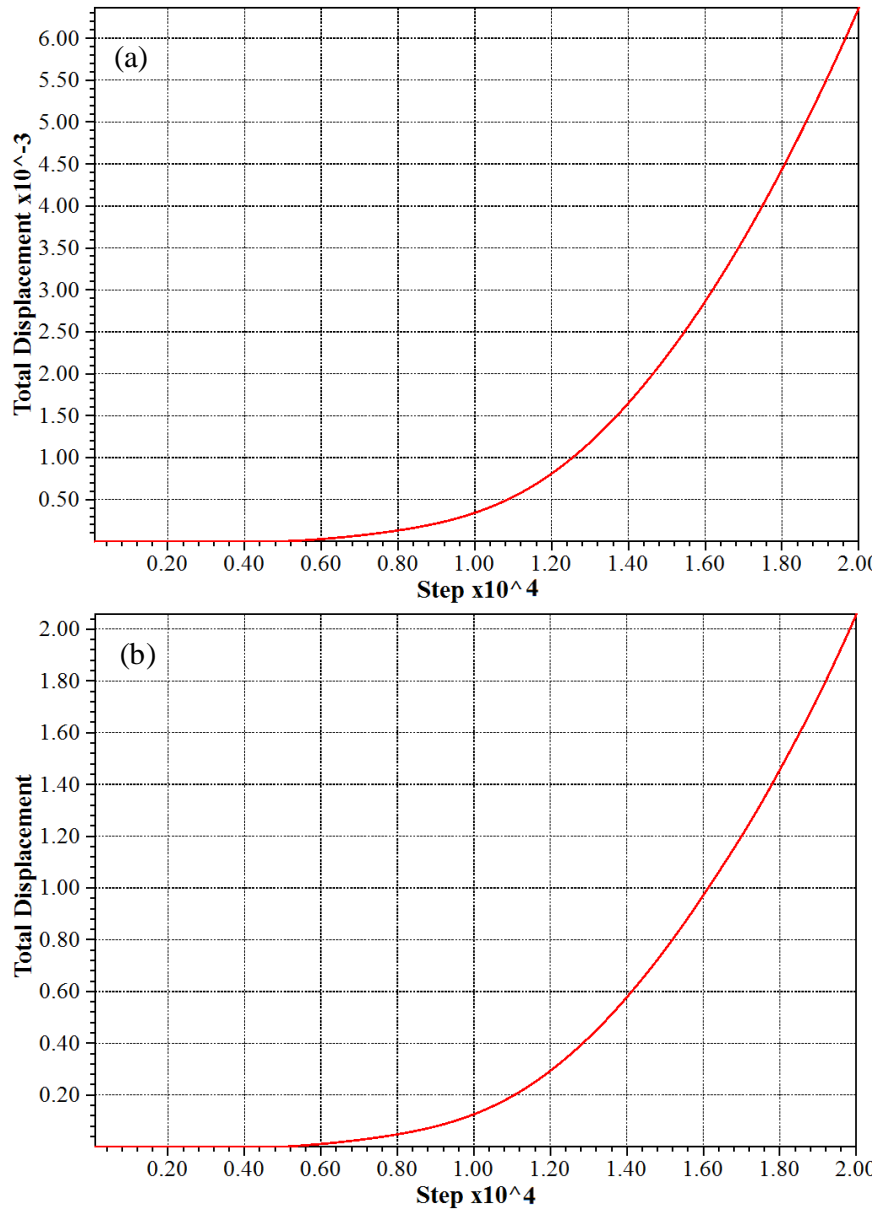
Figure 4.23 - History of total displacement in the centerpoint of (a) iteration one, (b) iteration twelve (m.).

The displacement vectors of the potential wedge in iteration one and twelve are shown in Figure 4.24. It is clear that the maximum total displacement occurs at the toe of the wedge which has good compatibility with site observations where evidances of fallen blocks exist. All the results of the history records are listed in Appendix E.

71
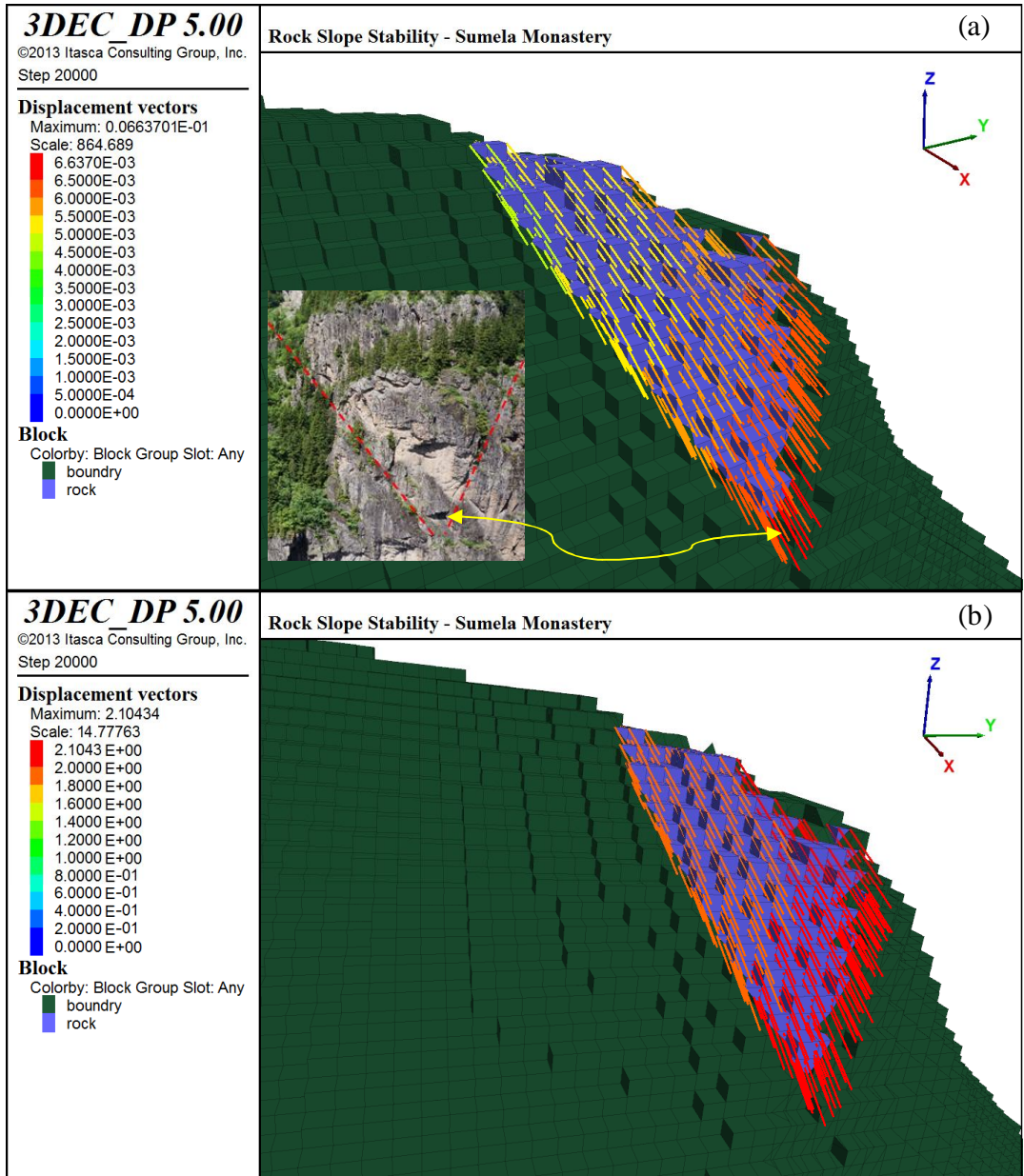
Figure 4.24 – Displacement vectors of the potential wedge failure in the centerpoint of (a) iteration one, (b) iteration twelve (m).

Figure 4.25 illustrates the maximum vertical velocity in centerpoint of each iteration and corresponding FOS. It is clear that, by converging to the failure region, vertical velocity increases. Slope instability is quite obvious by the sudden increase in the vicinity of the limit state failure region where FOS is almost 1.0.

72
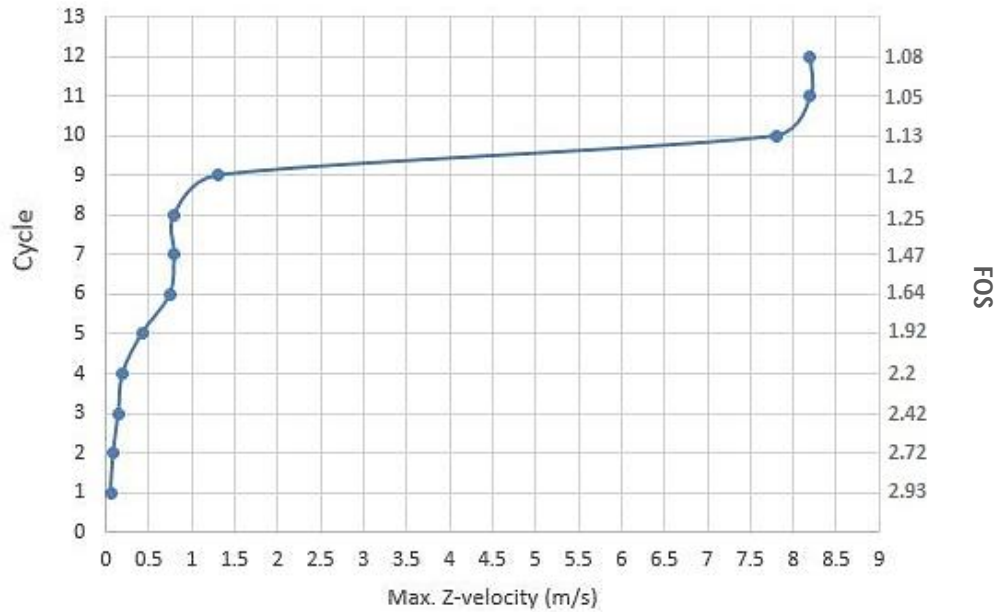
Figure 4.25 – Maximum vertical velocity in centerpoints vs. iteration number and FOS.

Similarly, Maximum total displacement graph is shown in Figure 4.26. The total displacements of the wedge block increases by converging to the failure surface. It can be stated that, in cases where such a large wedge with volume of 10 million m^3 is under concern, even low displacements of centimeters means a high hazard which can cause uncontrollable failure. According to Figure 4.26, the wedge shows unstable condition after 10 centimeters. By installing displacement monitoring systems in the study region, this graph can be very useful to understand in what rates of displacements the wedge is in critical conditions.
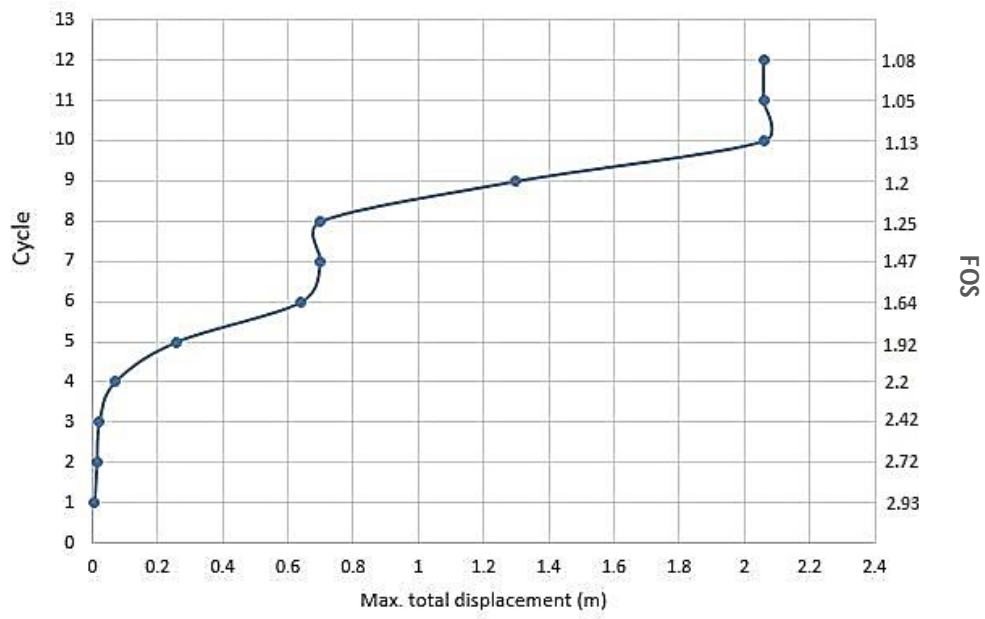
Figure 4.26- Maximum total displacement in centerpoints vs. iteration number and corresponding FOS.

CHAPTER 5

DISCUSSIONS AND CONCLUSIONS

In this Thesis, a method to analyze reliability of rock slopes using the response surface method is developed. The rock slope is modeled and analyzed by a three dimensional distinct element code, 3DEC. The numerical simulation which is usually expensive is repeated a limited number of times to give point estimates of the response of FOS corresponding to uncertainties in the model parameters. A graduating function is then fit to these point estimates so that the response given by the 3DEC code can be reasonably approximated by the graduating function within the region of interest. The approximating function, called the response surface, is used to replace the code in subsequent repetitive computations required in a reliability analysis. The procedure is applied to a large potential wedge in rock slope in Sumela monastery, Turkey, involving uncertain discontinuity properties.

The potential wedge is located at height of about 200 meters from the toe of the cliff with volume of about 10^6 m^3. Rockfall evidences on the wedge prove the instability hazard in the vicinity. The P_f of the wedge is calculated to be 16.3% by 84 simulations in 3DEC based on proposed methodology. Comparing this P_f by similar probabilistic rock slope stability studies in literature, this amount indicates a high hazard of failure in the region. The model is also created in Swedge program and probabilistic analysis is performed. The P_f is found to be lower (9.8%) by Swedge. On the other hand, the behavior of the slope is monitored in each simulation. It is concluded that by converging

to the limit state surface, slope instabilities occur inside the model and cause increase in total displacements and vertical velocity. It is also revealed that after about 10 cm of displacement, the slope represents a critical uncontrollable situation. Considering the P_f obtained by the proposed methodology and MCS by using Swedge, the slope shows quite a low level of safety which indicates the requirement of mitigation measures.

The MCS method is one of the widely probabilistic methods used for calculation of P_f. However, this method is applicable only when acceptable number of observations is provided. Generally, the number of experiments in MCS method is in orders of 10^3. This value becomes quite challenging as the state-of-the-art simulation codes get more sophisticated. Alternatively, the P_f of the concerning wedge is calculated by 84 number of experiments using RSM. It is shown that, by using the RSM, the behavior of the FOS can wisely be defined. Once the function of the FOS is obtained, the FORM can easily be performed to estimate the P_f. it is shown that the estimation of the P_f of the potential wedge according to the proposed methodology is performed within 10% of the number of simulations based on a direct MCS (e.g. assuming 1000 experiments for MCS).

Another advantage of the proposed methodology is that, a function can be defined to the FOS based on any desired effective parameter. Other probabilistic tools like MCS cannot provide a characteristic equation to the system. A function which can describe the stability quality of a slope based on effective parameters is quite applicable in designing practices. Generally, in the design and engineering practices of rock slopes, it is required to define certain values of slope properties for a desired FOS. This purpose can easily be achieved by sensitivity analysis in limit equilibrium methods. However, it is quite challenging by numerical simulations. By using RSM and defining a function to the FOS, this goal can efficiently be achieved in numerical methods along with considering the uncertainties of the parameters.

It is important to note that since the potential wedge has quite large size, depth of the discontinuities effect the cohesion of the discontinuity surface in different areas. Hence,

for the future studies, it is expected that assuming various cohesion values by depth will highly affect the estimated probability of failure.

REFERENCES

Adhikari, S., 2004. Reliability Analysis Using Parabolic Failure Surface Approximation. *Journal of Engineering Mechanics*, 130(12), pp.1407–1427.

Ang, A.H.S. & Tang, W.H., 1984. *Probability Concepts in Engineering Planning and Design. Vol.2. Decision, risk, and reliability*, John Wiley and Sons.

Anon, 2013. 3DEC v.5.0 Users' Manual.

Bishop, A., 1955. The Use of the Slip Circle in the Stability Analysis of the slopes. *journal of geotechnique*, 5(1), pp.7–17.

Bjerager, P., 1991. Methods for structural reliability computation. In F. Casciati & J. B. Roberts, eds. *Reliability Problems: General principles and Applications in Mechanics of Solids and Structures*. Springer-Verlag, pp. 89–136.

Box, G. & Draper, N.R., 1987. *Empirical Model Building and Response Surface*, John Willey and Sons.

Box, G.E.P. & Wilson, K.B., 1951. On the Experimental Attainment of Optimum Conditions. *Journal of the Royal Statistical Society*, 13(1), pp.1–45.

Brideau, M. et al., 2008. preliminary description and slope stability analyses of the 2008 little Salmon lake and 2007 Mt . Steele landslides , Yukon rEactivation. , pp.119–134.

Bucher, C. & Bourgund, U., 1990. fast and efficient response surface approach for structural reliability problems. *structural safety*, 7, pp.57–66.

Bucher, C.G. & Bourgund, Y.M., 1990. A fast and efficient response surface approach for structural reliability problems. *Structural Safety*, 7, pp.57–66.

Byrne, R., 1974. *Physical and numerical model in rock and soil-slope stability*. James Cook University of North Queensland, Townsville, Australia.

Chappel, B., 1974. Numerical and physical experiments with discontinua. In *Proceedings of the Third Congress on ISRM*. p. Volume 2A.

Chappel, B., 1972. *The mechanics of blocky material.* Australia National University, Canberra.

Chen, J., Zhong, F. & Chen, D., 2013. Upper and lower bound method applied in stability analysis of a plane sliding rock slope based on limit equilibrium theory. *Journal of Central South University (Science and Technology)*, 44(8), pp.3310–3315.

Cornell, C.A., 1969. Structural Safety Specifications Based on Second Moment Analysis. In *Bridge and Structural Engineers, Symposium on Concepts of Safety of Structures and Methods of Design*.

Cundall, P., 1971. A computer model for simulating progressive, large scale movements in blocky rock systems. In *Proceedings of the International Symposium Rock Fracture, ISRM*. p. Paper No. II–8.

Cundall, P., 1988. Formulation of a three-dimensional distinct element model—Part I. A scheme to detect and represent contacts in a system composed of many polyhedral blocks. *International Journal of Rock Mechanics and Mining* , 25(3), pp.107–116.

Cundall, P., 1974. *Rational design of tunnel supports: a computer model for rock mass behaviour using interactive graphics for the input and output of geomaterial data*,

Cundall, P. & Marti, J., 1979. Some new developments in discrete numerical methods for dynamic modelling of jointed rock masses. In *Rapid Excavation Tunnelling*. pp. 1464–6.

Cundall, P.A., 1980. *UDEC-A Generalised Distinct Element Program for Modelling Jointed Rock*,

Cundall, P.A. & Hart, R.D., 1985. Development of generalized 2-D and 3-D distinct element programs for modeling jointed rock. *Itasca Consulting Group, Miscellaneous Paper No. SL-85-1. US Army Corps of Engineers*.

Dadashzadeh, N., Dusgun, H.S.. & Gheibie, S., A Second-Order Reliability Analysis of Rock Slope Stability in Amasya, Turkey. In *international congress on rock mechanics*.

Diederichs, M.S. et al., 2007. Shear Strength Reduction Approach for Slope Stability Analyses. In *1st Canada-US Rock Mechanics Symposium*.

Dolezalova, M., Hladik, I. & Zemanova, V., 2001. Stability analysis of a motorway embankment on soft subsoil using FEM, FLAC and limit equilibrium methods. In *FLAC and Numerical Modeling in Geomechanics – 2001, Proceedings of the 2nd International Symposium, Lyon, France*. A.A Balkema, pp. 125–132.

Duncan, J.M., 2000. Factors of Safety and Reliability in Geotechnical Engineering. *Journal of Geotechnical and Geoenvironmental Engineering*, 126(4), pp.307–316.

Duncan, J.M., 1996. State of the Art: Limit Equilibrium and Finite Element Analysis of Slopes. *Journal of Geotechnical Engineering*, 122(7), pp.577–596.

Duzgun, H.S.B. & Bhasin, R.K., 2008. Probabilistic Stability Evaluation of Oppstadhornet Rock Slope, Norway. *Rock Mechanics and Rock Engineering*, 42(5), pp.729–749.

Duzgun, H.S.B., M.S., Y. & Pasamehmetoglu, A.G., 1995. Plane Failure Analysis of Rock Slopes: A Reliability Approach. *International Journal of Surface Mining and Reclamation*, 9, pp.1–6.

Duzgun, H.S.B., Yucemen, M.S. & Karpuz, C., 2003. A Methodology for Reliability-Based Design of Rock Slopes. *Rock Mechanics and Rock Engineering*, 36(2), pp.95–120.

Eberhardt, E., 2003. Rock Slope Stability Analysis – Utilization of Advanced Numerical Techniques.

ELFEN, 2001. ELFEN 2D/3D Numerical Modelling Package.

El-Ramly, H., Morgenstern, N.R. & Cruden, D.M., 2002. Probabilistic slope stability analysis for practice. *Canadian Geotechnical Journal*, 39(3), pp.665–683.

Faravelli, L., 1989. Response surface approach for reliability analysis. *Engineering Mechanics*, 115(12), pp.2763–2781.

Fiessler, B. & Rackwitz, R., 1979. Quadratic limit states in structural reliability. *Journal of the Engineering Mechanics Division*, 105(4), pp.661–676.

Firpo, G. et al., 2011. Use of Digital Terrestrial Photogrammetry in rocky slope stability analysis by Distinct Elements Numerical Methods. *International Journal of Rock Mechanics and Mining Sciences*, 48(7), pp.1045–1054.

Gelisli, K. et al., 2011. The Sumela Monastery slope in Macka, Trabzon, Northeast Turkey: rock mass properties and stability assessment. *Bulletin of Engineering Geology and the Environment*, 70, pp.577–583.

Gheibie, S., Duzgun, S.H.B. & Akgun, A., 2013. Probabilistic-Numerical Modeling of Stability of a Rock Slope in Amasya-Turkey. In *47th US Rock Mechanics / Geomechanics Symposium*. American Rock Mechanics Association.

Goodman, R.E. & G.-H., S., 1985. Block Theory and Its Application to Rock Engineering. *New Jersey: Prentice Hall.*

Griffiths, D. V. & Lane, P.A., 1999. Slope stability analysis by finite element. *journal of geotechnique*, 49(3), pp.387–403.

Guo, F. et al., 2013. Research on Deformation Stability of Soft Rock Slope under Excavation Based on FLAC3D. *Applied Mechanics and Materials*, 275-277, pp.290–294.

Gutiérrez, F. et al., 2010. Recent advances in landslide investigation: Issues and perspectives. *Geomorphology*, 124(3-4), pp.95–101.

Hammah, R.E., Yacoub, T.E. & Curran, J.H., 2009. Probabilistic Slope Analysis with the Finite Element Method. In *the 43rd US Rock Mechanics Symposium and 4th U.S.-Canada Rock Mechanics Symposium.*

Harr, M.E., 1989. Probabilistic estimates for multivariate analyses. *Applied Mathematical Modelling*, 13(5), pp.313–318.

Harrison, J. & Hudson, J., 2000. *Engineering rock mechanics. Part 2.*,

Hart, R., Cundall, P. a. & Lemos, J., 1988. Formulation of a three-dimensional distinct element model—Part II. Mechanical calculations for motion and interaction of a system composed of many polyhedral blocks. *International Journal of Rock Mechanics and Mining Sciences & Geomechanics Abstracts*, 25(3), pp.117–125.

Hasofer, A.M. & Lind, N.C., 1974. Exact and Invariant Second-Moment Code Format. *Journal of the Engineering Mechanics Division*, 100(1), pp.111–121.

Hoek, E., 1973. Methods for the rapid assessment of the stability of three-dimensional rock slopes. *Quarterly Journal of Engineering Geology and Hydrogeology*, 6(3-4), pp.243–255.

Hoek, E. & Bray, J., 1981. *Rock Slope Engineering*, Institute of Mining and Metallurgy.

Huang, Y.S. & Li, J.L., 2012. Study of the Three-Dimensional Global Limit Equilibrium Method Applied to the Stability of Rock Slope.

Hungr, O., Leroueil, S. & Picarelli, L., 2013. The Varnes classification of landslide types, an update. *Landslides*, 11(2), pp.167–194.

Itasca, 2013. 3 dimensional Discrete Element Code.

Itasca, Itasca Software Products - FLAC, FLAC3D, UDEC, 3DEC, PFC2D/3D.

J.C., W. et al., 2000. Reliability analysis of an open pit coal mine slope. *International Journal of Rock Mechanics and Mining Sciences*, 37(4), pp.715–721.

Jiang, H.D., Lee, C.F. & Zhu, D.Y., 2003a. Generalised framework of limit equilibrium methods for slope stability analysis. *Géotechnique*, 53(4), pp.377–395.

Jiang, H.D., Lee, C.F. & Zhu, D.Y., 2003b. Generalised framework of limit equilibrium methods for slope stability analysis. *Géotechnique*, 53(4), pp.377–395.

Jiang, Y.S., 1990. *Slope analysis using boundary elements*, New York: Springer-Verlag Publishers.

Jimenez-Rodriguez, R., Sitar, N. & Chacón, J., 2006. System reliability approach to rock slope stability. *International Journal of Rock Mechanics and Mining Sciences*, 43(6), pp.847–859.

Jing, L., 2003. A review of techniques, advances and outstanding issues in numerical modelling for rock mechanics and rock engineering. *International Journal of Rock Mechanics and Mining Sciences*, 40(3), pp.283–353.

Kainthola, A. et al., 2013. A Review on Numerical Slope Stability Analysis. *International Journal of Science, Engineering and Technology Research (IJSETR)*, 2(6), pp.1315–1320.

Kainthola, A., Singh, P.K. & Singh, T.N., 2014. Stability investigation of road cut slope in basaltic rockmass, Mahabaleshwar, India. *Geoscience Frontiers*.

Khuri, A.I. & Mukhopadhyay, S., 2010. Response surface methodology. *WIREs Computational Statistics*, 2, pp.128–149.

Kim, S. & Na, S., 1997. esponse surface method using vector projected sample points. *structural safety*, 19(1), pp.3–19.

Kim, S.H. & Na, S.W., 1997. Response surface method using vector projected sampling points. *Structural Safety*, 19(1), pp.3–19.

Lee, Y.-F. et al., 2012. Reliability Analysis of Rock Wedge Stability: Knowledge-Based Clustered Partitioning Approach. *Journal of Geotechnical and Geoenvironmental Engineering*, 138(6), pp.700–708.

Li, D. et al., 2009. A system reliability approach for evaluating stability of rock wedges with correlated failure modes. *Computers and Geotechnics*, 36(8), pp.1298–1307.

Li, D. et al., 2011. Stochastic response surface method for reliability analysis of rock slopes involving correlated non-normal variables. *Computers and Geotechnics*, 38(1), pp.58–68.

Lin, D. & Fairhurst, C., 1988. Static analysis of the stability of three-dimensional blocky systems around excavations in rock. *International Journal of Rock Mechanics and Mining Sciences and Geomechanics Abstracts*, 25(3), pp.139–147.

Lorig, L.J. & Brady, B.H.G., 1984. A hybrid computational scheme for excavation and support design in jointed rock media. In *Design and performance of underground excavations; ISRM Symposium*. London: British Geotech. Soc., p. 105.

Low, J., 1997. Reliability analysis of rock wedges. *geotechnical environmental engineering*, 123, pp.498–505.

Lowe, J. & Karafiath, L., 1960. Stability of Earth Dams upon Drawdown. In *The First PanAmerican Conference on Soil Mechanics and Foundation Engineering*. pp. 537–552.

Matsui, T. & San, K.C., 1992. Finite element slope stability analysis by shear strength reduction technique. *journal of soils and foundation*, 32, pp.59–70.

Miller, W., 1968. *Trebizond : the last Greek empire*, The Macmillan co.

Moellmann, A., Pieter, A. V. & Huber, M., 2008. a probabilistic finite element analysis of embankment stability under transient seepage conditions. In *Proceeding of the 6th international probabilistic workshop, Darmstadt*. pp. 551–562.

Montgomery, D.C., 1997. *Design and Analysis of Experiments*, John Wiley & Sons.

Morgenstern, N.R. & Price, V.E., 1965. The Analysis of the Stability of General Slip Surfaces. *journal of geotechnique*, 15(1), pp.79–93.

Munjiza, A., Owen, D.R.J. & Bicanic, N., 1995. A combined finite-discrete element method in transient dynamics of fracturing solids. *Engineering Computations*, 12(2), pp.145–174.

Myers, R.H. & Montgomery, D.C., 1995. *Response Surface Methodology : Process and Product Optimization Using Designed Experiments*, John Wiley & Sons, New York.

Nadim, F.Einstein, H.Roberds, W., 2005. Probabilistic stability analysis for individual slopes in soil and rock. In E. Hungr, O.Fell, R.Couture, R.Eberhardt, ed. *Landslides risk management*. A.A Balkema, pp. 63–98.

Nash, D.T.F., 1987. A comprehensive review of limit equilibrium methods of slope stability analysis. In M. G. Anderson & K. S. Richards, eds. *slope stability*. John Wiley & Sons, New York.

Nataf, A., 1962. determination des distribution dont les marges sont donnees. *Comptes rendus de lacademie des sciences*, 225, pp.42–43.

Noroozi, M., Jalali, S.E. & Yarahmadi-Bafghi, A.R., 2012. 3D key-group method for slope stability analysis. *International Journal for Numerical and Analytical Methods in Geomechanics*, 36(16), pp.1780–1792.

Park, H. & West, T.R., 2001. Development of a probabilistic approach for rock wedge failure. *engineering geology*, 59(3-4), pp.233–251.

Phoon, kok kwang, 2008. *Reliability-based design in geotechnical Engineering, computations and applications*, CRC Press.

Propst, A., Cornell, J. a. & Crocker, D.C., 1992. How to Apply Response Surface Methodology. *Technometrics*, 34(3), p.359.

Rajashekhar, M. & Ellingwood, B., 1993. A new look at the response surface approach for reliability analysis. *structural safety*, 12(3), pp.205–220.

Rathod, G.W. et al., 2012. 3 Dimensional Stability Assessment of Jointed Rock Slopes Using Distinct Element Modelling. In *GeoCongress, ASCE*. pp. 2382–2391.

Rocscience, Phase2.

Rosenblatt, M., 1952. Remarks on a Multivariate Transformation. *The Annals of Mathematical Statistics*, 23(3), pp.470–472.

Sainsbury, D.P. et al., 2007. Three-Dimensional Discontinuum Analysis of Structurally Controlled Failure Mechanisms at the Cadia Hill Open Pit. In *International Symposium, Rock Slope Stability in Open Pit Mining and Civil Engineering, Perth, Australia*. Itasca Australia Pty Ltd, Melbourne, Australia Australia.

Schultz, R.A., 1993. Brittle strength of basaltic rock masses with applications to Venus. *Journal of Geophysical Research*, 98(E6), p.10883.

Sdvizhkova, Y.A., Kovrov, A.S. & Kiriiak, K.K., 2014. GEOMECHANICAL ASSESSMENT OF LANDSLIDE SLOPE STABILITY BY FINITE ELEMENT METHOD. *scientific Bulletin of National Mining University*, (2), pp.86–92.

Shen, H., 2012. *Non-Deterministic Analysis of Slope Stability based on Numerical Simulation*. Technische Universität Bergakademie Freiberg.

Shen, H. & Abbas, S.M., 2013. Rock slope reliability analysis based on distinct element method and random set theory. *International Journal of Rock Mechanics and Mining Sciences*, 61, pp.15–22.

Spencer, E., 1967. A Method of Analysis of the Stability of Embankments Assuming Parallel Interslice Forces. *journal of geotechnique*, 17(1), pp.11–26.

Stanković, J.N. et al., 2013. RISK AND RELIABILITY ANALYSIS OF SLOPE STABILITYDETERMINISTIC AND PROBABILISTIC METHOD. *Journal of Trends in the Development of Machinery and Associated Technology*, 17(1), pp.97–100.

Stead, D. et al., 2001. Advanced numerical techniques in rock slope stability analysis – applications and limitations. In *International Conference on Landslides Causes, Impacts and Countermeasures*. pp. 615–624.

Suchomel, R. & Masin, D., 2008. Modelling of the Lodalen slide using probabilistic numerical methods. In *International Conference on Numerical Computation in Geotechnical Engineering*.

Swan, C.C. & Seo, Y.K., 1999. Limit state analysis of earthen slopes using dual continuum/FEM approaches. *International Journal for Numerical and Analytical Methods in Geomechanics*, 23, pp.1359–1371.

Tan, X. et al., 2013. Response Surface Method of Reliability Analysis and its Application in Slope Stability Analysis. *geotechnical geology engineering*, 31, pp.1011–1025.

Tang, W.H., Yucemen, M.S. & Ang, A.H.-S., 1976. Probability-based short term design of soil slopes. *Canadian Geotechnical Journal*, 13(3), pp.201–215.

Turner, A.K. & Schuster, R.L. eds., 1996. *Landslides: Investigation and Mitigation* first., National Research Council (U.S.) Transportation Research Board Special Report.

USGS, 2000. Landslide hazards. *U.S. Geological Survey, USGS Fact Sheet Fs-071-00.*

VIPS- Vector International Processing Systems, 2001. VISAGE - Vectorial Implementation of Structural Analysis and Geotechnical Engineering.

Voight, B. & Faust, C., 1992. Frictional heat and strength loss in some rapid landslides: error correction and affirmation ofmechanism for the Vaiont landslide. *journal of geotechnique*, 42(4), pp.641–643.

Wang, H., Chen, Z.X. & Zhang, D.M., 2012. Rock Slope Stability Analysis Based on FLAC3D Numerical Simulation. *Applied Mechanics and Materials*, 170-173, pp.375–379.

Wang, J. & Ji, H.G., 2013. Analysis of Rock Slope Stability on the Basis of Limit Equilibrium Method. *Advanced Materials Research*, 711, pp.333–337.

Wang, Z. De et al., 2013. Numerical Analysis of Stratified Rock Slope Stability Based on 3DEC. *Applied Mechanics and Materials*, 454, pp.133–139.

Warburton, P.M., 1981. Vector stability analysis of an arbitrary polyhedral rock block with any number of free faces. *International Journal of Rock Mechanics and Mining Sciences and Geomechanics Abstracts*, 18(5), pp.415–427.

Weida, N. et al., 2014. Dynamic Stability Analysis of Wedge in Rock Slope Based on Kinetic Vector Method. *Journal of Earth Science*, 25(4), pp.749–756.

Wikipedia, 2014. Sümela Monastery. Available at: http://en.wikipedia.org/wiki/Sumela_Monastery. [Last accessed on 15.01.2015]

Wong, F., 1985. Slope reliability and response surface method. *geotechnical engineering*, 111(1), pp.32–53.

Wu, T.H. & Kraft, L.M., 1970. Safety analysis of slopes. *journal of soil mechanics and foundation division*, 96(3), pp.609–630.

Yang, B., 2011. Application of FLAC strength reduction method to analysis of slope stability. In *2011 Second International Conference on Mechanic Automation and Control Engineering*. IEEE, pp. 5618–5621.

Ying Wei Liu & Moses, F., 1994. A sequential response surface method and its application in the reliability analysis of aircraft structural systems. *Structural Safety*, 16(1-2), pp.39–46.

Youliang, D., Aiqun, L. & Yang, D., 2008. A new look at the response surface method for reliability analysis using chaos theory. *EARTHQUAKE ENGINEERING AND ENGINEERING VIBRATION*, 7, pp.329–335.

Zangeneh, N. et al., 2002. Application of response surface methodology in numerical geotechnical analysis. In *55th Canadian Society for Geotechnical Conference, Hamilton, Ontario*.

Zeng, J. et al., 2006. Numerical simulation with FLAC3D on construction and excavation process of underground powerhouse of Fuziling pumped storage hydropower station. *Rock and Soil Mechanics*, 27(4), pp.637–642.

Zhang, J. & Du, X., 2010. A Second-Order Reliability Method With First-Order Efficiency. *Journal of Mechanical Design*, 132(10), p.101006.

Zhang, J., Huang, H.W. & Phoon, K.K., 2013. Application of the Kriging-Based Response Surface Method to the System Reliability of Soil Slopes. *Journal of Geotechnical and Geoenvironmental Engineering*, 139(4), pp.651–655.

Zhao, Y.G. & Ono, T., 1999. A general procedure for first/second-order reliability method (FORM/SORM). *structural safety*, 21(2), pp.95–122.

Zheng, Y. & Das, P., 2000. Improved response surface method and its application to stiffened plate reliability analysis. *engineering structure*, 22, pp.544–551.

Zou, J.Z. & Williams, D.J., 1995. Search for critical slip surface based on finite element method. *Canadian Geotechnical Journal*, 32(1), pp.233–246.

APPENDIX A

ROCK MASS RATING SYSTEM TABLE

The table of the Rock Mass Rating System (After Bieniawski 1989) is given in Figure A.1.

A. CLASSIFICATION PARAMETERS AND THEIR RATINGS

Parameter		Range of values						
1	Strength of intact rock material	Point-load strength index	>10 MPa	4 - 10 MPa	2 - 4 MPa	1 - 2 MPa	For this low range - uniaxial compressive test is preferred		
		Uniaxial comp. strength	>250 MPa	100 - 250 MPa	50 - 100 MPa	25 - 50 MPa	5 - 25 MPa	1 - 5 MPa	< 1 MPa
		Rating	15	12	7	4	2	1	0
2	Drill core Quality *RQD*		90% - 100%	75% - 90%	50% - 75%	25% - 50%	< 25%		
	Rating		20	17	13	8	3		
3	Spacing of discontinuities		> 2 m	0.6 - 2 . m	200 - 600 mm	60 - 200 mm	< 60 mm		
	Rating		20	15	10	8	5		
4	Condition of discontinuities (See E)		Very rough surfaces Not continuous No separation Unweathered wall rock	Slightly rough surfaces Separation < 1 mm Slightly weathered walls	Slightly rough surfaces Separation < 1 mm Highly weathered walls	Slickensided surfaces or Gouge < 5 mm thick or Separation 1-5 mm Continuous	Soft gouge >5 mm thick or Separation > 5 mm Continuous		
	Rating		30	25	20	10	0		
5	Groundwater	Inflow per 10 m tunnel length (l/m)	None	< 10	10 - 25	25 - 125	> 125		
		(Joint water press)/ (Major principal σ)	0	< 0.1	0.1, - 0.2	0.2 - 0.5	> 0.5		
		General conditions	Completely dry	Damp	Wet	Dripping	Flowing		
		Rating	15	10	7	4	0		

B. RATING ADJUSTMENT FOR DISCONTINUITY ORIENTATIONS (See F)

Strike and dip orientations		Very favourable	Favourable	Fair	Unfavourable	Very Unfavourable
Ratings	Tunnels & mines	0	-2	-5	-10	-12
	Foundations	0	-2	-7	-15	-25
	Slopes	0	-5	-25	-50	

C. ROCK MASS CLASSES DETERMINED FROM TOTAL RATINGS

Rating	100 ← 81	80 ← 61	60 ← 41	40 ← 21	< 21
Class number	I	II	III	IV	V
Description	Very good rock	Good rock	Fair rock	Poor rock	Very poor rock

D. MEANING OF ROCK CLASSES

Class number	I	II	III	IV	V
Average stand-up time	20 yrs for 15 m span	1 year for 10 m span	1 week for 5 m span	10 hrs for 2.5 m span	30 min for 1 m span
Cohesion of rock mass (kPa)	> 400	300 - 400	200 - 300	100 - 200	< 100
Friction angle of rock mass (deg)	> 45	35 - 45	25 - 35	15 - 25	< 15

E. GUIDELINES FOR CLASSIFICATION OF DISCONTINUITY conditions

Discontinuity length (persistence)	< 1 m	1 - 3 m	3 - 10 m	10 - 20 m	> 20 m
Rating	6	4	2	1	0
Separation (aperture)	None	< 0.1 mm	0.1 - 1.0 mm	1 - 5 mm	> 5 mm
Rating	6	5	4	1	0
Roughness	Very rough	Rough	Slightly rough	Smooth	Slickensided
Rating	6	5	3	1	0
Infilling (gouge)	None	Hard filling < 5 mm	Hard filling > 5 mm	Soft filling < 5 mm	Soft filling > 5 mm
Rating	6	4	2	2	0
Weathering	Unweathered	Slightly weathered	Moderately weathered	Highly weathered	Decomposed
Ratings	6	5	3	1	0

F. EFFECT OF DISCONTINUITY STRIKE AND DIP ORIENTATION IN TUNNELLING**

Strike perpendicular to tunnel axis		Strike parallel to tunnel axis	
Drive with dip - Dip 45 - 90°	Drive with dip - Dip 20 - 45°	Dip 45 - 90°	Dip 20 - 45°
Very favourable	Favourable	Very unfavourable	Fair
Drive against dip - Dip 45-90°	Drive against dip - Dip 20-45°	Dip 0-20 - Irrespective of strike°	
Fair	Unfavourable	Fair	

* Some conditions are mutually exclusive . For example, if infilling is present, the roughness of the surface will be overshadowed by the influence of the gouge. In such cases use A.4 directly.

** Modified after Wickham et al (1972).

Figure A.1 – Rock Mass Rating System (After Bieniawski 1989).

APPENDIX B

RESULTS OF TRIAXIAL COMPRESSIVE TESTS

Table C.1 – Results of triaxial compressive test.

Sample No.	Diameter (mm)	Effective area (mm²)	Lateral stress (MPa)	Axial stress (MPa)	Cohesion (Mpa)	Friction angle
1	51.33	2068.29	0.1	235.27		
2	52.04	2125.91	0.3	247.81	71	28˚
3	51.83	2108.78	0.5	258.33		
4	51.93	2116.93	0.7	274.86		

APPENDIX C

DEVELOPED CODES IN 3DEC

new

poly brick -500,500 -500,500 -500,100

group block 'rock'

densify nseg 4 4 3

join

geometry import 'topography.dxf'

densify gradlimit maxlength 10 repeat range geometry 'topography' distance 0 extent

join

group block 'rock-mass' range geometry 'topography' count odd

delet range group 'rock'

jset dip 90 dd 90 ori 244.89,-151.008,-283.333

jset dip 0 dd 90 ori 227.344,-437.5,-256.815

hide dip 0 dd 90 ori 227.344,-437.5,-256.815 below

hide dip 90 dd 90 ori 244.89,-151.008,-283.333 above

jset dip 82 dd 185 spacing 4 num 7 ori 135,27,-143

93

```
jset dip 82 dd 185 ori 26.6191,6.855,-134.015

jset dip 44 dd 38 spacing 6 num 4 origin 29.2388,-79.1577,-50.8439

group block 'rock'

seek

hide range group 'rock'

group block 'boundry'

seek

fix range group 'boundry'

gravity 0  0 -10

change cons 2 mat 1

prop mat=1 k 48.67e9 g 29.2e9 den 2650 bcoh=71e20 bfric=80 bten 15e20

prop jmat 1 jkn 30e9 jks 12e9 jcoh 4.5e20 jfric 89

hist zvel 126.255,-25.4155,-126.282

hist disp 126.255,-25.4155,-126.282

hist unbal

step 2000

change cons 2 mat 1

prop mat=1 k 48.67e9 g 29.2e9 den 2650 bcoh=0 bfric=31

prop jmat 1 jcoh 4.5e6  jfric 30 jkn 30e9 jks 12e9

step 18000

solve FOS associated

ret
```

APPENDIX D

GENERATION OF THE RESPONSE SURFACE OF FOS

The response surface of FOS is approximated by 84 simulations in 3DEC. All results of analysis are listed in Tables D.1 to D.12.

Table D.1 – Generation of the response function of FOS in iteration one.

NO.	Point Sets	Parameter Values		Coefficients of RSM		Response Surface Function / FOS
ITERATION 1	**POINT 1**	X_1 (MPa)	4.5	a_0	0.64928	**FOS (X^*) = 2.72**
		X_2 (GPa/m)	30			
		X_3 (GPa/m)	12			
		FOS	2.93			
	POINT 2	X_1 (MPa)	6.3	b_1	1.95261	
		X_2 (GPa/m)	39			
		X_3 (GPa/m)	14.4			
		FOS	4.22			
	POINT 3	X_1 (MPa)	2.7	b_2	-0.44480	
		X_2 (GPa/m)	21			Response Surface Function : FOS = (0.649) + (1.953*X_1) + (-0.445*X_2) + (0.509*X_3) + (-0.143*X_1^2) + (0.008*X_2^2) + (-0.023*X_3^2)
		X_3 (GPa/m)	14.4			
		FOS	1.45			
	POINT 4	X_1 (MPa)	2.7	b_3	0.50850	
		X_2 (GPa/m)	39			
		X_3 (GPa/m)	14.4			
		FOS	1.82			
	POINT 5	X_1 (MPa)	2.7	c_1	-0.14288	X^*_i (X^*_1, X^*_2, X^*_3) = (**3.85 , 28.3 , 12.6**)
		X_2 (GPa/m)	39			
		X_3 (GPa/m)	9.6			
		FOS	2.04			
	POINT 6	X_1 (MPa)	2.7	c_2	0.00773	
		X_2 (GPa/m)	21			
		X_3 (GPa/m)	9.6			
		FOS	1.7			
	POINT 7	X_1 (MPa)	6.3	c_3	-0.02310	
		X_2 (GPa/m)	21			
		X_3 (GPa/m)	14.4			
		FOS	3.35			

Table D.2 - Generation of the response function of FOS in iteration two.

NO.	Point Sets	Parameter Values		Coefficients of RSM		Response Surface Function : FOS = (0.671) + (1.903*X_1) + (-0.467*X_2) + (0.596*X_3) + (-0.164*X_1^2) + (0.009*X_2^2) + (-0.025*X_3^2)	FOS (X*) = 2.42
ITERATION 2	POINT 1	X_1 (MPa)	3.85	a_0	0.67063		
		X_2 (GPa/m)	28.3				
		X_3 (GPa/m)	12.6				
		FOS	2.72				
	POINT 2	X_1 (MPa)	5.65	b_1	1.90343		
		X_2 (GPa/m)	37.3				
		X_3 (GPa/m)	15				
		FOS	3.97				
	POINT 3	X_1 (MPa)	2.05	b_2	-0.46662		X^*_i (X^*_1, X^*_2, X^*_3) = (3.11 , 26.4 , 12. 9)
		X_2 (GPa/m)	19.3				
		X_3 (GPa/m)	15				
		FOS	1.29				
	POINT 4	X_1 (MPa)	2.05	b_3	0.59573		
		X_2 (GPa/m)	37.3				
		X_3 (GPa/m)	15				
		FOS	1.65				
	POINT 5	X_1 (MPa)	2.05	c_1	-0.16350		
		X_2 (GPa/m)	37.3				
		X_3 (GPa/m)	10.2				
		FOS	1.87				
	POINT 6	X_1 (MPa)	2.05	c_2	0.00860		
		X_2 (GPa/m)	19.3				
		X_3 (GPa/m)	10.2				
		FOS	1.51				
	POINT 7	X_1 (MPa)	5.65	c_3	-0.02546		
		X_2 (GPa/m)	19.3				
		X_3 (GPa/m)	15				
		FOS	3.1				

Table D.3 - Generation of the response function of FOS in iteration three.

NO.	Point Sets	Parameter Values		Coefficients of RSM		Response Surface Function : $\text{FOS} = (1.361) + (-0.132 * X_1) + (0.652 * X_2) + (-1.354 * X_3) + (0.123 * X_1^2) + (-0.011 * X_2^2) + (0.051 * X_3^2)$	$\text{FOS}(X^*) = 2.2$
ITERATION 3	POINT 1	X_1 (MPa)	3.11	a_0	1.35990		
		X_2 (GPa/m)	26.4				
		X_3 (GPa/m)	12.9				
		FOS	2.42				
	POINT 2	X_1 (MPa)	4.91	b_1	-0.13187		
		X_2 (GPa/m)	35.4				
		X_3 (GPa/m)	15.3				
		FOS	3.67				
	POINT 3	X_1 (MPa)	1.31	b_2	0.65235		
		X_2 (GPa/m)	17.4				
		X_3 (GPa/m)	15.3				
		FOS	1.07				
	POINT 4	X_1 (MPa)	1.31	b_3	-1.35441		$X^*_i (X^*_1, X^*_2, X^*_3) = (2.88, 25, 12.6)$
		X_2 (GPa/m)	35.4				
		X_3 (GPa/m)	15.3				
		FOS	1.4				
	POINT 5	X_1 (MPa)	1.31	c_1	0.12258		
		X_2 (GPa/m)	35.4				
		X_3 (GPa/m)	10.5				
		FOS	1.57				
	POINT 6	X_1 (MPa)	1.31	c_2	-0.01144		
		X_2 (GPa/m)	17.4				
		X_3 (GPa/m)	10.5				
		FOS	1.22				
	POINT 7	X_1 (MPa)	4.91	c_3	0.05112		
		X_2 (GPa/m)	17.4				
		X_3 (GPa/m)	15.3				
		FOS	2.8				

Table D.4 - Generation of the response function of FOS in iteration four.

NO.	Point Sets	Parameter Values		Coefficients of RSM		Response Surface Function : FOS = (1.368) + (-0.158*X_1) + (0.642*X_2) + (-1.321*X_3) + (0.133*X_1^2) + (-0.012*X_2^2) + (0.052*X_3^2) X_i^* (X_1^*, X_2^*, X_3^*) = (2.75 , 24.1 , 13.2)	FOS (X^*) = 1.92
ITERATION 4	**POINT 1**	X_1 (MPa)	2.88	a_0	1.36788		
		X_2 (GPa/m)	25				
		X_3 (GPa/m)	12.6				
		FOS	2.2				
	POINT 2	X_1 (MPa)	4.68	b_1	-0.15826		
		X_2 (GPa/m)	34				
		X_3 (GPa/m)	15				
		FOS	3.44				
	POINT 3	X_1 (MPa)	1.08	b_2	0.64156		
		X_2 (GPa/m)	16				
		X_3 (GPa/m)	15				
		FOS	0.89				
	POINT 4	X_1 (MPa)	1.08	b_3	-1.31964		
		X_2 (GPa/m)	34				
		X_3 (GPa/m)	15				
		FOS	1.19				
	POINT 5	X_1 (MPa)	1.08	c_1	0.13277		
		X_2 (GPa/m)	34				
		X_3 (GPa/m)	10.2				
		FOS	1.34				
	POINT 6	X_1 (MPa)	1.08	c_2	-0.01189		
		X_2 (GPa/m)	16				
		X_3 (GPa/m)	10.2				
		FOS	1.02				
	POINT 7	X_1 (MPa)	4.68	c_3	0.05168		
		X_2 (GPa/m)	16				
		X_3 (GPa/m)	15				
		FOS	2.59				

99

Table D.5 - Generation of the response function of FOS in iteration five.

NO.	Point Sets	Parameter Values		Coefficients of RSM		Response Surface Function	FOS
ITERATION 5	POINT 1	X_1 (MPa)	2.75	a_0	2.58893	Response Surface Function : FOS = (2.599) + (-3.622*X_1) + (1.862*X_2) + (-2.914*X_3) + (-0.742*X_1^2) + (-0.038*X_2^2) + (0.112*X_3^2)	FOS (X^*) = 1.64
		X_2 (GPa/m)	24.1				
		X_3 (GPa/m)	13.2				
		FOS	1.92				
	POINT 2	X_1 (MPa)	4.55	b_1	-3.62227		
		X_2 (GPa/m)	33.1				
		X_3 (GPa/m)	15.6				
		FOS	2.93				
	POINT 3	X_1 (MPa)	0.95	b_2	1.86185		$X_i^* (X_1^*, X_2^*, X_3^*) = (2.62, 21.9, 13)$
		X_2 (GPa/m)	15.1				
		X_3 (GPa/m)	15				
		FOS	0.71				
	POINT 4	X_1 (MPa)	0.95	b_3	-2.91369		
		X_2 (GPa/m)	33.1				
		X_3 (GPa/m)	15.6				
		FOS	0.94				
	POINT 5	X_1 (MPa)	0.95	c_1	0.74193		
		X_2 (GPa/m)	33.1				
		X_3 (GPa/m)	10.8				
		FOS	1.06				
	POINT 6	X_1 (MPa)	0.95	c_2	-0.03833		
		X_2 (GPa/m)	15.1				
		X_3 (GPa/m)	10.8				
		FOS	0.8				
	POINT 7	X_1 (MPa)	4.55	c_3	0.11210		
		X_2 (GPa/m)	15.1				
		X_3 (GPa/m)	15				
		FOS	2.36				

Table D.6 - Generation of the response function of FOS in iteration six.

NO.	Point Sets	Parameter Values		Coefficients of RSM		Response Surface Function : FOS = (4.923) + (0.812*X₁) + (-0.023*X₂) + (-0.821*X₃) + (-0.065*X₁²) + (0.001*X₂²) + (0.034*X₃²) X*ᵢ (X*₁ , X*₂ , X*₃) = (2.53, 21.2 , 13)	FOS (X*) = 1.47
ITERATION 6	POINT 1	X_1 (MPa)	2.62	a_0	4.92290		
		X_2 (GPa/m)	21.9				
		X_3 (GPa/m)	13				
		FOS	1.64				
	POINT 2	X_1 (MPa)	4.42	b_1	0.81243		
		X_2 (GPa/m)	30.9				
		X_3 (GPa/m)	15.4				
		FOS	2.82				
	POINT 3	X_1 (MPa)	0.82	b_2	-0.02289		
		X_2 (GPa/m)	14				
		X_3 (GPa/m)	13				
		FOS	0.54				
	POINT 4	X_1 (MPa)	0.82	b_3	-0.81950		
		X_2 (GPa/m)	30.9				
		X_3 (GPa/m)	15.4				
		FOS	0.68				
	POINT 5	X_1 (MPa)	0.82	c_1	-0.06545		
		X_2 (GPa/m)	30.9				
		X_3 (GPa/m)	10.6				
		FOS	0.77				
	POINT 6	X_1 (MPa)	0.82	c_2	0.00079		
		X_2 (GPa/m)	12.9				
		X_3 (GPa/m)	10.6				
		FOS	0.56				
	POINT 7	X_1 (MPa)	4.42	c_3	0.03440		
		X_2 (GPa/m)	14				
		X_3 (GPa/m)	13				
		FOS	2.23				

Table D.7 - Generation of the response function of FOS in iteration seven.

NO.	Point Sets	Parameter Values		Coefficients of RSM		Response Surface Function :	FOS(X*) = 1.25
ITERATION 7	POINT 1	X_1 (MPa)	2.53	a_0	4.92639	FOS = (4.926) + (0.81*X_1) + (-0.015*X_2) + (-0.799*X_3) + (-0.051*X_1^2) + (0.001*X_2^2) + (0.031*X_3^2)	
		X_2 (GPa/m)	21.2				
		X_3 (GPa/m)	13				
		FOS	1.47				
	POINT 2	X_1 (MPa)	4.33	b_1	0.81037		
		X_2 (GPa/m)	30.2				
		X_3 (GPa/m)	15.4				
		FOS	2.65				
	POINT 3	X_1 (MPa)	0.73	b_2	-0.01535		X_i^* (X_1^* , X_2^* , X_3^*) = (2.46 , 20.8 , 13.3)
		X_2 (GPa/m)	15.4				
		X_3 (GPa/m)	15.1				
		FOS	0.43				
	POINT 4	X_1 (MPa)	0.73	b_3	-0.79935		
		X_2 (GPa/m)	30.2				
		X_3 (GPa/m)	15.4				
		FOS	0.51				
	POINT 5	X_1 (MPa)	0.73	c_1	-0.04997		
		X_2 (GPa/m)	30.2				
		X_3 (GPa/m)	10.6				
		FOS	0.59				
	POINT 6	X_1 (MPa)	0.73	c_2	0.00058		
		X_2 (GPa/m)	12.2				
		X_3 (GPa/m)	10.6				
		FOS	0.42				
	POINT 7	X_1 (MPa)	4.33	c_3	0.03117		
		X_2 (GPa/m)	15.4				
		X_3 (GPa/m)	15.1				
		FOS	2.11				

Table D.8 - Generation of the response function of FOS in iteration eight.

NO.	Point Sets	Parameter Values		Coefficients of RSM		Response Surface Function : $\quad$ FOS $= (4.928) + (0.799^*X_1) + (-0.043^*X_2) + (-0.804^*X_3) +$ $(-0.066^*X_1^2) + (0.001^*X_2^2) + (0.033^*X_3^2)$	FOS $(X^*) = 1.2$
ITERATION 8	**POINT 1**	X_1 (MPa)	2.46	a_0	4.92822		
		X_2 (GPa/m)	20.8				
		X_3 (GPa/m)	13.3				
		FOS	1.25				
	POINT 2	X_1 (MPa)	4.26	b_1	0.79898		
		X_2 (GPa/m)	29.8				
		X_3 (GPa/m)	15.7				
		FOS	2.4				
	POINT 3	X_1 (MPa)	0.66	b_2	-0.04277		
		X_2 (GPa/m)	13.1				
		X_3 (GPa/m)	12.9				
		FOS	0.23				
	POINT 4	X_1 (MPa)	0.66	b_3	-0.80426	$X^*_i (X^*_1, X^*_2, X^*_3) = (2.39, 20.5, 13.2)$	
		X_2 (GPa/m)	29.8				
		X_3 (GPa/m)	15.7				
		FOS	0.3				
	POINT 5	X_1 (MPa)	0.66	c_1	-0.06613		
		X_2 (GPa/m)	29.8				
		X_3 (GPa/m)	10.9				
		FOS	0.34				
	POINT 6	X_1 (MPa)	0.66	c_2	0.00116		
		X_2 (GPa/m)	11.8				
		X_3 (GPa/m)	10.9				
		FOS	0.24				
	POINT 7	X_1 (MPa)	4.26	c_3	0.03302		
		X_2 (GPa/m)	13.1				
		X_3 (GPa/m)	12.9				
		FOS	1.89				

Table D.9 - Generation of the response function of FOS in iteration nine.

NO.	Point Sets	Parameter Values		Coefficients of RSM		Response Surface Function : $FOS = (4.906) + (1.183*X_1) + (-0.171*X_2) + (-0.618*X_3) + (-0.126*X_1^2) + (0.004*X_2^2) + (0.023*X_3^2)$	
ITERATION 9	**POINT 1**	X_1 (MPa)	2.39	a_0	4.90638		$FOS(X^*) = 1.13$
		X_2 (GPa/m)	20.5				
		X_3 (GPa/m)	13.2				
		FOS	1.2				
	POINT 2	X_1 (MPa)	4.19	b_1	1.18259		
		X_2 (GPa/m)	29.5				
		X_3 (GPa/m)	15.6				
		FOS	2.34				
	POINT 3	X_1 (MPa)	0.59	b_2	-0.16995		$X^*_i (X^*_1, X^*_2, X^*_3) = (2.27, 19.9, 13.4)$
		X_2 (GPa/m)	14.9				
		X_3 (GPa/m)	12.7				
		FOS	0.21				
	POINT 4	X_1 (MPa)	0.59	b_3	-0.61795		
		X_2 (GPa/m)	29.5				
		X_3 (GPa/m)	15.6				
		FOS	0.24				
	POINT 5	X_1 (MPa)	0.59	c_1	-0.12566		
		X_2 (GPa/m)	29.5				
		X_3 (GPa/m)	10.8				
		FOS	0.27				
	POINT 6	X_1 (MPa)	0.59	c_2	0.00424		
		X_2 (GPa/m)	11.5				
		X_3 (GPa/m)	10.8				
		FOS	0.2				
	POINT 7	X_1 (MPa)	4.19	c_3	0.02321		
		X_2 (GPa/m)	14.9				
		X_3 (GPa/m)	12.7				
		FOS	1.96				

Table D.10 - Generation of the response function of FOS in iteration ten.

NO.	Point Sets	Parameter Values		Coefficients of RSM		Response Surface Function : FOS = (4.91) + (1.099*X_1) + (-0.156*X_2) + (-0.616*X_3) + (-0.116*X_1^2) + (0.004*X_2^2) + (0.023*X_3^2) X_i^* (X_1^* , X_2^* , X_3^*) = (2.17 , 19.7 , 13.4)	FOS (X^*) = 1.05
ITERATION 10	**POINT 1**	X_1 (MPa)	2.27	a_0	4.91029		
		X_2 (GPa/m)	19.9				
		X_3 (GPa/m)	13.4				
		FOS	1.13				
	POINT 2	X_1 (MPa)	4.07	b_1	1.09980		
		X_2 (GPa/m)	28.9				
		X_3 (GPa/m)	15.8				
		FOS	2.26				
	POINT 3	X_1 (MPa)	0.47	b_2	-0.15591		
		X_2 (GPa/m)	14.6				
		X_3 (GPa/m)	12.5				
		FOS	0.16				
	POINT 4	X_1 (MPa)	0.47	b_3	-0.61637		
		X_2 (GPa/m)	28.9				
		X_3 (GPa/m)	15.8				
		FOS	0.19				
	POINT 5	X_1 (MPa)	0.47	c_1	-0.11559		
		X_2 (GPa/m)	28.9				
		X_3 (GPa/m)	11				
		FOS	0.21				
	POINT 6	X_1 (MPa)	0.47	c_2	0.00399		
		X_2 (GPa/m)	10.9				
		X_3 (GPa/m)	11				
		FOS	0.16				
	POINT 7	X_1 (MPa)	4.07	c_3	0.02284		
		X_2 (GPa/m)	14.6				
		X_3 (GPa/m)	12.5				
		FOS	1.91				

Table D.11 - Generation of the response function of FOS in iteration eleven.

NO.	Point Sets	Parameter Values		Coefficients of RSM			
ITERATION 11	POINT 1	X_1 (MPa)	2.17	a_0	5.13848	Response Surface Function : $FOS = (5.138) + (-0.191*X_1) + (0.704*X_2) + (-1.787*X_3) + (0.172*X_1^2) + (-0.016*X_2^2) + (0.067*X_3^2)$	$FOS(X^*) = 1.09$
		X_2 (GPa/m)	19.7				
		X_3 (GPa/m)	13.4				
		FOS	1.05				
	POINT 2	X_1 (MPa)	3.97	b_1	-0.19127		
		X_2 (GPa/m)	28.7				
		X_3 (GPa/m)	15.8				
		FOS	2.17				
	POINT 3	X_1 (MPa)	0.37	b_2	0.70358		$X^*_i (X^*_1 , X^*_2 , X^*_3) = (2.18 , 19.1 , 13.3)$
		X_2 (GPa/m)	14.1				
		X_3 (GPa/m)	12.8				
		FOS	0.17				
	POINT 4	X_1 (MPa)	0.37	b_3	-1.78667		
		X_2 (GPa/m)	28.7				
		X_3 (GPa/m)	15.8				
		FOS	0.17				
	POINT 5	X_1 (MPa)	0.37	c_1	0.17208		
		X_2 (GPa/m)	28.7				
		X_3 (GPa/m)	11				
		FOS	0.17				
	POINT 6	X_1 (MPa)	0.37	c_2	-0.01642		
		X_2 (GPa/m)	14.1				
		X_3 (GPa/m)	11				
		FOS	0.16				
	POINT 7	X_1 (MPa)	3.97	c_3	0.06667		
		X_2 (GPa/m)	14.1				
		X_3 (GPa/m)	12.8				
		FOS	1.8				

Table D.12 - Generation of the response function of FOS in iteration twelve.

NO.	Point Sets	Parameter Values		Coefficients of RSM		Response Surface Function : FOS = (5.124) + (-0.073*X_1) + (0.682*X_2) + (-1.758*X_3) + (0.147*X_1^2) + (-0.016*X_2^2) + (0.066*X_3^2)	FOS (X^*) = 1.08
ITERATION 12	**POINT 1**	X_1 (MPa)	2.18	a_0	5.12445		
		X_2 (GPa/m)	19.1				
		X_3 (GPa/m)	13.3				
		FOS	1.09				
	POINT 2	X_1 (MPa)	3.98	b_1	-0.07330		
		X_2 (GPa/m)	28.1				
		X_3 (GPa/m)	15.7				
		FOS	2.22				
	POINT 3	X_1 (MPa)	0.38	b_2	0.68235		
		X_2 (GPa/m)	13.9				
		X_3 (GPa/m)	12.9				
		FOS	0.17			X_i^* (X_1^* , X_2^* , X_3^*) = (**2.06, 18.9 , 13.5**)	
	POINT 4	X_1 (MPa)	0.38	b_3	-1.75750		
		X_2 (GPa/m)	28.1				
		X_3 (GPa/m)	15.7				
		FOS	0.17				
	POINT 5	X_1 (MPa)	0.38	c_1	0.14742		
		X_2 (GPa/m)	28.1				
		X_3 (GPa/m)	10.9				
		FOS	0.17				
	POINT 6	X_1 (MPa)	0.38	c_2	-0.01623		
		X_2 (GPa/m)	13.9				
		X_3 (GPa/m)	10.9				
		FOS	0.16				
	POINT 7	X_1 (MPa)	3.98	c_3	0.06607		
		X_2 (GPa/m)	13.9				
		X_3 (GPa/m)	12.9				
		FOS	1.84				

APPENDIX E

HISTORY RECORDS OF THE CENTERPOINTS IN EACH ITERATION

The history plots of the centerpoint of iterations one to twelve are illustrated in figures E.1 to E.12.
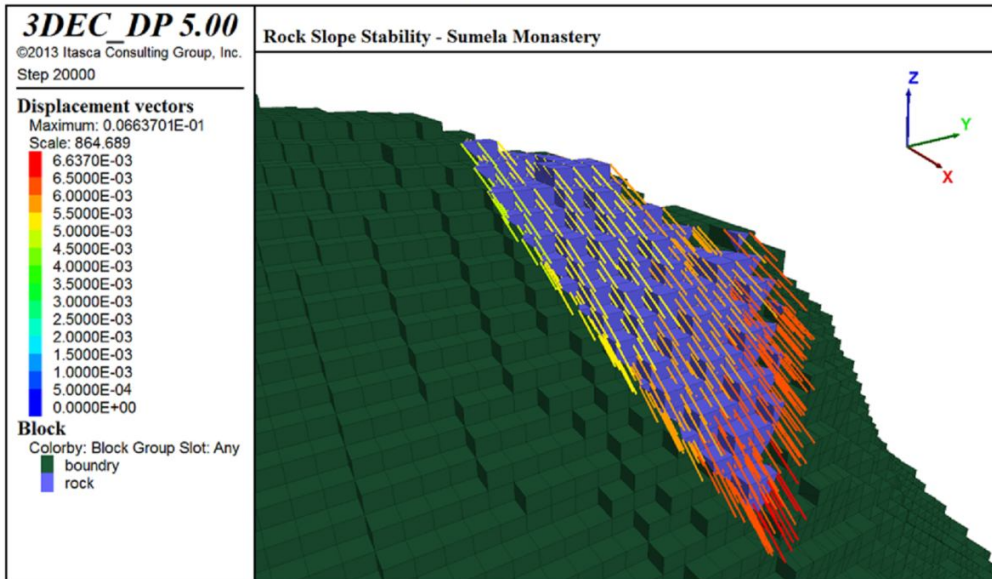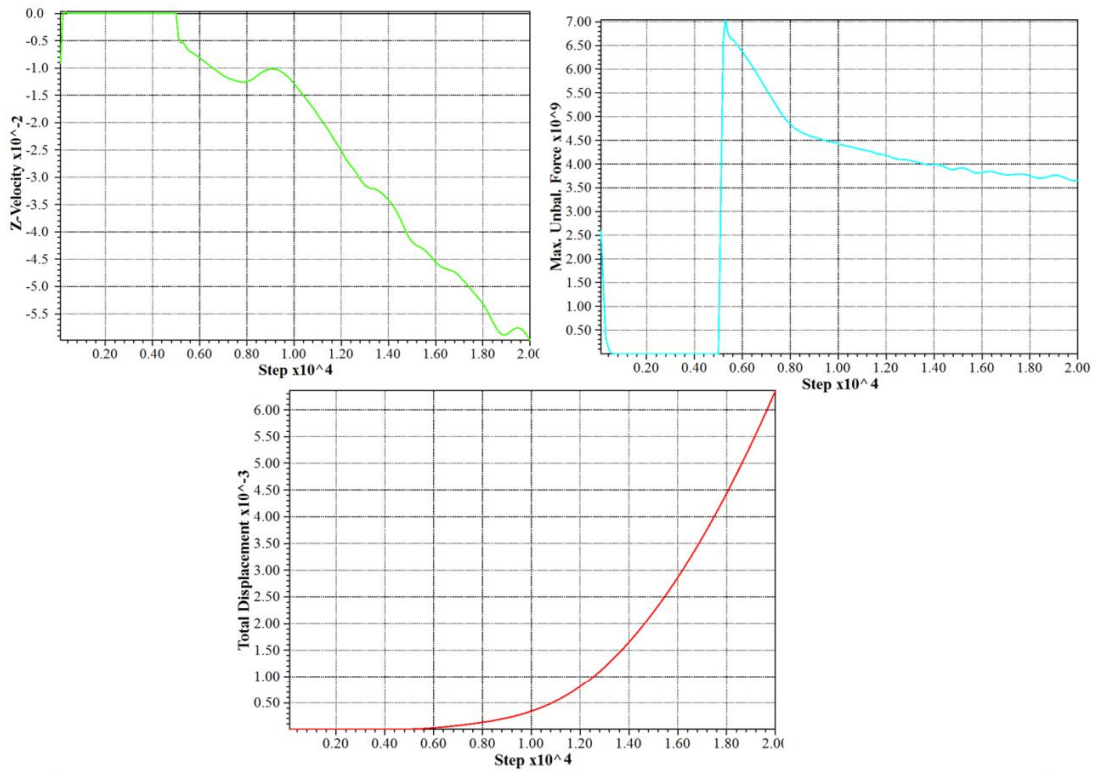
Figure E.1 - History plots of the centerpoint of iteration one (a) vertical velocity (m/s), (b) unbalanced force (N), (c) total displacement (m), (d) total displacement vectors (m).

110
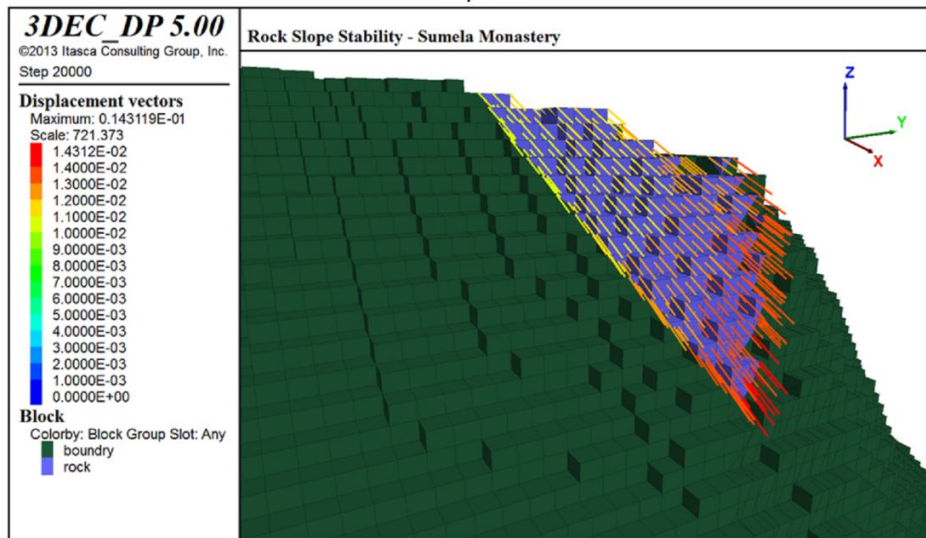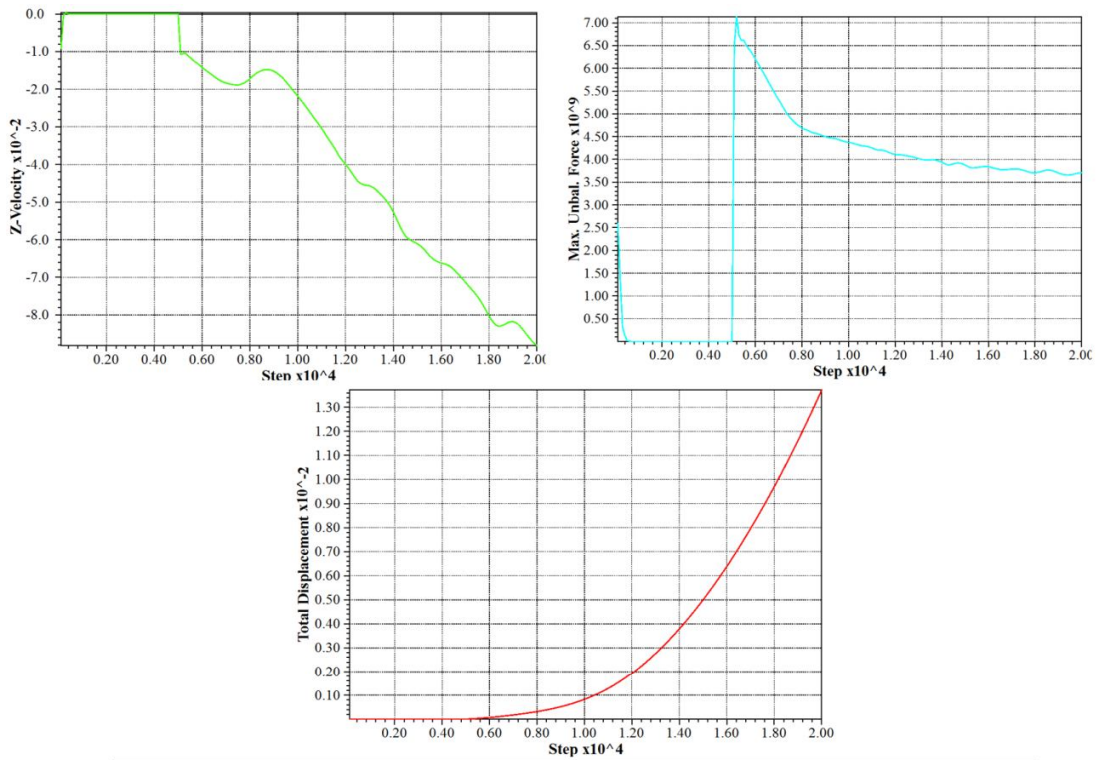
Figure E.2 - History plots of the centerpoint of iteration two (a) vertical velocity (m/s), (b) unbalanced force (N), (c) total displacement (m), (d) total displacement vectors (m).

111
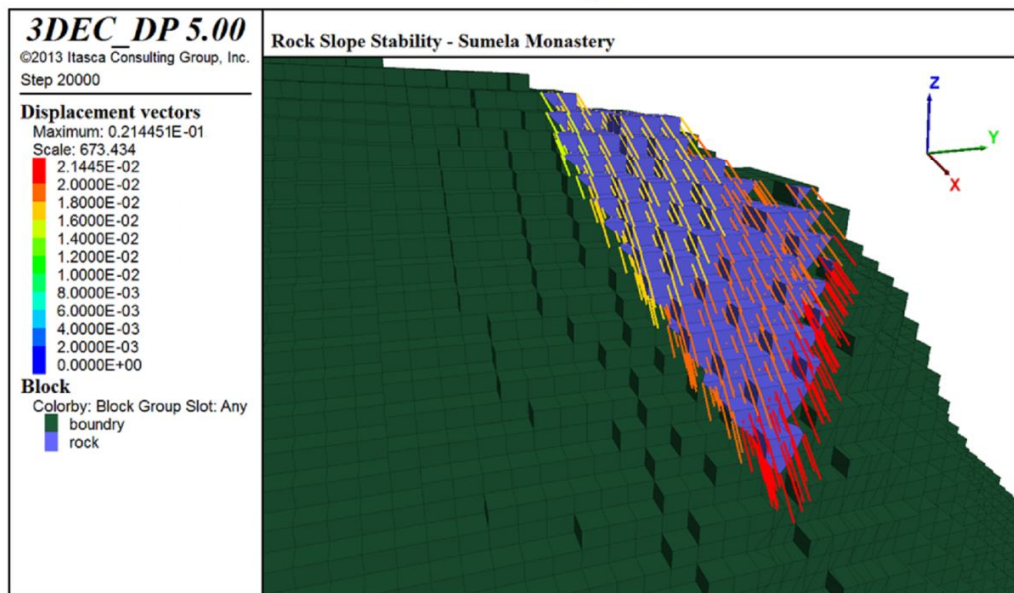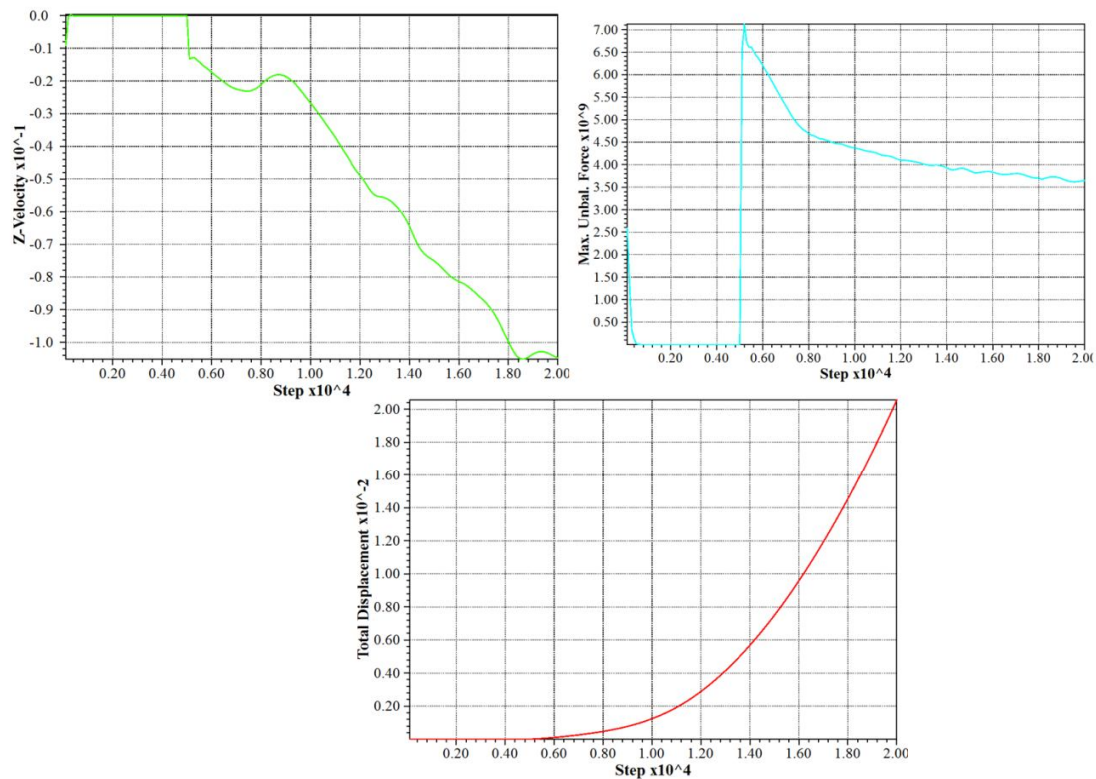
Figure E.3 - History plots of the centerpoint of iteration three (a) vertical velocity (m/s), (b) unbalanced force (N), (c) total displacement (m), (d) total displacement vectors (m).
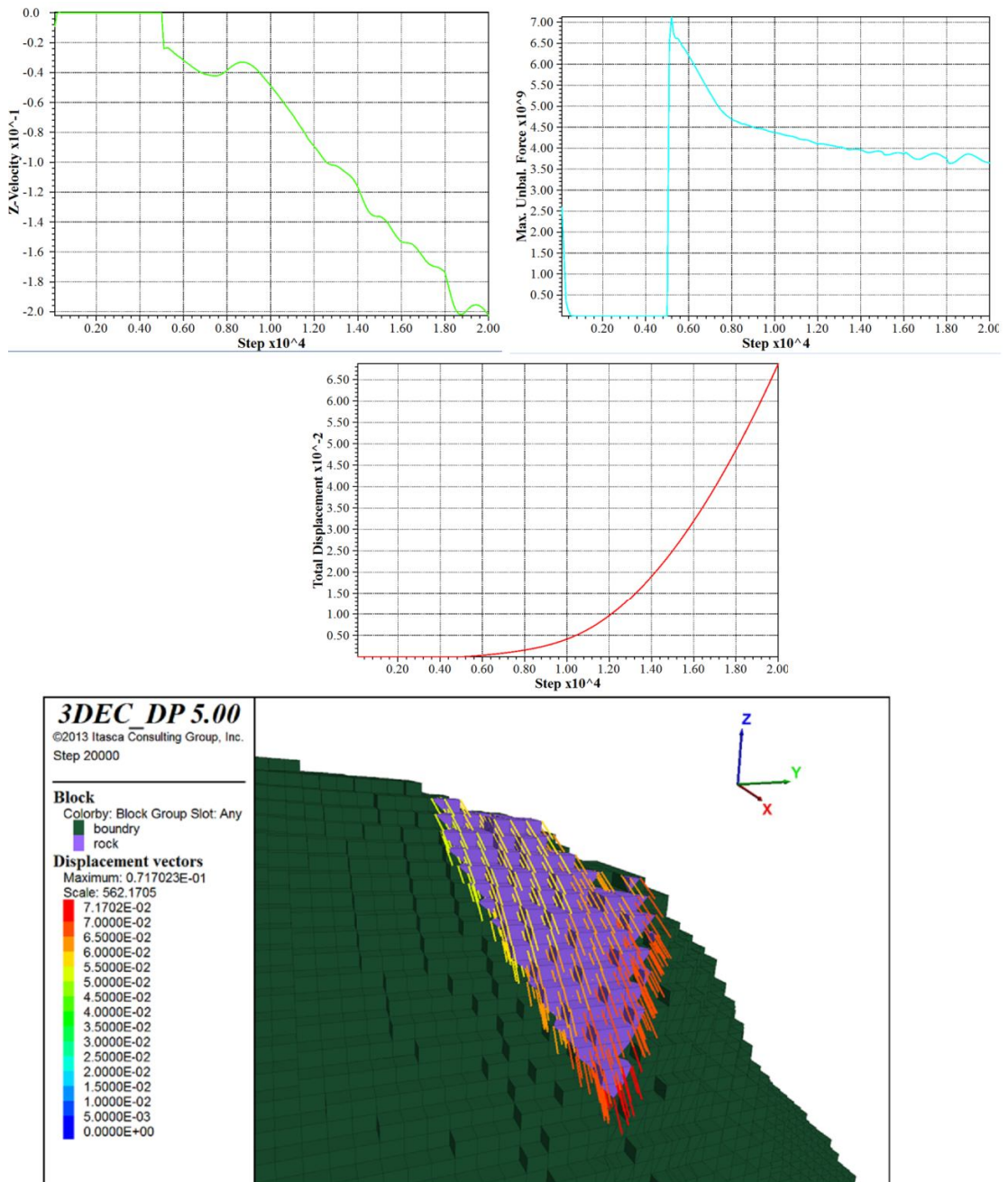
Figure E.4 - History plots of the centerpoint of iteration four (a) vertical velocity (m/s), (b) unbalanced force (N), (c) total displacement (m), (d) total displacement vectors (m).
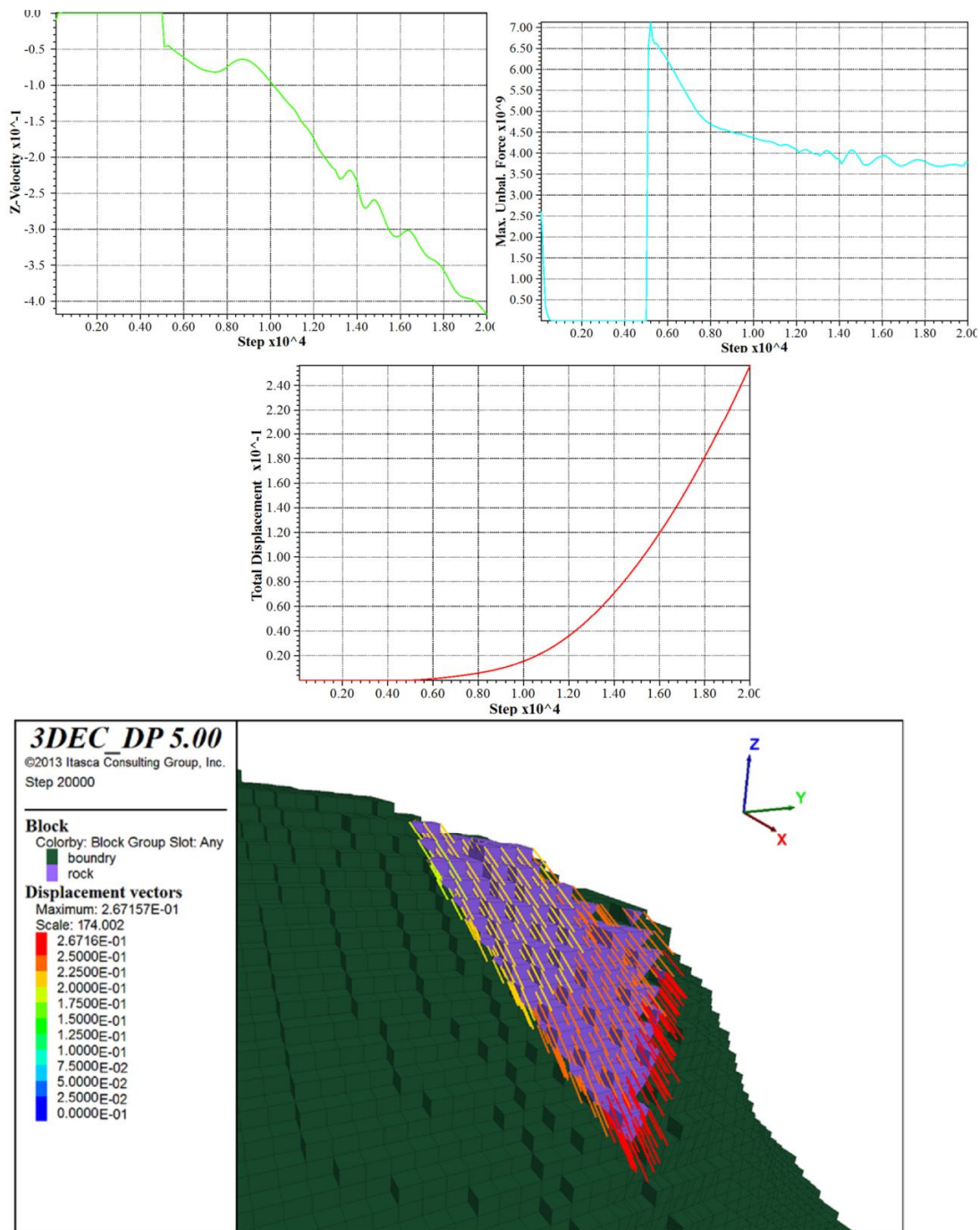
Figure E.5 - History plots of the centerpoint of iteration five (a) vertical velocity (m/s), (b) unbalanced force (N), (c) total displacement (m), (d) total displacement vectors (m).
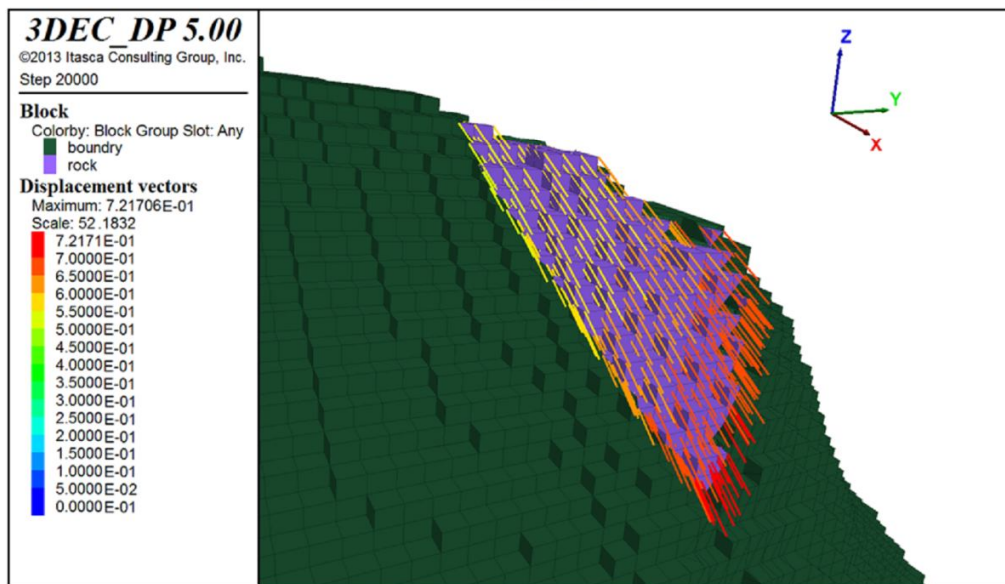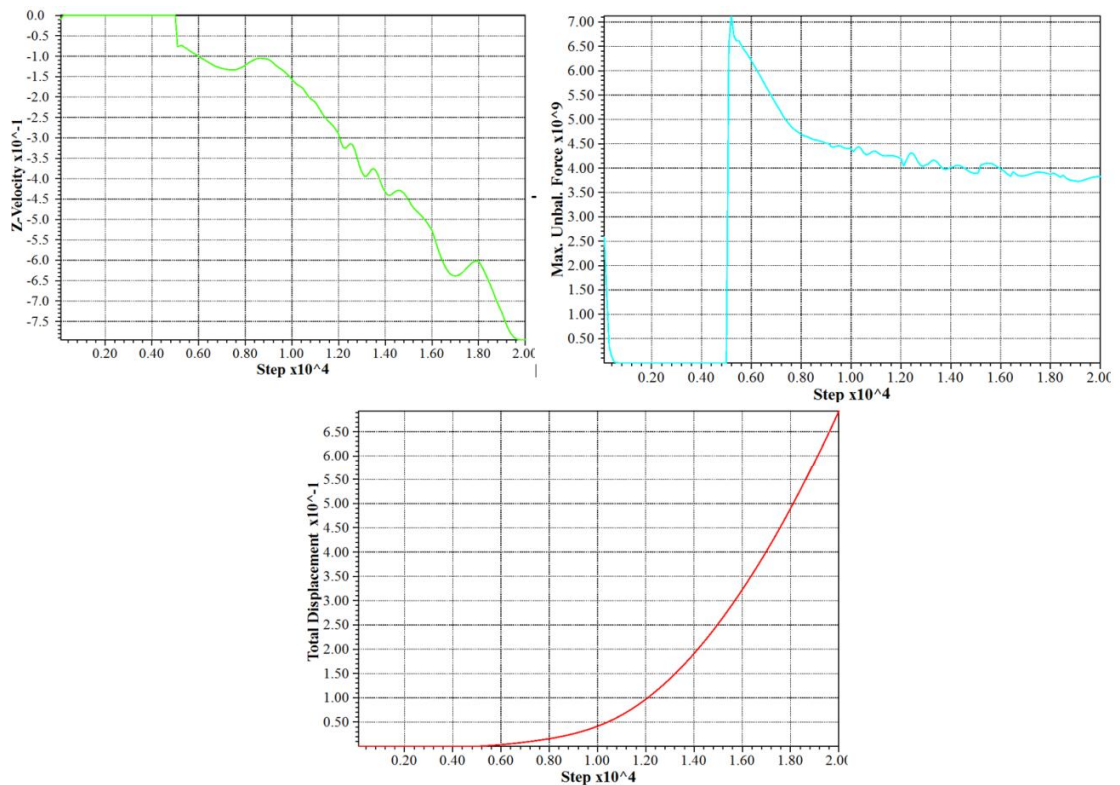
Figure E.6- History plots of the centerpoint of iteration six (a) vertical velocity (m/s), (b) unbalanced force (N), (c) total displacement (m), (d) total displacement vectors (m).
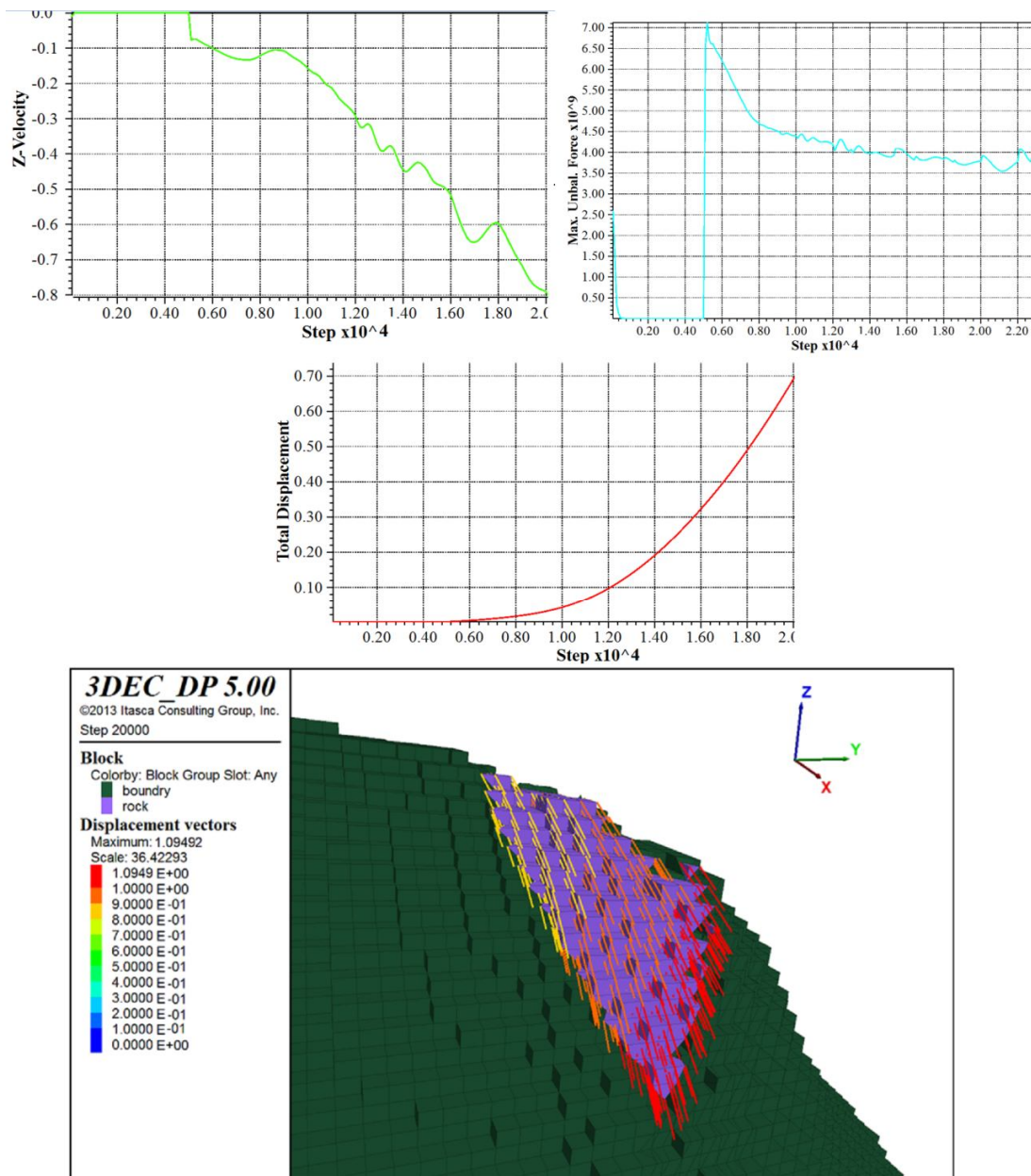
Figure E.7 - History plots of the centerpoint of iteration seven (a) vertical velocity (m/s), (b) unbalanced force (N), (c) total displacement (m), (d) total displacement vectors (m).

116
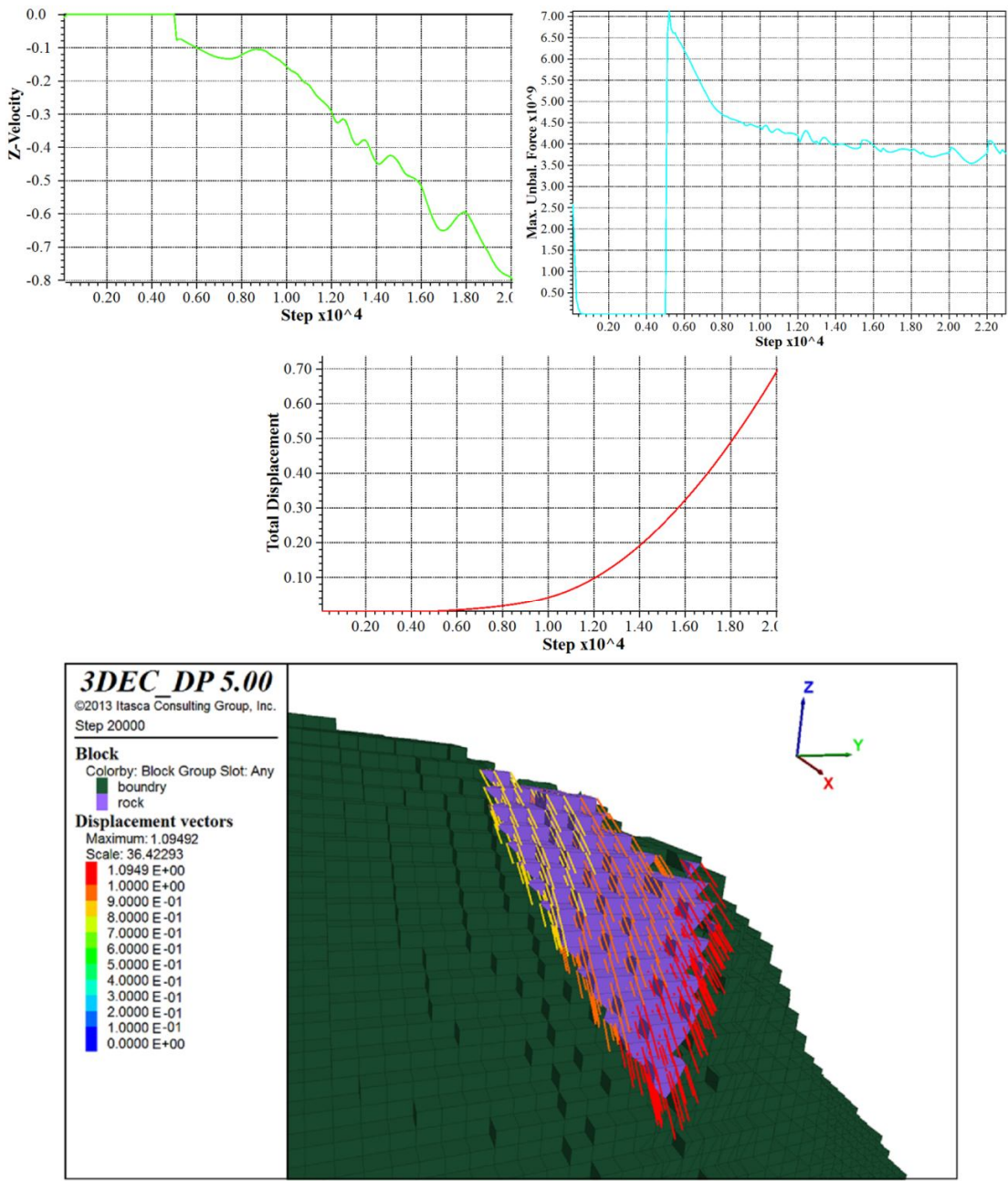
Figure E.8 - History plots of the centerpoint of iteration eight (a) vertical velocity (m/s), (b) unbalanced force (N), (c) total displacement (m), (d) total displacement vectors (m).

117
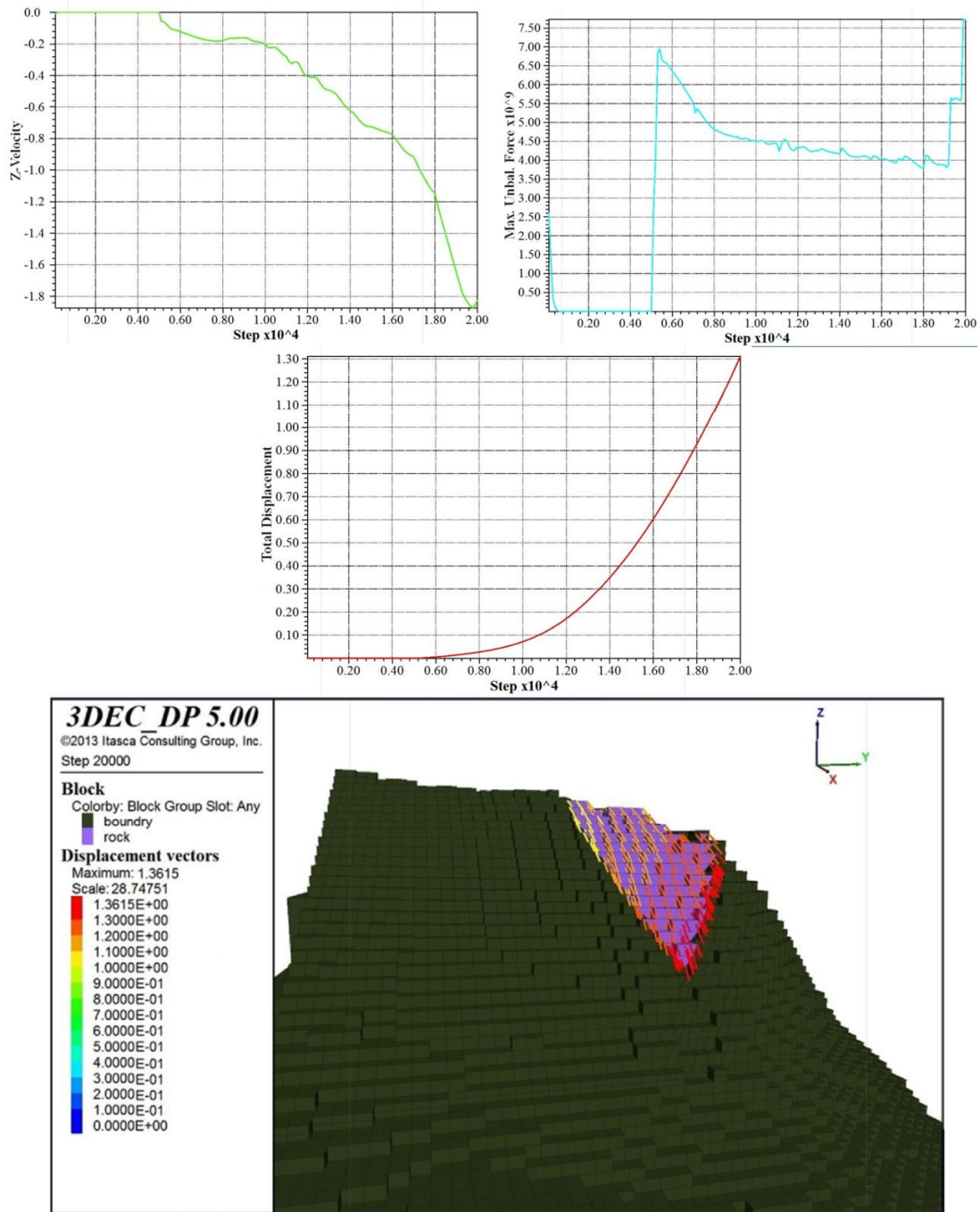
Figure E.9 - History plots of the centerpoint of iteration nine (a) vertical velocity (m/s), (b) unbalanced force (N), (c) total displacement (m), (d) total displacement vectors (m).

118
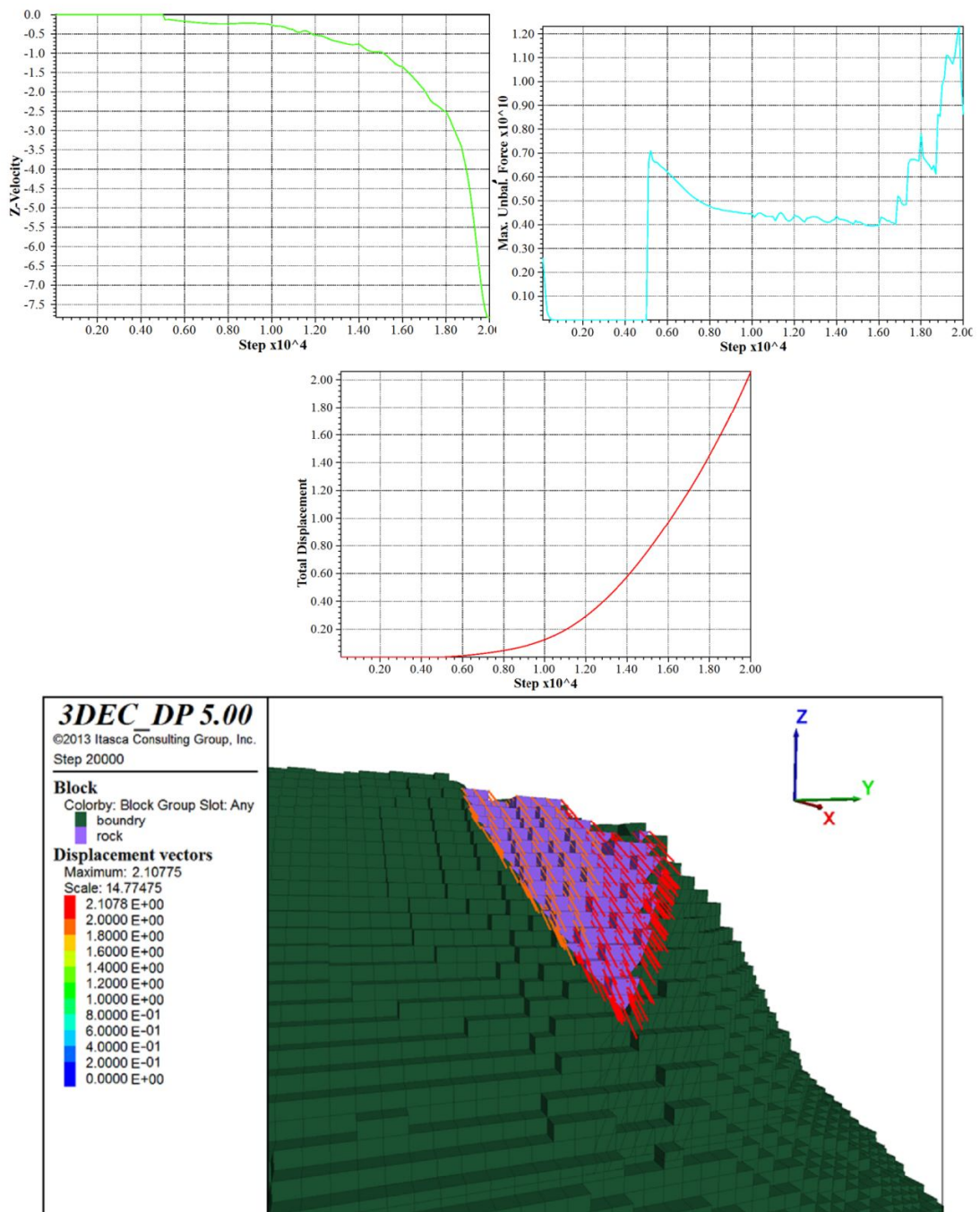
Figure E.10 - History plots of the centerpoint of iteration ten (a) vertical velocity (m/s), (b) unbalanced force (N), (c) total displacement (m), (d) total displacement vectors (m).

119
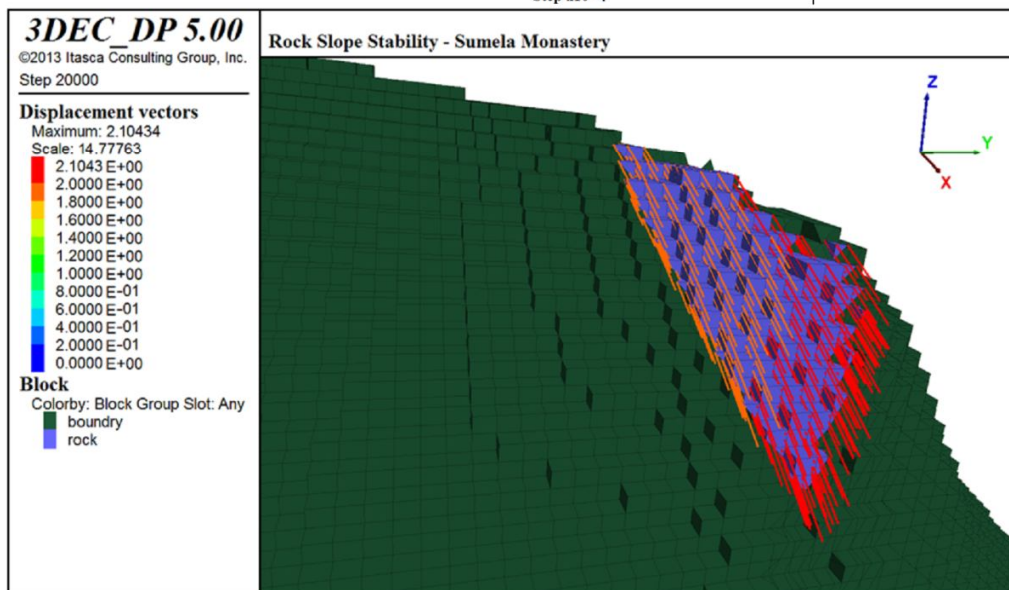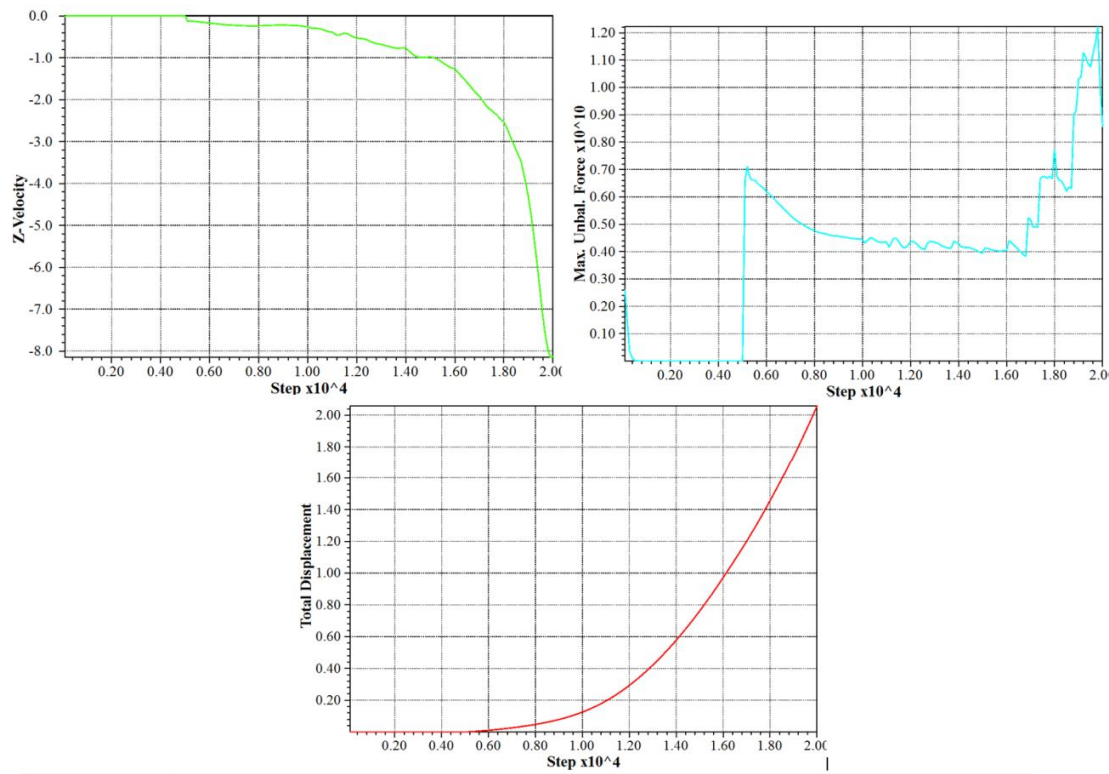
Figure E.11 - History plots of the centerpoint of iteration eleven (a) vertical velocity (m/s), (b) unbalanced force (N), (c) total displacement (m), (d) total displacement vectors (m).

120
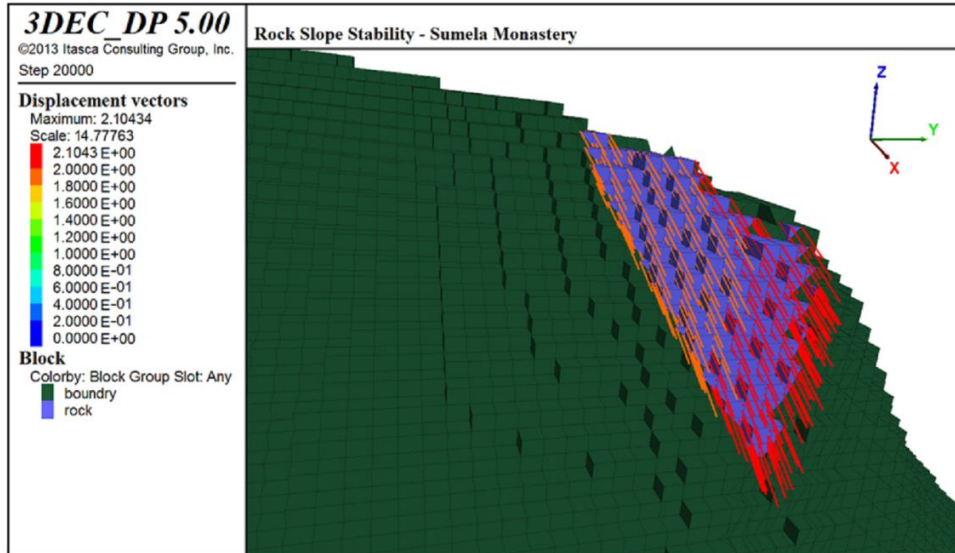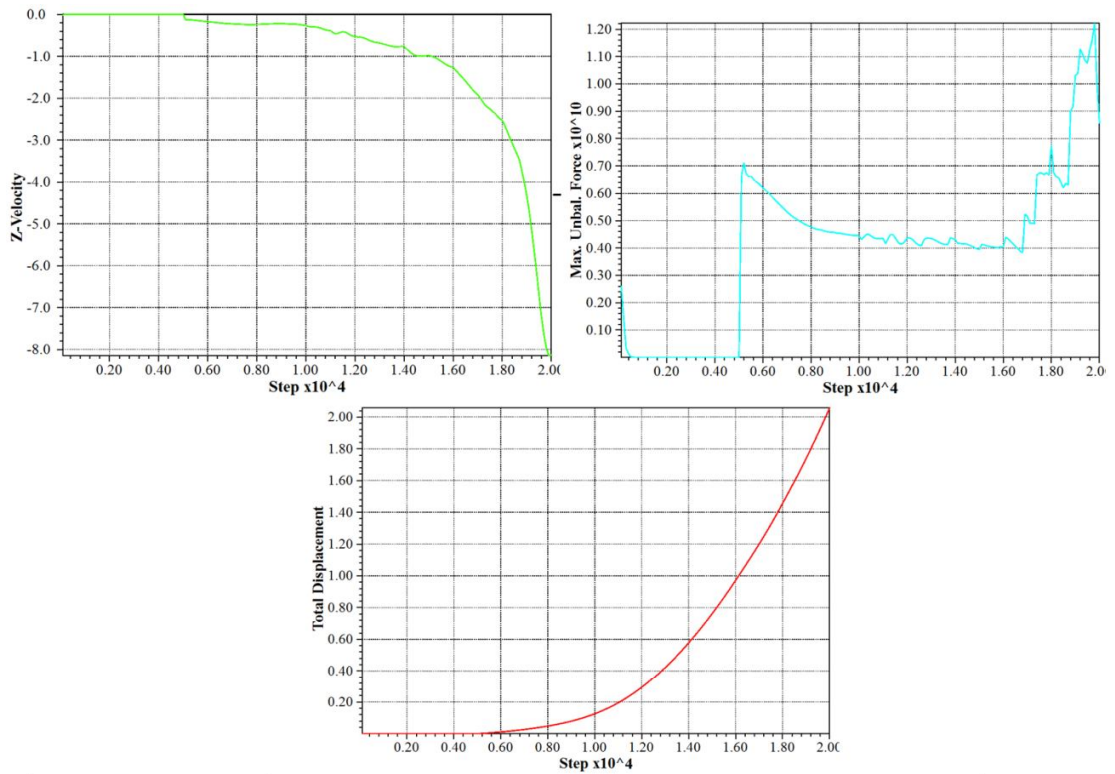
Figure E.12 - History plots of the centerpoint of iteration twelve (a) vertical velocity (m/s), (b) unbalanced force (N), (c) total displacement (m), (d) total displacement vectors (m).